



**NTNU – Trondheim**  
Norwegian University of  
Science and Technology

# Analysis of Ice-Induced Damages to a Cargo Carrier and Implications wrt. Rule Requirements

**Nora Helen Lund Lyngra**

Marine Technology

Submission date: May 2014

Supervisor: Jørgen Amdahl, IMT

Co-supervisor: Sverre Bergli, DNV-GL

Norwegian University of Science and Technology  
Department of Marine Technology



MASTER THESIS SPRING 2014  
for  
Stud. Techn. Nora Helen Lund Lyngra  
**Analysis of Ice-Induced Damages to a Cargo Ship and Implications  
wrt. Rule Requirements**  
*Analyse av is-skalde på lasteskip og implikasjoner mht. regelkrav*

Due to global warming the ice cover in the Arctic has been reduced substantially and the Northern Sea Route (NSR) has become virtually ice-free in the summer season. As a consequence of this shipping activity in this area has increased significantly. Ships with no or light ice reinforcement have sailed the route, and the classification society DNV-GL has recently experienced incidents of ice-induced hull damages for ships classed by the Society. This is of concern as penetration of hull may cause spill of dangerous cargo to the vulnerable Arctic environment, and put the safety of ship and crew in jeopardy.

For DNV-GL it is essential to establish a good understanding of the forces that have caused these damages because this will provide information as to the ice actions that are to be expected during sailing in the nominal ice-free waters in the NSR. Further, this knowledge will constitute a basis for formulation of strength requirements/ice classes, maintenance, and new rules for ships in such traffic.

The master thesis shall address the following topics:

1. Review of the DNV-GL and IACS Unified Requirements for structural design of Polar ships, with emphasis on requirements to plates, stiffeners and girders/frames. A review of various ice pressure-area relationships shall be given. Emphasis shall be on ships designed for moderate ice actions
  2. Perform a detailed description of hull damages reported for a cargo ship according to information obtained from DNV-GL. The amount of damage shall be quantified as far as possible; if no other information is available from measurements shall be taken from photographic evidence combined with structural drawings. The uncertainty range of the measured deformations shall be estimated. The likely material strength (engineering stress-strain curve) shall be estimated.
  3. Initial assessment of the ice pressures causing the reported damages shall be made based on plastic methods of analysis.
-

4. A finite element model of the structure in the damaged area shall be established for nonlinear finite element with Abaqus. The size of the model shall be evaluated with respect to required mesh fineness, computer time and modelling of boundary conditions. It shall also be considered how application of various pressure distributions can easily be facilitated.
5. Perform a series of nonlinear finite element analyses. The load levels and pressure distributions shall be varied so as to reproduce the reported damage pattern as far as possible. The resulting load levels shall be compared with those of the simplified analysis.
6. Compare the ice pressure obtained from the numerical simulations with those for relevant ice classes in the DNV-GL and IACS rules (to the extent it is possible to single out the ice pressures in the design rules). Alternatively, to what ice class would it be necessary to design the actual bulk carrier to avoid hull damage?
7. Conclusions and recommendations for further work

Literature studies of specific topics relevant to the thesis work may be included.

The work scope may prove to be larger than initially anticipated. Topics may be deleted from the list above or reduced in extent, subject to approval from the supervisor.

In the thesis the candidate shall present his personal contribution to the resolution of problems within the scope of the thesis work.

Theories and conclusions should be based on mathematical derivations and/or logic reasoning identifying the various steps in the deduction.

The candidate should utilise the existing possibilities for obtaining relevant literature.

The thesis should be organised in a rational manner to give a clear exposition of results, assessments, and conclusions. The text should be brief and to the point, with a clear language. Telegraphic language should be avoided.

The thesis shall contain the following elements: A text defining the scope, preface, list of contents, summary, main body of thesis, conclusions with recommendations for further work, list of symbols and acronyms, references and (optional) appendices. All figures, tables and equations shall be numerated.

The supervisor may require that the candidate, in an early stage of the work, presents a written plan for the completion of the work. The plan should include a budget for the use of computer and laboratory resources which will be charged to the department. Overruns shall be reported to the supervisor.

---

The original contribution of the candidate and material taken from other sources shall be clearly defined. Work from other sources shall be properly referenced using an acknowledged referencing system.

The report shall be submitted in two copies:

- Signed by the candidate
- The text defining the scope included
- In bound volume(s)
- Drawings and/or computer prints which cannot be bound should be organised in a separate folder.

**Supervisor:**

Prof. Jørgen Amdahl

**Advisor at DNV-GL:**

Sverre Bergli

**Deadline: June 2, 2014**

Trondheim, January 6, 2014

Jørgen Amdahl

---



# Preface

This thesis is an individual master thesis carried out at the Department of Marine Technology, Norwegian University of Science and Technology, Trondheim, in cooperation with DNV-GL, Tankers and Dry Cargo Section, Høvik, Norway. The scope is a case study of the damage loads on a ship which has undergone severe deformation of the hull structure after sailing in ice infested waters. The thesis was done over a period of 20 weeks, for 12 of these I was located at DNV-GL's main office at Høvik.

A considerable amount of time was spent searching for errors in the finite element models, which gave less time for running analyses. Therefore, the number of analyses performed is less than initially intended.

I would like to thank my supervisor Professor Jørgen Amdahl for providing me with a very interesting scope for the thesis, and for the supervision he has given me. I would also like to thank Ivar Håberg and Sverre Bergli at the Division of Tankers and Dry Cargo, who provided me with information about the ship studied, and put me in contact with people who could help me along the way. Thanks to Carl-Johan Åkerstöm and the rest of the Department of Tankers and Dry Cargo for supervising me and including me in the department during my stay at Høvik. Last but not least, thanks to the Department of Structures, Technical Advisory, Maritime for crucial help with the element models. Nonlinear analyses are not straight forward, and without you this thesis would lack proper results.

Trondheim, May 30<sup>rd</sup> 2014



Nora Helen Lund Lyngra





# Summary

In this thesis, an ice-induced damage to a DNV-GL registered cargo ship is investigated by looking into its damage survey report, and running nonlinear finite element analyses. The analyses are used for regeneration of the damage deformations and estimation the damage loading. The results are compared with design and capacity ice loads calculated from DNV-GL and IACS' rule requirements for the ice class of the ship studied, [1], [2].

The Finnish-Swedish Ice Class Rules (FSICR), which are adopted by DNV-GL, and the International Association of Classification Societies Unified Requirements for Polar Class (IACS UR PC), are derived and explained with focus on plating and framing requirements. From the rules design loads and capacity loads for the frames in the side bow of the case study ship, are calculated and applied to three different finite element models for analysis. The first model is a single frame with plate flange. The second is two neighbouring frames with two tripping brackets in between. The third model is the ship side damage area. In addition to the design loads from the rules, five proposed load cases are analyzed for the ship side model. The resulting model deformations are compared with deformation measurements from photos given in the surveyor report, in order to evaluate the applied load cases. A resemblance in the deformations indicates a load case that resembles the original damage load.

The analyses of the frame models with design and capacity loads from the rules show that the frames have a considerable amount of capacity beyond the rule calculations. In one of the analyses a frame capacity of  $15\text{MPa}$  is obtained, while the design capacity is  $5\text{MPa}$ . For the ship side model, only one of the five proposed load cases proves to be successful. Measurements of the deformation of the model are done, and they coincide with the photos where the deformations are large, but give a poor match elsewhere. A pressure of  $6.9\text{MPa}$  over an area of

$5.8m^2$  is needed to reproduce the largest of the deformations seen in the photos.

The ship side analysis shows that a force about ten times the FSICR design load, or twice the IACS PC design load, is needed to produce the deformations seen in the photos. The large difference in the ratio for the FSICR and the IACS PC force originate from the difference in the size of the load application area. The rules appear to present very conservative design loads, as the finite element analyses reveal a considerable amount of load carrying capacity beyond the design load level. This is because the rules are derived to be conservative, hence, they are not suited for calculation of the actual capacity of a structure. For the ship side model, an ice class 3-5 notations higher than the notation it is classified for is needed to withstand the damage loading, depending on how the numbers are evaluated. This implies that the ship in question has been sailing in waters with ice conditions it was not designed for.

Due to a lot of uncertainty related to the photo measurements, and the many assumptions made for the analyses' input, an uncertainty is related to the output of the analyses, and the conclusions based on these.

This thesis is conducted in cooperation with DNV-GL, Tankers and Dry Cargo Section, Høvik, Norway. They supplied survey reports, ship drawings, and supervision along the way. The vessel documents are applied anonymously within the production of this report. In order to realize the true potential of ice damage investigation, more precise documentation of the scale of the actual damages must be recorded.

---

# Sammendrag

I denne oppgaven er et is-skadet DNV-GL registrert skip undersøkt gjennom studie av inspeksjonsrapporten og ved å kjøre ikke-lineære elementanalyser. Analysene er gjort for å gjenskape skadedeformasjonene, samt estimere skadelasten. Resultatene er sammenlignet med design- og kapasitetslaster beregnet etter DNV-GL og IACS' regelkrav for isklassen til skipet som er undersøkt, [1], [2].

“The Finnish-Swedish Ice Class Rules”(FSICR), som DNV-GL har inkludert i sine regler, og “the International Association of Classification Societies Unified Requirements for Polar Class”(IACS UR PC), er forklart og utledet med fokus på kravene for plater og stivere. Design- og kapasitetslaster for stiverne i siden på baugen til det skadede skipet er beregnet og brukt i elementanalyse av tre modeller. Den første modellen er en enkelt stiver med plateflens. Den neste er to stivere ved siden av hverandre, med vippebraketter mellom. Den tredje modellen er skadeområdet på siden av baugen. I tillegg til designlastene fra reglene er fem foreslåtte lasttilfeller analysert for den tredje modellen. Deformasjonene fra den analyserte modellen er sammenlignet med målinger av deformasjoner gjort fra bilder gitt i inspeksjonsrapporten, for å kunne gjøre en bedømming av de foreslåtte lasttilfellene. Likheter i deformasjonene gir en indikasjon om at lasttilfellet ligner den originale lasten som førte til skaden.

Analysene av stivermodellene med design- og kapasitetslaster fra reglene viser at stiverne har en betydelig restkapasitet utover det regelberegningene viser. I den ene analysen nås en stiverkapasitet på  $15MPa$ , mens designkapasiteten er  $5MPa$ . For modellen av siden av baugen er kun en av de foreslåtte lasttilfellene som leder til en fullført analyse. Deformasjonene blir målt, og de stemmer godt med målene fra bildene i området er deformasjonene er størst, men stemmer ikke like godt andre steder. For å oppnå en deformasjon lik den største sett på bildene er et trykk på  $6.9MPa$  over et areal lik  $5.8m^2$  nødvendig.

Baugsideanalysen viser at en last ti ganger designlasten fra FSICR, og to ganger designlasten fra IACS PC, er nødvendig for å oppnå ønsket deformasjoner. Den store forskjellen i nødvendig rate fra FSICR- og IACS PC-lastene kommer fra forskjellen i størrelsen på arealet lastene virker på. Reglene ser ut til å gi veldig konservative designlaster, da elementanalysene viser at modellene har lastkapasitet langt utover designlastene. Dette kommer fra reglene som er utledet for å være konservative, og de gir derfor dårlige estimater for den faktiske kapasiteten til konstruksjonen. For modellen av sidebaugen er en økning av isklasse med 3-5 notasjoner nødvendig for å ha et design som kan motstå lasten, alt etter som hvordan tallene er tatt i betraktning. Dette impliserer at skipet har seilet under forhold det ikke var designet for å tåle.

På grunn av stor usikkerhet knyttet til målingene gjort fra bildene, og mange antagelser gjort for inndataene til elementanalysene, er usikkerhet knyttet til resultatene fra analysene og konklusjonene basert på disse.

Denne oppgaven er utført i samarbeid med DNV-GL, Avdeling for Tank- og Tørrlast, Høvik, Norge. De fremskaffet inspeksjonsrapporter, skrogtegninger, og gav veiledning underveis. Alle dokumenter relatert til skadeskipet er gjengitt i anonymisert form i denne oppgaven. For å kunne utnytte potensialet i informasjonen fra en undersøkelse av et isskadet skip, må deformasjonene dokumenteres mer detaljert under skadeinspeksjonen.

---

# Contents

<b>Preface</b>	<b>V</b>
<b>Summary</b>	<b>VII</b>
<b>Sammendrag</b>	<b>IX</b>
<b>Table of Contents</b>	<b>XIII</b>
<b>List of Tables</b>	<b>XVI</b>
<b>List of Figures</b>	<b>XIX</b>
<b>Nomenclature</b>	<b>XXI</b>
<b>1 Introduction</b>	<b>1</b>
<b>2 Rules for Structural Design of Polar Ships</b>	<b>3</b>
2.1 DNV-GL: “Ice Strengthening for the Northern Baltic” . . . . .	4
2.1.1 Design Ice Pressure . . . . .	5
2.1.2 Shell Plate Requirement . . . . .	5
2.1.3 Requirement for Frames . . . . .	8
2.1.4 Ice Stringer Requirements . . . . .	10
2.1.5 Requirements for Web Frames . . . . .	11
2.2 IACS: “Requirements Concerning Polar Class” . . . . .	12
2.2.1 Design Ice Load . . . . .	13
2.2.2 Shell Plate Requirements . . . . .	17
2.2.3 Requirements for Framing . . . . .	18
<b>3 Description of Ship Side Damage</b>	<b>23</b>
3.1 Description of External Damage . . . . .	23
3.2 Description of Internal Damage, An Overview . . . . .	25

---

3.3	Inwards Deformation of Plates and Frames . . . . .	26
3.4	Tripping of Frames . . . . .	29
3.5	Web Frames . . . . .	34
3.6	Stringers . . . . .	37
3.7	Discussion of Deformations . . . . .	37
3.8	Sources of Error . . . . .	38
3.9	Load Calculation from Rules . . . . .	38
3.9.1	Design Loads Calculated from Rules . . . . .	39
3.9.2	Capacities Calculated from Rules . . . . .	40
3.9.3	Capacity Calculated from Simplified Theory . . . . .	41
<b>4</b>	<b>Damage Reproduction with Finite Element Analyses</b>	<b>43</b>
4.1	Material Properties . . . . .	44
4.1.1	Plate Materials . . . . .	45
4.1.2	Frame Materials . . . . .	48
4.1.3	Material Summary . . . . .	49
4.2	Analysis Procedures . . . . .	50
4.3	Simplified Frame Analysis . . . . .	52
4.3.1	Element Meshing . . . . .	53
4.3.2	Boundary Conditions . . . . .	53
4.3.3	Loading . . . . .	54
4.3.4	Double Frame . . . . .	55
4.4	Analysis of Ice Damaged Hull Structure . . . . .	56
4.4.1	Element Meshing . . . . .	57
4.4.2	Boundary Conditions . . . . .	58
4.4.3	Loading . . . . .	58
4.4.4	FSICR and IACS Ice Patch . . . . .	59
4.4.5	Proposed Ice Patches . . . . .	59
4.5	Analysis Challenges . . . . .	63
4.5.1	Verification of the Model . . . . .	66
<b>5</b>	<b>Results from Finite Element Analyses</b>	<b>69</b>
5.1	Simplified Frame Analyses . . . . .	69
5.1.1	Initial Loads, Centred . . . . .	69
5.1.2	FSICR and IACS Ice Patch Analysis of Single and Double Frame . . . . .	74
5.2	Main Model Analysis . . . . .	78
5.2.1	Analysis with FSICR and IACS Ice Patch . . . . .	78
5.2.2	Analyses with Proposed Load Cases . . . . .	81
<b>6</b>	<b>Discussion of Results</b>	<b>87</b>

---

6.1	Comparison of Analysis Results and Real Damage . . . . .	87
6.1.1	Single and Double Frame . . . . .	87
6.1.2	Main Model . . . . .	89
6.1.3	Discussion of Validity of Comparisons . . . . .	93
6.2	Comparison of Photos and Analysis Model . . . . .	94
<b>7</b>	<b>Conclusion</b>	<b>99</b>
<b>8</b>	<b>Recommendations for Further Work</b>	<b>101</b>
<b>A</b>	<b>Drawings</b>	<b>A1</b>

---





# List of Tables

2.1	Main particulars . . . . .	4
2.2	Polar Class. . . . .	13
3.1	Displacement of web frames . . . . .	25
3.2	Displacement of hull plate . . . . .	26
3.3	Displacement of hull plate . . . . .	29
3.4	Displacement of frame flanges . . . . .	29
3.5	Displacement of frame flanges . . . . .	32
3.6	Displacement of frame flanges . . . . .	33
3.7	Displacement of frames . . . . .	33
3.8	Displacement of frames . . . . .	34
3.9	Comparison of different measures for the same frame . . . . .	37
3.10	Definition of ice load length according to the FSICR, [3] . . . . .	39
4.1	Stress-strain values from DNV-GL test curves . . . . .	46
4.2	Material details for plating used in model, true stress and strain . . . . .	47
4.3	Material data for frames and stiffeners used in model, true stress and strain . . . . .	48
4.4	Material data calculated from mean values . . . . .	49
4.5	Summary of material data . . . . .	50
4.6	Scantlings of frame #232 1/2 . . . . .	52
4.7	Materials of frame #232 1/2 . . . . .	53
5.1	Initial load analysis for center loading, FSICR rules . . . . .	70
5.2	Initial load analysis for center loading, IACS PC rules . . . . .	70
5.3	Results from nonlinear FEA of single and double frame with FSICR patch at water line . . . . .	74
5.4	Results from nonlinear FEA of single and double frame with IACS patch at water line . . . . .	74
5.5	Results from nonlinear FEA of single and double frame with patch at water line . . . . .	75

5.6	Results from nonlinear FEA of main model with FSICR and IACS PC ice patch at water line . . . . .	81
5.7	Comparison of measurements from photos and from analysis . . .	84
5.8	Comparison of measurements from photos and from analysis . . .	84
6.1	Calculated capacities for a single frame, $[MPa]$ . . . . .	88
6.2	Capacities for a single frame from FEA, $[MPa]$ . . . . .	88
6.3	Comparison of design loads from IACS PC and FEA results . . .	91
6.4	Summary results from load case 1-4 . . . . .	93

# List of Figures

2.1	Ice belt regions . . . . .	6
2.2	Bending moment factor (m-values) . . . . .	7
2.3	Values of $m_0$ . . . . .	9
2.4	Design scenario - flexural failure during glancing collision . . . . .	14
2.5	Combination of crushing and flexural forces . . . . .	15
2.6	Ice load patch configuration . . . . .	16
2.7	General formulation of collapse state . . . . .	18
2.8	The three limit states considered for frames . . . . .	19
2.9	Bending/shear interaction diagram . . . . .	19
3.1	Shell expansion with damage area sketched . . . . .	24
3.2	Port side indent . . . . .	27
3.3	Port side indent . . . . .	27
3.4	Indent seen from inside fore peak tank . . . . .	28
3.5	Indent seen from inside fore peak tank . . . . .	28
3.6	Deformation of plates and frames #227 - #230 . . . . .	30
3.7	Deformation of plates and frames #231 - #233 . . . . .	30
3.8	Deformation of plates and frames #230 - #233 . . . . .	31
3.9	Deformation of plates and frames #233 - #235 . . . . .	31
3.10	Frame detail . . . . .	32
3.11	Deformation of plates and frames #233 - #237 . . . . .	35
3.12	Deformation of plates and frames #232 1/2 - #235 . . . . .	35
3.13	Deformation of frames and web frames #229 1/2 - #233 . . . . .	36
3.14	Deformation of frames and web frames #233 - #234 1/2 . . . . .	36
3.15	Frame capacities as a function of load height . . . . .	41
4.1	Example of distribution of steel quality, strictly illustrative . . . . .	44
4.2	Stress-strain curves from test data, DNV-GL . . . . .	46
4.3	Different materials used in different parts of the model . . . . .	50
4.4	Single and double frame with mesh, boundary conditions, and load . . . . .	56
4.5	Main analysis model with mesh . . . . .	57

---

4.6	Comparison plots of model with and without hydrostatic pressure	59
4.7	Load and boundary conditions applied in LC1, from Abaqus . . .	60
4.8	Load distribution of load case 2 . . . . .	61
4.9	Load distribution of load case 3 . . . . .	62
4.10	Load distribution of load case 4 and 5 . . . . .	62
4.11	The full model as it initially was intended to be, seen from center line . . . . .	63
4.12	Deformed stringer junction with beam and shell elements, respec- tively - von Mises stress distribution . . . . .	65
4.13	Curve of the applied force and the reaction force . . . . .	66
4.14	Curve of the internal energy and the external work . . . . .	67
5.1	Load-displacement curves for frames under FSICR capacity loading	72
5.2	Load-displacement curves for frames under IACS PC capacity loading . . . . .	72
5.3	Force-displacement curves for centred loaded frames, FSICR and IACS . . . . .	72
5.4	Distribution of U2 displacement at $U2_{max} = 168mm$ , for single and double frame with centred FSICR patch . . . . .	73
5.5	Distribution of U2 displacement at $U2_{max} = 168mm$ , for single and double frame with centred IACS PC patch . . . . .	73
5.6	Load-displacement curves for frames under FSICR capacity loading	76
5.7	Load-displacement curves for frames under IACS capacity loading	76
5.8	Force-displacement curves for frames under loading at the center line . . . . .	76
5.9	Distribution of U2 displacement at $U2_{max} = 168mm$ , for single and double frame with FSICR patch at the water line . . . . .	77
5.10	Distribution of U2 displacement at $U2_{max} = 168mm$ , for single and double frame with IACS patch at the water line . . . . .	77
5.11	Load-displacement curve of main model loaded with FSICR patch at water line and web frame #233 . . . . .	79
5.12	Load-displacement curve of main model loaded with IACS patch at water line and web frame #233 . . . . .	79
5.13	Load-displacement curve of main model loaded with IACS patch at water line and at frame #232½ . . . . .	79
5.14	Distribution of U2 displacement at $U2_{mac} = 285mm$ , FSICR patch	80
5.15	Distribution of U2 displacement at $U2 = 200mm$ , IACS PC patch	80
5.16	Distribution of U2 displacement for LC1 . . . . .	82
5.17	Load-displacement curve for LC1 . . . . .	83
5.18	Distribution of von Mises stress for LC1 . . . . .	83
5.19	Comparison of load-displacement curve from LC1 and LC2 . . .	85

---

---

5.20	Load-displacement curve from LC3 analysis . . . . .	86
5.21	Load-displacement curve from LC4 . . . . .	86
6.1	Transition from elastic to plastic region, from figure 5.2 . . . . .	89
6.2	Comparison of real damage and single and double frame from analysis . . . . .	90
6.3	Ship kinetic energy as function of velocity . . . . .	92
6.4	Comparison of figure 3.3 and analysis model . . . . .	95
6.5	Comparison of figure 3.5 and analysis model . . . . .	95
6.6	Comparison of figure 3.7 and analysis model . . . . .	95
6.7	Comparison of figure 3.8 and analysis model . . . . .	96
6.8	Comparison of figure 3.11 and analysis model . . . . .	96
6.9	Comparison of figure 3.12 and analysis model . . . . .	97
6.10	Comparison of photo and analysis model . . . . .	97
A.1	Shell expansion . . . . .	A2
A.2	Center Line . . . . .	A3
A.3	Fore peak tank top . . . . .	A4
A.4	No. 2 side stringer . . . . .	A5
A.5	No. 3 side stringer . . . . .	A6
A.6	No, 4 side stringer . . . . .	A7
A.7	Side longitudinal 4 . . . . .	A8
A.8	Side longitudinal 2 and 3 . . . . .	A9
A.9	Inner bottom . . . . .	A10
A.10	Longitudinal 4 and 8 . . . . .	A11
A.11	Web frame #227 . . . . .	A12
A.12	Web frame #230 . . . . .	A13
A.13	Web frame #233 . . . . .	A14
A.14	Web frame #237 . . . . .	A15
A.15	Web frame #241 . . . . .	A16

---



# Nomenclature

$A$	Cross section area	$[cm^2]$
$B$	Breadth	$[m]$
$b$	Ice patch height	$[m]$
$D$	Depth	$[m]$
$\varepsilon$	Strain	$[mm/mm]$
$F$	Force	$[N]$
$h$	Design ice height	$[m]$
$h_0$	Level ice thickness	$[m]$
$I$	Moment of inertia	$[mm^4]$
$LBP$	Length between perpendiculars	$[m]$
$LWL$	Length in water line	$[m]$
$M$	Bending moment	$[Nm]$
$m$	Boundary condition variable	$[-]$
$N$	Shear capacity	$[MPa]$
$p$	Ice pressure	$[MPa]$
$Q$	Line load	$[N/m]$
$s$	Frame spacing	$[m]$
$\sigma$	Stress	$[MPa]$
$T_{scant}$	Draught	$[m]$
$t$	Plate thickness	$[mm]$
$\tau$	Shear stress	$[MPa]$
$V_{max}$	Maximum service speed	$[kn]$
$w$	Ice patch width	$[m]$
$Z$	Section modulus	$[cm^3]$





# Chapter 1

## Introduction

The increase in interest for the Polar areas as transportation routes and source of oil and gas, demands knowledge about the harsh environment and how to design structures that can withstand the extreme loads. Investigation of damages that a structure has undergone can give indications about the load a structure has been exposed to, and thus be used as a basis for the development of structural designs and rules. This has been the practice when developing the Finnish-Swedish Ice Class Rules (FSICR), which today can be considered an “industry standard” for the design of ships for light ice conditions, [3]. This thesis is a case study of a DNV-GL classed cargo ship which met challenging conditions when sailing through the Northern Sea Route (NSR). Interaction with multi-year ice was reported, and when arriving at port, large deformations were seen at the port side of the ship, [4]. DNV-GL is interested in knowing what kind of load caused the damage, in order to assess whether or not rules and standards should be updated, and ships of similar construction upgraded.

The ship side deformations are estimated from photographs, and nonlinear element analyses carried out with different load cases in order to reproduce the estimated deformations. The load applied when obtaining a reproduction resembling the estimated deformations, gives indications about the characteristics of the original load.

This thesis has been composed throughout 20 weeks, time has therefore been the main limiting factor of the work. The main analysis model has been simplified and assumptions have been made on almost every part of the input. If more time were available analyses could have been run to verify the element size, the nonlinear material curves, boundary conditions, and load distribution and intensity. More focus would also have been given to finding a proper way to compare the loads

found with the design loads from the rules.

Photos of the deformations and a short description are the only available information, making it challenging to estimate the range, distribution, velocity, acceleration, magnitude, and duration of the actual load. Therefore the focus of this thesis is limited to a couple of these parameters: distribution and magnitude.

The aim of this thesis is to estimate the ice load that inflicted the hull damage to the case study ship. The work is divided into four main sections. The first section is a review of the FSICR, which are adopted by DNV-GL [1], and the International Association of Classification Societies' (IACS) Unified Requirements for Polar Class [2], for structural design of Polar ships. In the second section the photographs documenting the case study ship's hull damage are described thoroughly. Measurements of the deformations, from the photos, are also done. The third section deals with the modelling of finite element models, including discussion of material inputs, element meshing, boundary conditions, and load cases. The fourth and final section include the results from the finite element analyses, discussion of the results, and comparison of these results with the design load from the first section, and the deformations measured in the second section.

The vessel documents are applied anonymously within the production of this report.

## Chapter 2

# Rules for Structural Design of Polar Ships

Ice classes and rule requirements are made to confirm that maritime structures and facilities comply with the standards of the classification societies, as a safeguard to life, property and environment. Navigation in waters with ice conditions is associated with higher risk, therefore special class rules have been developed, e.g. DNV-GL's "Rules for Classification of Ships" Part 5, Chapter 1: "Ships for Navigation in Ice", [1]. In this chapter Section 3 "Ice Strengthening for the Northern Baltic" and Section 8 "Polar Class" are of interest when investigating the structural capacity of the ship studied in this thesis. Section 3 has been developed by the Finnish Transport Safety Agency (TRAFI) through cooperation between the Finnish and the Swedish Maritime Authorities. The rules are a requirement for all ships that will sail in the Bothnian Bay during the winter season and are thus referred to as "Ice Strengthening for the Northern Baltic" but is also known under the name "The Finnish-Swedish Ice Class Rules" (FSICR). The Polar Class is developed by the International Association of Classification Societies (IACS) as one of their unified requirements (UR). IACS are developing the UR for all of their member societies to incorporate in their own rules, with the goal of gaining consistency of the general philosophy on which the rules of the societies are established.

In the following, TRAFI's FSICR and IACS' Polar Class will be explained with regard to design ice pressure, and plating and framing requirements.

The ship considered in this case study is a cargo ship with a length over 100 *m* and ice class notation **ICE-1A**, and it is with this specific ship in mind the following rule explanation is done.

**Table 2.1:** Main particulars, [5]

<b>Class</b>	<b>ICE-1A</b>
<b>LBP</b>	220 <i>m</i>
<b>LWL</b>	225 <i>m</i>
<b>B</b>	32 <i>m</i>
<b>D</b>	20 <i>m</i>
<b>T<sub>scant</sub></b>	14 <i>m</i>
<b>V<sub>max</sub></b>	14.5 <i>kn</i>
<b>Min req. prop. power</b>	13300 <i>kW</i>

## 2.1 DNV-GL: “Ice Strengthening for the Northern Baltic”

In DNV-GL’s “Rules for Classification of Ships” Part 5, Chapter 1: “Ships for Navigation in Ice” [1], Section 3: “Ice Strengthening for the Northern Baltic” it is stated that “The requirements shall be regarded as supplementary to those given in assignment of main rules.” [1]. The main rules are found in Part 3 Chapter 1 “Hull Structural Design, Ships with Length 100 Metres and Above” [6]. In Section 3, A101, it is pointed out that the requirements “apply to vessels for service in the Northern Baltic in winter or areas with similar conditions”.

A large number of hull damages to ships sailing in the Baltic Sea led to the development of the Finnish-Swedish Ice Class Rules (FSICR). Common ice class rules were introduced in Finland and Sweden in 1971, TRAFI [7]. The Finnish-Swedish ice classes address ships which can operate independently and/or behind an ice breaker in ridged ice fields. These ships are also able to sail independently in opened fairways leading to ports. Vessels which operate without any assistance in the Baltic Sea requires Baltic ice class notation **1A Super** or higher and must fulfill propulsion power requirements.

The FSICR are adopted by DNV-GL and DNV-GL’s class **ICE-1A** is considered to be equal to the Finnish-Swedish ice class 1A. The dimensioning of the ship in the most ice prone areas is found from capacity calculations when applying a design ice load to the structure. The operation of an **ICE-1A** class ship is defined as “capable of navigation in difficult ice conditions, with the assistance of ice breakers when necessary”. Since the ship studied has the class notation **ICE-1A**, focus will be on this notation in the following. It is assumed that a ship of this class will be assisted by an ice breaker to avoid heavy ice jamming, which is stated in DNV-GL’s Hull Structural Rules Background notes [8]. For **ICE-1A** the level ice thickness is not to exceed  $h_0 = 0.80m$ , while the design ice thickness  $h = 0.30m$

and is “assumed to be only a fraction of the ice thickness”.

### 2.1.1 Design Ice Pressure

The design ice pressure is based on a nominal ice pressure of  $5600\text{ kN/m}^2$  and calculated from equation (2.1). The formula is derived from results of full scale measurements done by the Finnish-Swedish Winter Navigation Board, [8]. In DNV-GL’s “Development, Background, Motives” note values for the uniaxial crushing strength of ice is given. The value varies from  $1.5 - 3.0\text{ MPa}$  for first-year to multi year ice. To account for the fact that the ice is confined in the transverse direction, the values should be at least doubled, i.e.  $3.0 - 6.0\text{ MPa}$ . The standard value of  $5.6\text{ MPa}$  has been chosen for the first year ice conditions in the Baltic, and is thus utilized in the FSICR and adopted by DNV-GL’s **ICE**-rules.

$$p = 5600 \cdot c_d \cdot c_1 \cdot c_a \quad (2.1)$$

$c_d$  = a factor based on experience which takes into account the influence of the size and engine output of the ship. This because it was found that the damage frequency was higher for larger ships, background note [8]

$c_a$  = a factor which takes account of the probability that the full length of the area under consideration will be under pressure at the same time. In other words: regulates the reduction in design pressure with increasing size of the load area. Short load length are more probable than long ones [8]

$c_1$  = a factor that accounts for the design pressure occurring in a certain region of the hull for the ice class in question

Here  $c_d$  and  $c_a$  are constants calculated from the main specifications of the ship, while  $c_1$  is a class dependent constant.  $p$  has the unit  $\text{kN/m}^2$ .

### 2.1.2 Shell Plate Requirement

Figure 2.1 shows the extension of ice belt region for frames defined by TRAFI and adopted in DNV-GL’s rules, [1]. There are three main regions: the bow, the midbody, and the stern region. These are found as a fraction of the rule length in combination with the water line and center line. The extreme draughts the upper ice water line (UIWL) and the lower ice water line (LIWL) are also sketched in figure 2.1. The extent of ice strengthening is defined from the UIWL and LIWL.

In the damage case considered here, the damage is located in the bow region, above the lower ice water line (LIWL) and below the upper ice water level (UIWL).

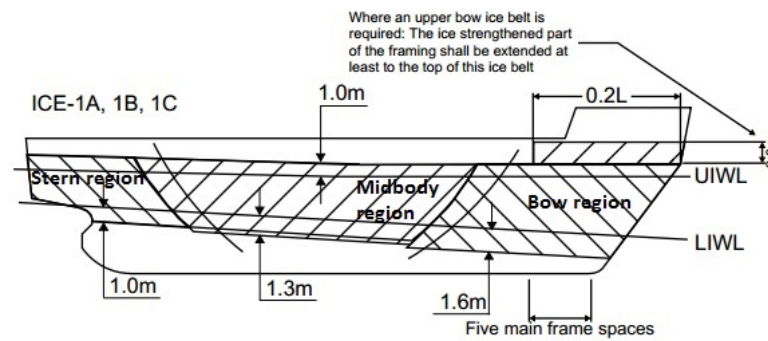


**Figure 2.1:** Ice belt regions, [1]

According to the rules for class notation **ICE-1A**, the vertical extension of ice strengthening of plating is not to be less than  $0.50m$  above UIWL anywhere along the ship, and not less than  $0.90m$  below LIWL in the bow area and not less than  $0.75m$  elsewhere.

The FSICR uses first yield as limit state, therefore only the elastic response of the structure needs to be derived, [3]. In its simplest form the stress for a plate strip is given as:

$$\sigma = \frac{M}{I} \cdot \frac{t}{2} \quad (2.2)$$

By inserting the second moment of inertia for a strip with unit width, and the moment including a boundary condition variable  $m$ , the equation becomes:

$$\sigma = \frac{6000 \cdot p \cdot s^2}{m \cdot t^2} \quad (2.3)$$

A factor of 1000 is included in the numerator since the DNV-GL rule dimension of the load  $p$  is  $kN/m^2$ . From this equation  $t$  is found:

$$t = 77.5 \cdot s \cdot \sqrt{\frac{p}{m \cdot \sigma}} \quad (2.4)$$

The bending moment factor  $m$  in the above equation is derived for decks under wheel loading in DNV-GL “Rules for Classification of Ships” Part 5, Chapter 2: “Passenger and Dry Cargo Ships”, Section 4: “General Cargo Carriers”, [9]. Figure 2.2 shows the curves of  $m$  as a function of  $x$  for four different cases of loading and boundary conditions.  $x$  is defined as  $x = b/s$  not greater than 1.0 for plates, or  $x = a/l$  for stiffeners.  $b$  is the extent of the load area perpendicular to the stiffeners,  $a$  is the extent of the load area parallel to the stiffeners,  $s$  is the

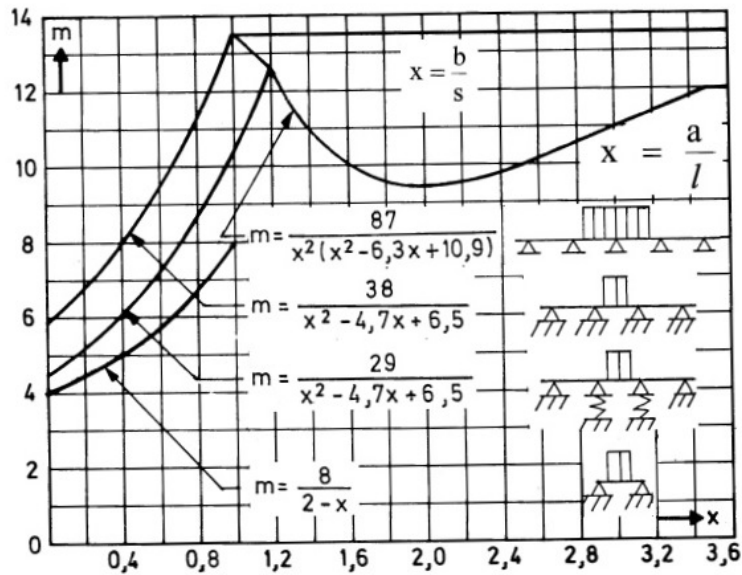


Figure 2.2: Bending moment factor ( $m$ -values), [9]

stiffener spacing, and  $l$  the stiffener span. The two upper boundary curves are valid for the plating.

“With uniform pressure on adjacent plate fields the boundary condition is assumed as fixed, and the  $m$ -factor at the ends will be 12, and at the midpoint 24.” When considering “a short ice load equal to the frame spacing (as this gives the highest ice pressure), we use  $m = 13.5$ ”, [8]. This is found from figure 2.2 by assuming  $s/l$  to be less than 0.4, and  $b = s$ . This is valid for transversely stiffened plating. Documentation of the development of the  $m$ -formulas haven’t been obtained, and it’s therefore hard to say anything about the background of the equations. However, the form of the equations, an integer divided by a polynomial, suggests these formulas have been found by regression of experiment data.  $m = 16$  indicates full plasticity by hinge mechanisms. In figure 2.2 14.5 is the highest value of  $m$ , indicating there being some limit to where the elastic part ends and where plastic theory should be applied.

$$t = 21.1 \cdot s \cdot \sqrt{\frac{p}{\sigma}} \quad (2.5)$$

In the DNV-GL rules, [1], the required plate thickness in  $mm$  for shell plating in the ice belt with transverse framing is given by equation (2.6).

$$t = 21.1s \sqrt{\frac{f_1 \cdot p_{PL}}{\sigma_F}} + t_c \quad (2.6)$$

$s$  = frame spacing

$f_1$  = a factor representing the load reduction due to redistribution to the adjacent plate fields

$p_{PL}$  = “75% of the mean ice pressure due to redistribution of pressure from plating to stiffeners/girders” [8]

$\sigma_F$  = yield stress of the material

$t_c$  = increment for abrasion and corrosion

In the DNV-GL rules, elastic theory is used for dimensioning of stiffener and girder strengthened plate fields subjected to lateral loads. However, the membrane effect and reserve strength of a plate after reaching the elastic limit have been considered when regarding the allowable stresses. [8]

DNV-GL’s rules follow the elastic theory, but makes conservative assumptions and compare the results to the limit for full plasticity:  $1.5 \cdot \sigma_y$ . This limit is found by combining an approximate approach with plate experiments, [8]. When a plate is loaded above the elastic limit, plastic hinges will occur. “Calculations show that the start and early development of the permanent deflection is entirely due to the edge hinges, and this continues until complete plastic hinges are formed. Beyond this point, elastic-plastic theory is no longer valid, and the deflection and permanent set will further increase with the plastic membrane formation.” “With loading and deflection above the elastic limit, the plate develops plastic hinges, firstly along the edges and finally in the middle, then developing into a fully plastic membrane for which the rupture load is very large. This extreme level of load may be relevant in some special case, such as for ice breakers and for protection against blast or collision.” [8].

### 2.1.3 Requirement for Frames

The rules state that the vertical extension of the ice strengthening of the framing of **ICE-1A** classed ships shall be at least  $1.0m$  above UIWL, at least  $1.6m$  below LIWL in the bow region, at least  $1.3m$  below LIWL in the midship region, and at least  $1.0m$  below LIWL in the stern.

The rules provide formulae for calculation of section modulus of longitudinal and transverse frames, and the effective shear area. Since the case study ship has transverse frames the focus will be on this design.

The bending stress equation can be expressed in terms of section modulus as equation (2.7).

$$\sigma = \frac{M}{Z} \quad (2.7)$$



By rearranging and inserting the bending moment:

$$Z = \frac{M}{\sigma} \quad (2.8)$$

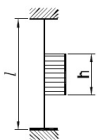
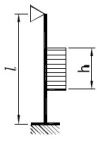
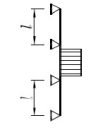
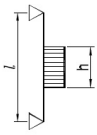
$$Z = \frac{p \cdot s \cdot h \cdot l}{m \cdot \sigma} \quad (2.9)$$

$h$  is the height of the ice load area and  $l$  is the stiffener span. As for the plate thickness the load is given as  $kN/m^2$ .

$$Z = \frac{p \cdot s \cdot h \cdot l}{m_t \cdot \sigma_F} \cdot 10^3 \quad (2.10)$$

$Z$  has the unit  $cm^3$ .

$m_t$  is the bending moment factor covering the boundary conditions of the stiffener, and is a function of  $h$ ,  $l$ , and  $m_0$ . The values of  $m_0$  for different boundary conditions are given in figure 2.3. For the damaged plate field in the studied incident the case described as “Continuous frames between several decks or stringers” fits the geometry best of the alternatives.

Boundary condition	$m_0$	Example
	7	Frames in a bulk carrier with top wing tanks
	6	Frames extending from the tank top to a single deck
	5.7	Continuous frames between several decks or stringers
	5	Frames extending between two decks only

**Figure 2.3:** Values of  $m_0$ , [1]

The effective shear area is derived from the equation of shear stress in the frame web, equation (2.11), and the equation for yield shear stress, equation (2.12), Kendrick and Daley [10]. Here a symmetric load is assumed.

$$\tau = \frac{p \cdot h \cdot s}{2 \cdot A_w} \quad (2.11)$$

$$\tau_y = \frac{\sigma_F}{\sqrt{3}} \quad (2.12)$$

To find the minimum allowable web area,  $A_0$ , the shear stress under design load is set equal to the yield shear stress:

$$\tau_y = \frac{p \cdot h \cdot s}{2 \cdot A_0} = \frac{\sigma_F}{\sqrt{3}} \quad (2.13)$$

Solving for the web area gives the effective shear area as written in the rules:

$$A_0 = \frac{\sqrt{3} \cdot p \cdot h \cdot s}{2 \cdot \sigma_F} = \frac{8.7 \cdot f_3 \cdot p \cdot h \cdot s}{\sigma_F} \quad (2.14)$$

$f_3$  = a factor which takes into account the maximum shear force versus the location and shear stress distribution, to be taken as 1.2

The shear area has the unit  $cm^2$ .

#### 2.1.4 Ice Stringer Requirements

The equation for the section modulus for the ice stringers is derived in the same order as for the frames, but here  $l$  is the length of both the patch and the stringer.  $h$  is still the height of the ice load.

$$Z = \frac{f_6 \cdot f_7 \cdot p \cdot h \cdot l^2}{m_1 \cdot \sigma_F} \cdot 10^3 \quad (2.15)$$

$m_1$  = boundary condition factor

$f_6$  = factor which takes into account the distribution of load to transverse frames, to be taken as 0.9

$f_7$  = factor of stringers, to be taken as 1.8

The unit of  $Z$  is  $cm^3$ .

The shear area for ice stringers is basically the same as for the transverse frames, only the stringer length is included instead of the stiffener spacing.

$$A = \frac{8.7 \cdot f_6 \cdot f_7 \cdot f_8 \cdot p \cdot h \cdot l}{\sigma_F} \quad (2.16)$$

$f_8$  = factor that takes into account the maximum shear force versus load location and the shear distribution, to be taken equal to 1.2.

The dimension of  $A$  is  $cm^2$

### 2.1.5 Requirements for Web Frames

In the FSICR background notes, [8], it is stated that “web frames are to be constructed in such a way that the bending stress and the shear stress do not exceed the values  $\sigma_y$  and  $0.58\sigma_y$ , respectively, when the load is located on any point of the web frame within the ice belt.” No further explanation is given to the values. In the rule derivation the point is chosen to inflict maximum bending and shear stress in the web frame in any load condition.

Ice stringers will transfer a design load to the web frames calculated from:

$$F = f_{12} \cdot p \cdot h \cdot s \quad (2.17)$$

$p$  is ice pressure,  $h$  is the height of the load area, and  $s$  the web frame spacing. The equation gives thus the total force an ice load  $p$  inflicts on an area of load height  $h$  and load width  $s$ .  $f_{12}$  is a web frame factor which accounts for the actual transferred load from stringer to web frame, to be taken as 1.8.

Following the formulae of bending moment capacity and shear capacity interaction is given:

$$M = M_p \sqrt{1 - \left(\frac{N}{N_p}\right)} \quad (2.18)$$

Where  $M$  is the moment capacity and  $N$  is the shear capacity. By inserting the formulas for moment and shear, and solving for the section modulus the rule equation for the web frame section modulus is gained, equation (2.19).

$$Z = \frac{M}{\sigma_F} \sqrt{\frac{1}{1 - \left(\gamma \frac{A}{A_a}\right)^2}} 10^3 \quad (2.19)$$

$M$  = maximum calculated bending moment under load calculated in equation (2.17).  $M = 0.193 \cdot F \cdot l$

$\gamma$  = factor dependent of the ratio  $A_f/A_w$

$A_f$  = cross sectional area of free flange

$A_w$  = actual effective cross section area of web plate

$A$  = required shear area, defined by equation (2.20)

$A_a$  = actual cross section area of web frame,  $A_f + A_w$

Equation (2.19) is the general equation for the section modulus with a reduction factor based on the required shear area. The unit is  $cm^3$ .

The formula for the shear area of a web frame is derived in the same order as equation (2.14) but here the load is based on the design load  $F$  from equation (2.17).

$$A = \frac{\sqrt{3} \cdot \alpha \cdot f_{13} \cdot Q}{\sigma_F} = \frac{17.3 \cdot \alpha \cdot f_{13} \cdot Q}{\sigma_F} \quad (2.20)$$

$Q$  = maximum calculated shear force under the load calculated in equation (2.17).

$f_{13}$  = factor that takes into account the shear force distribution, to be taken as 1.1

$\alpha$  = factor dependent of the ratio  $A_f/A_w$

$A$  has the dimension  $cm^2$ .

## 2.2 IACS: “Requirements Concerning Polar Class”

The International Association of Classification Societies (IACS) has published what they call “unified requirements” which are “adopted resolutions on matters directly connected to or covered by specific Rule requirements and practices of classification societies and the general philosophy on which the rules and practices of classification societies are established”. One of these is the “UR I, Polar Class” which “apply to ships constructed of steel and intended for navigation in ice-infested polar waters, except ice breakers”. As for the FSICR the UR rules are in addition to the open water requirements.

The unified requirements for Polar Ship construction is made to provide a common rule set for all the member societies. The Polar Class (PC) is as described in table 2.2

The Polar Class rule is adopted by DNV-GL in their rules meaning e.g. DNV-GL class **ICE-1A** can be set equal to Polar Class **PC-7** [1], Section 8, provided that the engine power requirement is fulfilled. This is strictly one way equivalent.

Kendrick and Daley, [10], argues the use of plastic ship design:

- “Using plastic design can help ensure a better balance of material distribution to resist design and extreme loads. This is particularly important because extreme ice loads can be considerably in excess of design values. This is more likely for ice loads than (for example) for wave loadings. The use of plastic methods ensures a considerable strength reserve, which may or may not be the case with elastic design.”

**Table 2.2:** Polar Class [11]

<b>Polar Class</b>	<b>General description</b>
<b>PC-1</b>	Year-round operation in all ice-covered waters
<b>PC-2</b>	Year-round operation in moderate multi-year ice conditions
<b>PC-3</b>	Year-round operation in second-year ice which may include old ice inclusions
<b>PC-4</b>	Year-round operation in thick first-year ice which may include old ice inclusions
<b>PC-5</b>	Year-round operation in medium first-year ice which may include old ice inclusions
<b>PC-6</b>	Summer/autumn operation in medium first-year ice which may include old ice inclusions
<b>PC-7</b>	Summer operation in thin first-year ice which may include old ice inclusions

- “Plastic design can allow considerably lighter structure, particularly when the return period for design loads is relatively long and when cumulative damage (deformation, fatigue cracking, etc.) is not a major consideration.”
- “Plastic design methods are more applicable to damage analysis, which will allow the assumptions in the URs to be tested against experience and refined in future as necessary.”

The derivation of the UR PC is based on energy methods: the balance between internal and external work under the proposed load models. It should be noted that strain and deflection predictions can’t be predicted from these methods.

### 2.2.1 Design Ice Load

The design ice load which IACS use is derived from a design scenario: a glancing collision between the ship side and an ice edge, [12]. The load is derived from equating the kinetic energy from the ship at speed, and the energy used for crushing the ice. The derivation is done in three steps: “First the total load is found as the minimum of the crushing and flexural limiting loads for the design ice. Second, the patch over which this load is applied is determined and idealized. Third, the distribution of load within the patch is modified to account for local loading peaks.” Variables which are accounted for in the derivation are the ice thickness, ice strength, hull form, ship size and ship speed.

The collision scenario which the design ice load for plating and framing design is based on is an impact between ice and the shoulder of the ship’s bow, while the ship is heading forward at design speed. In the derivation Daley assumes the ship speed, ice thickness, and ice strength to be class dependent, [12]. Since the ice crushing force can’t exceed the force required to fail the ice in bending the ice crushing is the limiting failure mode and will thus define the design ice force through the equality in normal kinetic energy and energy used to crush the ice, see equation (2.21). The right hand side gives the kinetic energy in terms of ship mass and velocity, the left hand side gives the crushing energy in terms of integration of the normal force over the penetration depth.

$$\frac{1}{2}M_e \cdot V_n^2 = \int_0^\delta F_n(\delta) \cdot d\delta \quad (2.21)$$

Figure 2.4 shows the design scenario: a ship moving forward into ice which will crush in a certain contact area and break due to bending at some distance from the contact area. The derivation of the design load is valid for the bow area only but corresponding loads can be found for the rest of the hull by the use of empirical hull area factors.

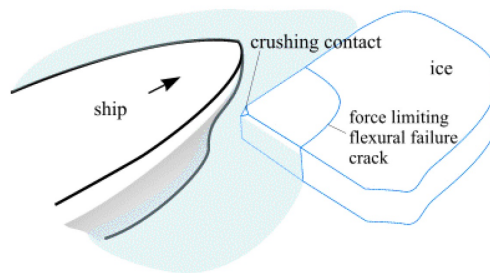


**Figure 2.4:** Design scenario - flexural failure during glancing collision, [12]

Daley uses a collision model called “Popov” when deriving the load from the oblique ice-bow interaction. The normal ice load is found through a complex equation accounting for ice pressure, ice edge opening angle, normal frame angle, ship mass and velocity. When equating the kinetic energy and the energy used to crush the ice, and solving for the force, the force equation will only account for the crushing interaction. But we’re interested in the flexural force as well. The limiting flexural force equation is dependent on the ice thickness, the flexural strength of the ice, and the normal (true) frame angle.

Whether the ice fails due to crushing or bending depends on the ice quality, frame angle, water line angle, velocity, mass, ship length, pressure, and where on the

ship the collision is located. Daley proposes an angle factor,  $f_a$  which takes the above variables into consideration and accounts for the two types of failure, and gives a limiting maximum value for the crushing failure to avoid extreme values. Equation (2.22) gives the design ice force deduced from equation (2.21).  $P_o$  is the class dependent ice pressure at  $1m^2$ .

$$F_n = f_a \cdot P_o^{36} \cdot \Delta_{ship}^{64} \cdot V_{ship}^{1.28} \quad (2.22)$$

The combination of crushing and flexural force is shown in figure 2.5. Daley states that the crushing force tends to drop with increasing distance from the bow, while the flexural force tends to rise with increasing distance. The intersection of the curves defines the maximum force value. “The circle represents the peak force (the design force) and its location.”

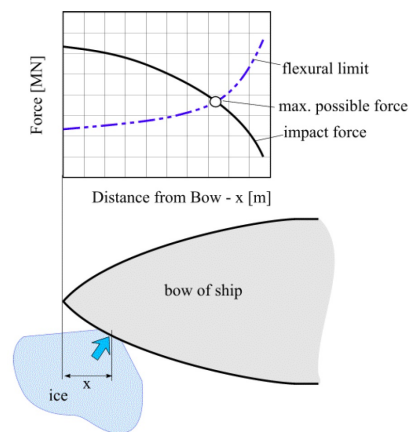


**Figure 2.5:** Combination of crushing and flexural forces over the bow of a ship (example), [12]

The design load patch, to which the design ice load will be applied, is derived from the relationship between the design force and the class dependent ice pressure as the nominal contact area. This area is used to deduce the patch height and width. From the force and the patch dimensions the line load and pressure can be derived. Figure 2.6 shows the configuration of the ice patch load.  $w$  is the patch width,  $b$  the patch height, and  $p$  the ice pressure.

In the rules for the Polar Class, [2], equation (2.22) is simplified by inserting factors for the class dependent physical parameters: crushing class factor, flexural class factor, or patch class factor. This results in the rule force, equation (2.23), for the bow region.

$$F_n = f_a \cdot C F_C \cdot \Delta_{ship}^{64} \quad (2.23)$$

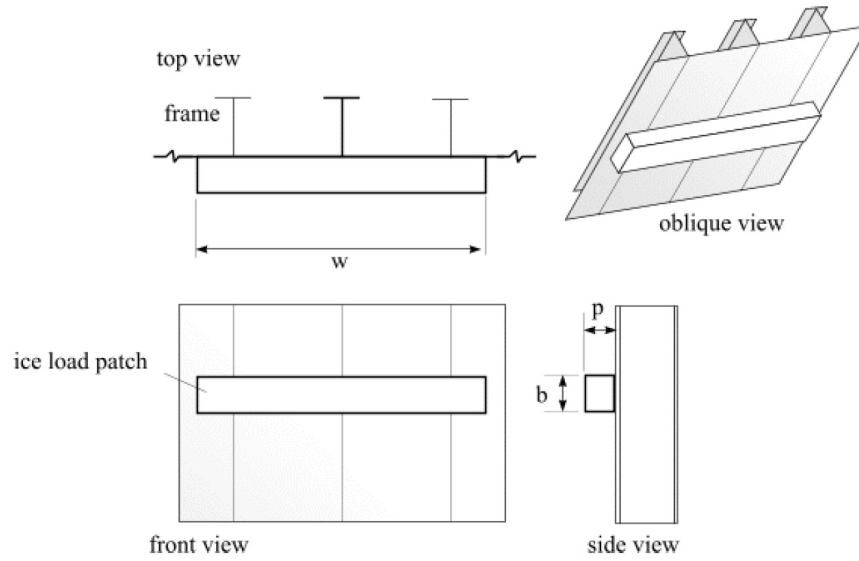


**Figure 2.6:** Ice load patch configuration, [12]

Here  $CF_C$  is the crushing class factor. When developing a design for an ice class ship in accordance with the Polar Class, equation (2.23) shall be calculated for several locations around the bow to ensure that the peak values of the force, line load, and pressure are found. The line load is expressed as:

$$Q = F_n^{0.61} \cdot \frac{CF_D}{AR^{0.35}} \quad (2.24)$$

where  $CF_D$  is the “load patch dimension class factor” and  $AR$  is the load patch aspect ratio. From these values the “conservative load patch” can be found, see equation (2.25) and (2.26).

$$w_{bow} = \frac{F_{max}}{Q_{max}} \quad (2.25)$$

$$b_{bow} = \frac{Q_{max}}{p_{max}} \quad (2.26)$$

$Q$  is the line load. From this the average pressure within the load patch can be found from equation (2.27).

$$P_{avg} = \frac{F}{b \cdot w} \quad (2.27)$$

The focus area of the above derivations has been the bow since the bow is the area of interest in this thesis. Formulas for the non-bow regions can be found in the rules [2].



## 2.2.2 Shell Plate Requirements

The plating and framing requirements proposed by IACS are based on plastic response criteria, [13]. Daley et al. argues that extreme ice loads can be considerably in excess of design values, and is more likely for ice loads than e.g. wave loads. By using plastic methods for deriving scantling requirements a considerable strength reserve is ensured. This may not be the case for elastic methods.

In elastic methods the yield point is used as limit state for the design. For plastic methods there are several alternatives for limit states, from yield until fracture. In the derivation of the UR the onset of idealized plastic collapse mechanisms are used as design limit state. E.g. membrane stresses and strain hardening have been neglected in the derivations for the design scantlings to be on the conservative side.

The minimum plate thickness requirement is derived from the plastic hinge collapse of a general plate, see figure 2.7, by setting the internal work of the system of hinges equal to the external work, respectively equation (2.28) and (2.29).

$$T = -FY \cdot t^2 \cdot \frac{f}{2} \left( \frac{0.5S}{n} + \frac{m}{S} \right) \quad (2.28)$$

$$V = \int_F p_u \cdot W(x, y) d\delta \quad (2.29)$$

$FY$  = yield stress

$t$  = plate thickness

$f$  = nominal displacement

$S$  = stiffener spacing

$m, n$  = hinge location parameters

$p_u$  = nominal collapse pressure

$W(x, y) = f \cdot \phi(x, y)$  = plate deflection in a point with coordinates  $(x, y)$

$F$  = area of plate assumed deflected from its initial shape

$b$  = load height

By manipulating and combining the equations the result is a nonlinear system. Numerical techniques are used to find that in general  $m$ , the failure area length, is equal to the load height  $b$ . After some rewriting the plate thickness becomes equation (2.30)

$$t = 0.5 \cdot S \sqrt{\frac{p}{FY}} \cdot \frac{1}{1 + \frac{0.5S}{b}} = 500 \cdot s \sqrt{\frac{p}{\sigma_y}} \cdot \frac{1}{1 + \frac{0.5s}{b}} \quad (2.30)$$

In the rules  $p$  is expressed as the product of a hull area factor, a peak pressure factor, and the average patch pressure. In this way it accounts for the fact that an

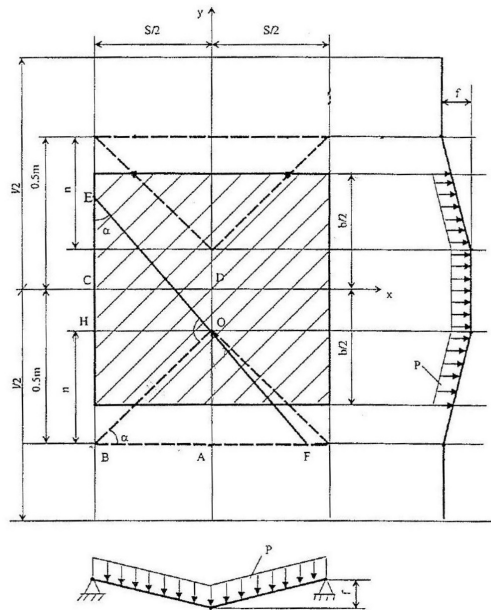


**Figure 2.7:** General formulation of collapse state, [13]

ice load consists of areas of higher, concentrated pressure, and that different hull areas are associated with different relative load magnitudes, [2].

### 2.2.3 Requirements for Framing

In order to derive framing requirements from the energy method, some plastic mechanisms must be assessed. The purpose is to find the mechanism that gives the lowest capacity of the structure, i.e. the capacity most similar to the true capacity. The energy method assumes elastic/perfectly plastic materials and does not include conservative contributions as strain hardening or membrane effects. Three mechanisms are used for the derivation:

- a) a pure bending hinge
- b) a combined shear/bending hinge
- c) a shear hinge

The above listed mechanisms are illustrated in figure 2.8. The pure bending hinge comes from an ice load applied midspan of a frame. Having the load concentrated towards one of the ends of the frame gives the combined shear/bending hinge where the dominating mechanism depends on the type of load and frame cross section. The shear hinge is the result of a centered ice load and leads to plastic

web collapse.

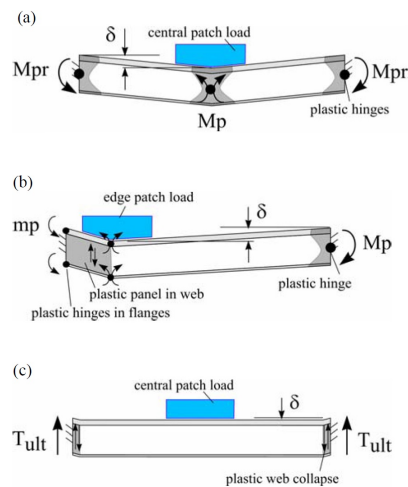


**Figure 2.8:** The three limit states considered for frames, [14]

In the UR much concern is given to the capacity of a frame under combined shear and moment loading. The presence of one of the above loads will reduce the capacity of the other load. Figure 2.9 shows the diagram for bending/shear interaction for two different cross sections. In the UR the only the web is assumed to contribute to shear capacity. When all of the web shear capacity is utilized only capacity from the free flange is left to withstand bending moment. Hence, a stiffener without a free flange will not have any moment capacity after being fully shear loaded. In pure bending the interaction with shear won't be a problem.

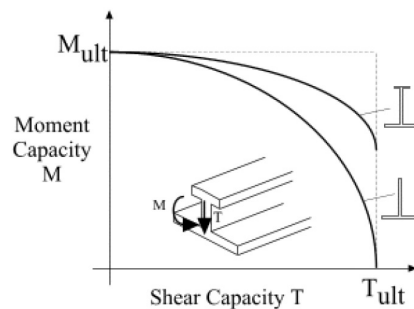


**Figure 2.9:** Bending/shear interaction diagram, [10]

The derivations of the frame requirements given in the IACS rules are not all straight forward. Kendrick and Daley [10] presents a summary of the procedure. For the symmetric load case:

1. Define the minimum web area required to carry the load in pure shear

$$A_0 = \frac{1}{2} P \cdot b \cdot S \cdot \frac{\sqrt{3}}{\sigma_y} \quad (2.31)$$

2. Develop the energy balance equation for external and internal work

$$(P \cdot b \cdot S) \left(1 - \frac{b}{2 \cdot L}\right) = 4 \cdot \frac{\sigma_y}{L} \cdot \left(Z_p + \frac{j}{2} \cdot Z_{pr}\right) \quad (2.32)$$

3. Establish the full section modulus,  $Z_p$ , for the center hinge

$$Z_p = Af \cdot \left(\frac{tf}{2} + hw + \frac{tp}{2}\right) + Aw \cdot \left(\frac{hw}{2} + \frac{tp}{2}\right) \quad (2.33)$$

4. Establish the reduced section modulus,  $Z_{pr}$  for the end hinges, including the section shape dependency effect

$$Z_{pr} = Z_p \cdot \left[1 - kw \cdot \left[1 - \sqrt{1 - \left(\frac{A_0}{Aw}\right)^2}\right]\right] \quad (2.34)$$

where

$$kw = \frac{1}{1 + 2 \cdot \frac{Af}{Aw}} \quad (2.35)$$

The rule requirement for section modulus can now be found from equation (2.33, 2.34, 2.35):

$$Z_p = \frac{P \cdot b \cdot S \cdot L}{4 \cdot \sigma_y} \left(1 - \frac{b}{2 \cdot L}\right) \cdot \frac{1}{2 + kw \left[\sqrt{1 - \left(\frac{A_0}{Aw}\right)^2} - 1\right]} \quad (2.36)$$

In some cases the asymmetric loading case will dominate the frame capacity requirements. For fully developed hinges the configuration is basically the same as for the centered load discussed above, but the process of getting there can be quite different. With a centered load the three hinges will form simultaneously, as for the end loading a shear hinge will develop at the end closest to the load at a much lower load level than for a bending hinge in the other end. This can result in a significantly higher local plastic strain than experienced in a centered load case.

The derivation of the rule requirements for the asymmetric load case is summarized as follows, [10]:

1. Balance the internal and external work

$$(P \cdot b \cdot S) \left(1 - \frac{b}{2 \cdot L}\right) = \sigma_y \cdot \left[ \frac{Aw}{\sqrt{3}} + \frac{Z_p}{L} \cdot fz \right] \quad (2.37)$$

where  $fz$  can be approximated as:

$$fz = 1.1 + 5.75 \cdot kz^{0.7} \quad (2.38)$$

and  $kz$  is the ratio of the combined flange moduli to the total section modulus:

$$kz = \frac{z_p}{Z_p} \quad (2.39)$$

The rule requirement is found by combining the above equations.

$$Z_p = \frac{P \cdot b \cdot S \cdot L}{\sigma_y \cdot (1.1 + 5.75 \cdot kz^{0.7})} \left(1 - \frac{b}{2 \cdot L}\right) \cdot \left[1 - \frac{Aw}{2 \cdot A_0 \left(1 - \frac{b}{2 \cdot L}\right)}\right] \quad (2.40)$$

Rewriting:

$$Z_p = \frac{P \cdot b \cdot S \cdot L}{4 \cdot \sigma_y} \left(1 - \frac{b}{2 \cdot L}\right) \cdot A_1 \quad (2.41)$$

Equation (2.41) is on the same form as the requirement equation given in the rules [2].  $A_1$  is dependent of the type of loading, either center or end. The area in the rules, which the actual net effective shear area is required to be greater than, is the same as equation (2.31). The pressure is to be taken as calculated in section (2.2.1) and scaled with respect to hull area and peak pressure.

The patch load for web frames and load-carrying stringers is to be applied at locations where the capacity of these members under the combined effects of bending and shear is minimized.

Web frames and load-carrying stringers are to be dimensioned such that the combined effects of shear and bending do not exceed the limit state(s) defined by the society.



# Chapter 3

## Description of Ship Side Damage

The ship studied in this thesis is a DNV-GL registered cargo ship. During one journey through the Northern Sea Route (NSR), the ship got a damage to the port side shell in the area of the fore peak tank after interaction with ice. Extensive deformation of the shell, frames, ice stringers, and web frames was reported by the surveyor assessing the damage. In order to make an assessment of the material strength and capacity for the estimation of the ice load, knowing the exact deformations in the structure in the affected area is related to the strength, capacity, and load calculations.

The surveyor report involved in this case was available but no detailed information was given since a surveyor would make an assessment of the measures necessary to repair the ship, and give no more details. In this case the deformations were of such severity that a replacement of a considerable area of the hull structure had to be done.

About 30 photographs from the survey are available. Due to the lack of detailed information about the deformations, the photos are used for estimating the buckling, tripping, and fracturing of the structural components.

### 3.1 Description of External Damage

The ice damage is located at the port side in the vicinity of the fore peak tank, see figure 3.1. In this area the hull is strengthened by transverse frames, web frames, and stringers. The collision bulk head provides transverse strength aft of the damage, web frame #241 provides transverse strength fore of the damage. The

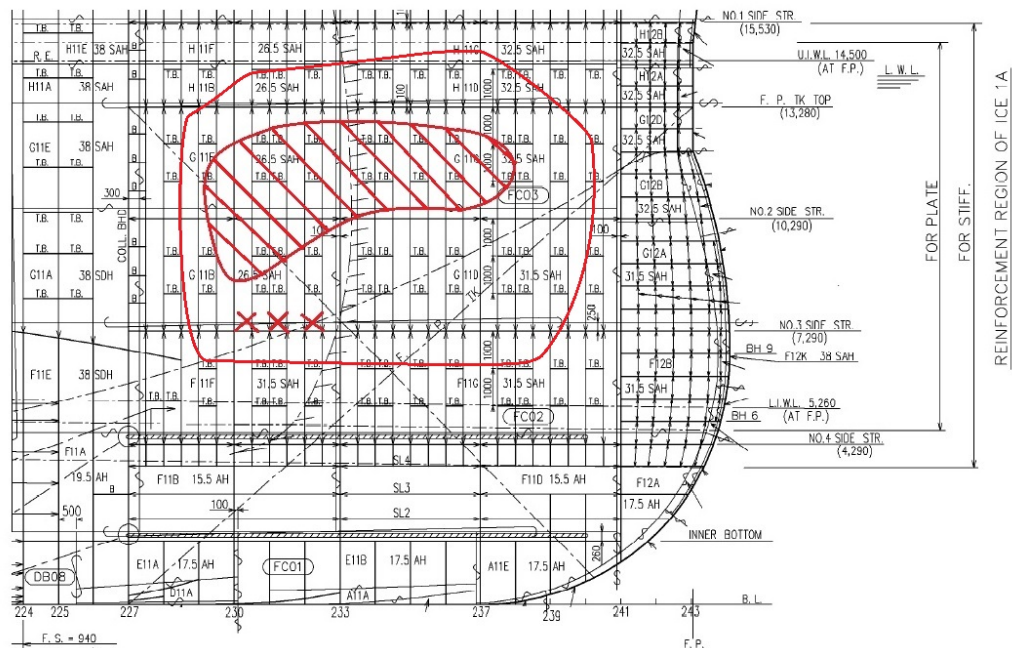


**Figure 3.1:** Shell expansion with damage area sketched, [5]

3<sup>rd</sup> side stringer gives additional strength longitudinally. The fore peak tank top supports the transverse structures. See figure A.3 to A.14 in appendix A.

The deformations are mainly limited to the area between bulk head #227 and #241, in between the 4<sup>th</sup> side stringer and the fore peak tank top, while the most severe damage is located in web frames #230, #233, and #237 and the area in between. It is reported that the collision bulkhead #227 is not affected. In figure 3.1 the general damage area is circled by a red line, while the most affected area with extensive deformations is shaded.

In figure 3.2, photo of the port side from the outside, the damage is visible as a dent with a length of about 9.4m and height of about 4.5m, located around web frame #233. The hull coating has been torn off in several places. Between #230 and #237, and along the fore peak tank top, the main part of the coating is completely removed. The same goes for the #230 web frame and its junction with the 2<sup>nd</sup> side stringer. On #229, #229½, #232½, and #237 the coating has also been torn off. Shallow scratches can be seen along the skin from #227 all the way to #241.

Table 3.1 gives the estimated maximum inwards displacement of web frame #230 and #233, measured from photo 3.3. Due to the uncertainties connected to measurements from a photograph two values are found for each frame, one maximum and one minimum value. The mean of these values are calculated. Subjective



gradings of each measurement have been done. The grading scale has three values: poor, OK, good. Poor is given to measurements which are hard to define due to e.g. rough photo resolution or the lack of a sufficient component to scale by. Good is given to a measurement thought to be close to the real deformation. Structure deforming towards the center line or forward are considered as positive. Deformations in the aft direction is considered to be negative.

**Table 3.1:** Displacement of web frames measured from figure 3.3

<b>Frame #</b>	<b>Span <i>mm</i></b>	<b>Scale <i>mm</i></b>	<b>Range <i>mm</i></b>	<b>Mean disp. <i>mm</i></b>	<b>Quality</b>
230	2990	1:27	±34	199	O.K.
232 ½	2990	1:31	±39	168	O.K.
233	2990	1:33	±67	285	O.K.

## 3.2 Description of Internal Damage, An Overview

Figure 3.4 and 3.5 shows the damaged area from inside the fore peak tank. The first photo shows large deformations in the plating between the 2<sup>nd</sup> side stringer and the fore peak tank top. The area where the coating has peeled due to the deformation of the steel has a shape similar to shaded area drawn by the surveyor in figure 3.1. The 2<sup>nd</sup> side stringer is clearly deformed close to the web frames. The web frames are buckles, especially web frame #230. This is most evident in figure 3.5.

In the following the state of the different structural components, plates, frames, web frames, stringers, decks and details, have been tried described from aft to fore of the damage area.

### 3.3 Inwards Deformation of Plates and Frames

Figure 3.6 shows parts web frames #227 and #230 and the frames in between. The buckle at the top of frames #228½ to #229½ and the cracked painting disclose the inwards bending of the hull plating. Unfortunately, the angle from where the photo is taken makes it difficult to estimate any values for the displacements.

The next descriptive photo, photo 3.7 shows frame #231 to #232½, web frame #233, the 2<sup>nd</sup> side stringer, and the fore peak tank top. The skin is bent inwards, which can be seen from the curve of the skin-to-frame welds. The frame flanges have displaced forward, and are twisted relative to the frame web. The webs are heavily bent forward, clearly seen from the cracked coating. Frame #232½ has been bent so that the weld connecting the top tripping bracket to the frame web has fractured. Local deformations at the upper frame brackets are seen as buckling, coming from both the bracket and frame being forced inwards and forwards. On the stringer the painting has cracked in vertical lines which can indicate an inward force perpendicular to the stringer. When assessing the stringer with a ruler the stringer appears to be slightly bent, but this can merely be a result of camera properties as a wide angle lens.

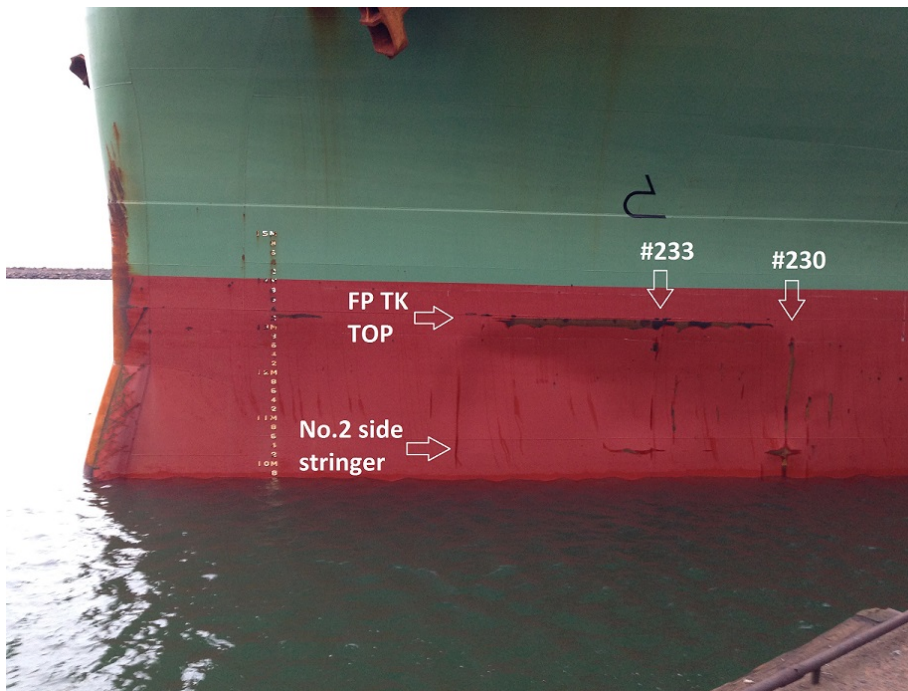
The plate deformation was measured by using the vertical paint cracks on the 2<sup>nd</sup> side stringer as guide lines, assuming these to be parallel to the original shape of the skin. Table 3.2 gives the measured plate deformations.

**Table 3.2:** Displacement of hull plate measured from figure 3.7

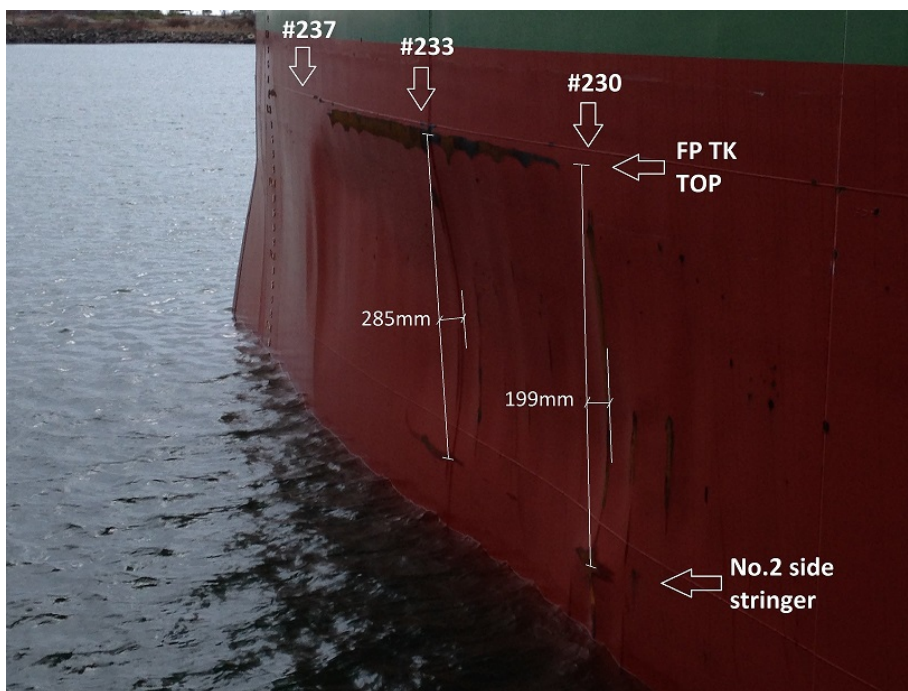
Frame #	Span	Scale <i>mm</i>	Range <i>mm</i>	Mean disp. <i>mm</i>	Quality
232	2990	1:19	±24	62	Poor
232½	2990	1:11	±24	162	Poor
233	2990	1:11	±35	85	Poor

Photo 3.8 shows the same as photo 3.7, but here more of the lower structure is visible. The inwards buckle of the plate was again measured by drawing straight lines from the top plate/frame web/tank top corner to the bottom edge of the weld between plate and frame web. The results are displayed in table 3.3.

Only pieces of the lower hull structure in the damage area i.e. over the 3<sup>rd</sup> side stringer and below the 2<sup>nd</sup> side stringer, are visible in the photos; figures 3.12, 3.14, 3.13. Hence haven't any estimates of the hull deformation been done for this area.



**Figure 3.2:** Port side indent, [5]



**Figure 3.3:** Port side indent, [5]



**Figure 3.4:** Indent seen from inside fore peak tank, [5]

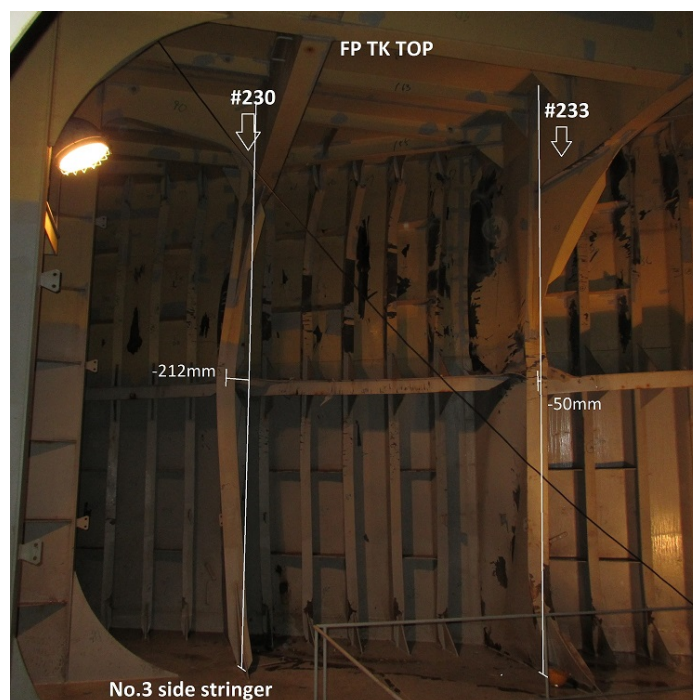


**Figure 3.5:** Indent seen from inside fore peak tank, [5]

Frame #	Span <i>mm</i>	Scale <i>mm</i>	Range <i>mm</i>	Mean disp. <i>mm</i>	Quality
232	2990	1:25	±13	100	O.K.
232½	2990	1:19	±10	86	O.K.
233	2990	1:19	±10	133	O.K.

**Table 3.3:** Displacement of hull plate measured from figure 3.8

### 3.4 Tripping of Frames

To simplify the assessment of the deformations the force from the ice load have been assumed to act perpendicular to the skin. The frames are welded to the skin at an angle of about  $52^\circ$ . Figure 3.10 shows how the frames are oriented relative to the skin. The dashed line is the 2<sup>nd</sup> side stringer. This construction forces the frames to bend forward when the skin is buckled inwards. Thus will there be a new angle to the flange, which is not accounted for in the measurements in table 3.4.

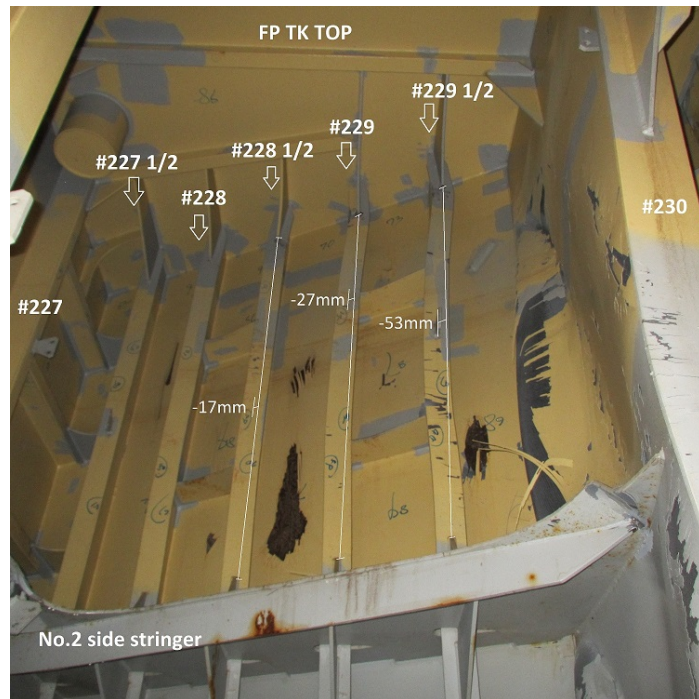
Figure 3.6 displays web frame #227 to #230, and from the 2<sup>nd</sup> side stinger to the fore peak tank top. The frames are deformed, easiest seen at the top of the frames. The webs are not visible but the flanges are almost normal to the camera and an approximate offset was measured. If one assumes that the brackets at the ends of the frames have their original position and not undergone any significant deformations, it is possible to measure the displacement of the frame. This was done by drawing a straight line from the top to the bottom bracket and measure how much the flange center had shifted relative to the bracket-bracket line. Only the maximum displacement of the flange is considered for each frame. The measurement was scaled using the width of the flange. The deformation measured is assumed to be the flange's forward displacement resulting from the shell's buckling towards the center line. This is also known as tripping.

Table 3.4 shows the forward flange displacement measured from the photo. No apparent displacement was found at frame#228.

**Table 3.4:** Displacement of frame flanges measured from photo 3.6

Frame #	Span <i>mm</i>	Scale <i>mm</i>	Range <i>mm</i>	Mean disp. <i>mm</i>	Quality
228½	2990	1:17	±9	-17	O.K.
229	2990	1:18	±9	-27	O.K.
229½	2990	1:17	±9	-53	O.K.

By assuming the relative tripping of the frame flange to be equal to the inwards buckling of the hull, the results from table 3.4 can be interpreted as estimates of



**Figure 3.6:** Deformation of plates and frames #227 - #230, [5]

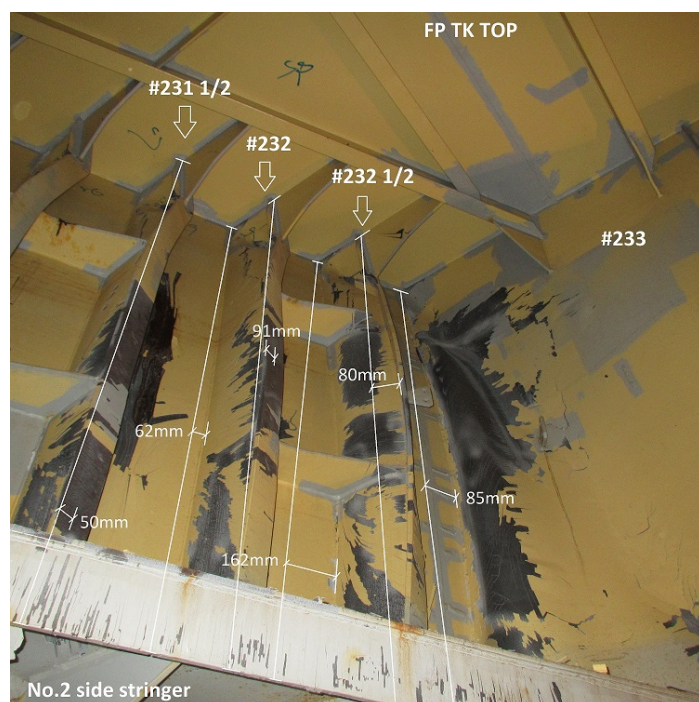


**Figure 3.7:** Deformation of plates and frames #231 - #233, [5]



**Figure 3.8:** Deformation of plates and frames #230 - #233, [5]



**Figure 3.9:** Deformation of plates and frames #233 - #235, [5]

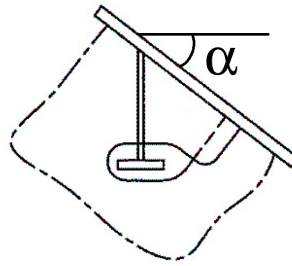


**Figure 3.10:** Frame detail, [15]

the plate buckling in the same location.

In figure 3.7 the displacement of the frames was found by using lines parallel to vertical the lines used for the plate measurements. By using the weld connecting the top of the frame to the fore peak tank top and the bracket as a reference point the offset of the frame flange was estimated. There are uncertainties connected to these measurements due to the lack of a proper reference point at the lower end of the frame.

**Table 3.5:** Displacement of frame flanges measured from figure 3.7

Frame #	Span	Scale <i>mm</i>	Range <i>mm</i>	Mean disp. <i>mm</i>	Quality
231½	2990	1:11	±21	50	Poor
232	2990	1:14	±21	91	Poor
232½	2990	1:11	±15	80	Poor

Due to the irregular shape of the tripping brackets in figure 3.7 it was hard to determine whether they had undergone deformations. The lower tripping bracket between frame #232 and #232½ has deformed due to the large deformation of the latter frame. The paint at the bracket's fore corner has fallen off due to the strains in the material. At the fore corner of the upper tripping bracket the strain had become high enough to fracture the weld between the bracket and frame #232½. The fracture spanned over half of the weld length. The size of the crack opening is estimated to 55*mm*.

Figure 3.9 shows the next section of frames; #233-#235. The frames here have deformations similar to those of the previously described frames. The translation of the frame flanges have been estimated by drawing straight lines from the weld corner at the top bracket to the weld corner at the bracket visible below the 2<sup>nd</sup> side stringer. In figure 3.11 frames #235-#237 are in focus, and the same method has been used to determine the flange displacements. The results are displayed in table 3.6. The estimates have been done around mid span of the frames, and at



the top of a few. The angles from where the photos are taken makes it difficult to assess whether the frames deform forward or to the aft.

**Table 3.6:** Displacement of frame flanges measured from figure 3.9 and 3.11

<b>Frame #</b>	<b>Span <i>mm</i></b>	<b>Scale <i>mm</i></b>	<b>Range <i>mm</i></b>	<b>Mean disp. <i>mm</i></b>	<b>Quality</b>
233½ mid	2990	1:11	±6	-66	O.K.
233½ top	2990	1:14	±7	42	O.K.
234	2990	1:13	±7	-17	O.K.
234 top	2990	1:14	±7	-84	O.K.
234½	2990	1:21	±11	94	Poor
235	2990	-	-	56	Good
235½	2990	-	-	-56	Good
236	2990	-	-	-56	Good
236½	2990	1:13	±7	-27	Good

No scales are given for frame #235, #235½ and #236 since the translation appeared to be equal to the flange width after deducting the upper bracket thickness.

In figure 3.12 the buckling of the frames was found by assuming the flange to be straight and close to its original position in the upper part of the photo. An elongation of this line was drawn and the gap at the bracket weld measured at its maximum. The bracket thickness, flange thickness and width were all used for scaling at different frames. Table 3.7 shows the findings. Frame #235 appears to be deformed due to the loss of paint, but no significant is present between the elongated line and the flange edge. Most likely is the deformation parallel to the camera angle.

**Table 3.7:** Displacement of frames measured from figure 3.12

<b>Frame #</b>	<b>Span <i>mm</i></b>	<b>Scale <i>mm</i></b>	<b>Range <i>mm</i></b>	<b>Mean disp. <i>mm</i></b>	<b>Quality</b>
232½	3000	1:11	±3	-23	Good
234	3000	1:19	±3	38	OK
234½	3000	1:21	±5	31	Good

## 3.5 Web Frames

The whole length of the two most affected web frames, #230 and #233, are shown in figure 3.5. Both are clearly buckled, but the angle from where the photo is taken makes it hard to determine the deformations of web frame #233. Never the less are the estimates given in table 3.8

**Table 3.8:** Displacement of frames measured from figure 3.5

Frame #	Span <i>mm</i>	Scale <i>mm</i>	Range <i>mm</i>	Mean disp. <i>mm</i>	Quality
230	5990	1:39	±24	-212	Good
233	5990	1:33	±20	-50	Poor

Figure 3.7: The web plate of web frame #233 is heavily buckled towards the skin. The paint has fallen off over a frame sized area, and yield lines are apparent in the steel. The fore peak tank top appear not to have any damages, although the bracket of one of the longitudinal tank top stiffeners looks slightly deformed.

Figure 3.6: Web frame #230 is heavily deformed which is seen from the buckled web plate, skewed flange, and the sharp angle of the weld connecting the 2<sup>nd</sup> side stringer and the web frame. The lack of sufficient reference points challenging to estimate the deformations. At best a educated guess could be made, thus have no guess been made.

Figure 3.6 The plate web of web frame #230 is severely deformed. Its flange is just partly visible in the photo but also appears to be deformed.

Figure 3.12: The structures in this photo was not as heavily deformed as the structures in the previous photos. It displays the 3<sup>rd</sup> side stringer and the lower two thirds of frames #232½ to #235, including web frame #233. Frame #233½ is hidden behind the web frame. Buckling of the frames is seen as a modest displacement in the flange just above the lower bracket, revealed by the cracked and flaking paint. The frame aft the web frame buckles aft while the frames fore of the web frame have buckled forward. The web frame flange has a more distinct deformation and appears twisted. The plate web of the web frame has buckled but it is hard to determine the magnitude. Due to the shadows from the camera blitz it looks like the plate buckles backward close to the flange, forward on the middle and towards the hull skin, and backwards again next to the skin. A lashing plate which one can assume to originally have been welded normal to the web, pointing backwards, has twisted down and inwards. One can thus assume the apex of the buckled plate is located somewhere above and further from the center line than the location of the lashing plate. There are two brown areas on the top of the 3<sup>rd</sup> side



Figure 3.11: Deformation of plates and frames #233 - #237, [5]



Figure 3.12: Deformation of plates and frames #232 1/2 - #235, [5]



**Figure 3.13:** Deformation of frames and web frames #229 1/2 - #233, [5]



**Figure 3.14:** Deformation of frames and web frames #233 - #234 1/2, [5]

**Table 3.9:** Comparison of different measures for the same frame

Figure	#232	#232 ½	#233
3.3	-	168	285
3.7	62	162	85
3.8	100	86	133

stringer. They look like dried ponds of rusty water, which indicates deformation of the stringer plate allowing water to collect.

The buckling of web frame #233 is challenging to quantify due to the lack of reference point. Just from looking at it the displacement at the bracket weld on the bottom part of the flange appears to be half of the flange width, in other words  $-63mm$ . This is a measurement of poor quality.

### 3.6 Stringers

Figure 3.6 In addition are the brackets between the 2<sup>nd</sup> side stringer and web frame #227 and #230 largely buckled. As previously mentioned are the brackets between the 2<sup>nd</sup> side stringer and web frames #227 and #230 heavily deformed. By drawing the line assumed to be the original location of the bracket and using the bracket thickness to scale, a measure of the deformation was estimated. The bracket between the stringer and #230 is N-shaped and the upward pointing bend was estimated to be  $31mm$  off its original location at its maximum. The downward bend was estimated to be  $8mm$  off at maximum. 1 :  $7.7mm$  was the assumed scale.

### 3.7 Discussion of Deformations

In the above sections the deformation of the ship side has been described. Some of the structures are occurring in several photos, and the deformations have therefore been estimated several times. Examples of this are frames #232, #232 ½, and web frame #233. Table 3.9 gives a comparison of the different measurements. The numbers are the deformations given in  $mm$ , as in table 3.1, 3.2, and 3.3. The measurements of the deformations varies a lot from figure to figure. For frame #232 ½ numbers from figure 3.3 and 3.7 coincides well, but for web frame #233 the numbers are very inconsistent. The measurements from figure 3.7 are assumed to be the least reliable since the damage extends beyond the area seen in the photo,

hence only local deformation within the photo can be measured. Figure 3.8 is assumed to be somewhat better since more of the ship side is visible. Figure 3.3 is considered to give the most realistic measurements since most of the damage is visible. Therefore the measures of  $168\text{mm}$  and  $285\text{mm}$  used as reference measures when performing the finite element analysis described in the following Chapters.

### 3.8 Sources of Error

The estimation of deformations from photos is challenging, and the validity of the measurements is uncertain. Therefore are some of the sources to these uncertainties listed below.

- The brackets have most likely been deformed and can't be used as reference points without accounting for these deformations.
- The visual estimate of where a flange has the maximum offset is imprecise.
- The scaling of the offset by using the flange width may be inaccurate due to the angle of the flange which is difficult to determine.
- The measured deformation is assumed to be purely a forward translation, while it in reality in addition would be a combination of translation toward the center line and forward bending of the web.
- The camera used to take the photos might have had a wide angle lens which would make structures photographed appear slightly bent
- Several of the close up photos of the structure inside the fore peak tank contain nothing but deformed structures and are thus lacking sufficient reference points for measurements.
- On the photos from the outside the water (line) hides the structure under the 2<sup>nd</sup> side stringer and it is impossible to see what the deformations on that side looks like
- Other factors are e.g. the angle from where the photo is taken, the loss of depth in the photo, the oblique construction of the shell and frames, and the light from the blitz making optical illusions of straight plates being bent.

### 3.9 Load Calculation from Rules

The following load calculations are partly based on equations given in the rules discussed previously in this Chapter, and partly on simplified theories. The loads are calculated with respect to frame#232 1/2 of the cargo ship in question because

Structural element	Length of the load area $l_a$
Transversely stiffened plates	Frame spacing
Transverse frames	Frame spacing
Ice stringers	Spacing of web frames
Web frames	Spacing of web frames

**Table 3.10:** Definition of ice load length according to the FSICR, [3]

the deformation is global and this specific frame appears to have the largest deformation, as will be discussed in the next Chapter. In the derivation of the FSICR it is stated that the ice load will concentrate more on the framing than on the plating because the plating is more flexible and will thus deform, leaving the frames as the load carrying structure, [3].

### 3.9.1 Design Loads Calculated from Rules

The design ice load for ships covered by the FSICR is calculated from equation (2.1). The calculation of  $c$ -factors is given in the rule [1] and will not be included here. For the cargo ship in this case study, with frame #232  $\frac{1}{2}$ , the following constants are found:

$$\begin{aligned} c_d &= 0.72 \\ c_1 &= 1.00 \\ c_a &= 0.80 \end{aligned}$$

The design ice pressure for the above mentioned frame then becomes:

- $p = 3.23 \text{ MPa}$

The area, to which this load should be applied, is defined by the load height  $h$  given to be  $300 \text{ mm}$  for **ICE-1A** in the rules, and the length of the load area  $l_a$ , given in table 3.10

The UR PC design ice load is calculated from equations (2.23-2.27). The specification and calculation of class factors, hull angles, and shape coefficients is not included here, but can be found in the rule document [2]. As in the design load calculation from the FSICR is frame #232  $\frac{1}{2}$  used as reference. The force  $F$  on the bow is found to be  $18.84 \text{ MN}$ , the line load  $Q = 6.05 \text{ MN/m}$ , and the pressure:

- $p = 2.54 \text{ MPa}$

Further is the design patch found to have the width  $w = 3104 \text{ mm}$  and height  $b = 2390 \text{ mm}$ , which gives an average design pressure within the patch of  $p_{avg} =$

2.55MPa.

### 3.9.2 Capacities Calculated from Rules

In order to find the actual capacity of frame #232  $\frac{1}{2}$  the design equations of the frame section modulus have been solved for the pressure  $p$ . By doing this one gets an indication of how much pressure the structures should be able to withstand.

For the FSICR the capacity ice pressure is calculated from equation (2.10).

$$p = \frac{Z \cdot m_t \cdot \sigma_F}{s \cdot l \cdot h} \quad (3.1)$$

The capacity pressure is calculated from equation (3.1) by inserting the elastic section modulus of the actual frame  $Z$ , bending moment factor  $m_t$ , yield stress  $\sigma_F$ , frame spacing  $s$ , frame span  $l$ , and load height  $h$ . The load height is taken to be 300mm as given in the rules for **ICE-1A**. The capacity pressure is then calculated to be:

- $p = 4.94MPa$

Note that the capacity is higher than the design load.

The IACS load calculation is done following the equations for the three failure mechanisms outlined in section 2.2.3, equations (2.31, 2.36, 2.40). By solving these equation for  $P$  and inserting the full section modulus according to equation (2.33) and the other parameters, the frame capacity is found for the three mechanisms.

For web collapse equation (2.31) becomes:

$$P_{web} = \frac{2 \cdot A \cdot \sigma_y}{b \cdot S \sqrt{3}} \quad (3.2)$$

Capacity for 3-hinge collapse from equation (2.36) becomes:

$$P_{3h} = \frac{(2 - kw) + kw \cdot \sqrt{1 - 48 \cdot Zpns(1 - kw)}}{12 \cdot Zpns \cdot kw^2 + 1} \cdot \frac{Zp \cdot \sigma_y \cdot 4}{\left[ S \cdot b \cdot L \cdot \left( 1 - \frac{b}{2L} \right) \right]} \quad (3.3)$$

And the capacity for asymmetric loading from equation (2.40) becomes:

$$P_{asym} = \frac{\sigma_y}{b \cdot S \left( 1 - \frac{b}{2L} \right)} \cdot \left[ \frac{Aw}{\sqrt{3}} + \frac{Zp}{L} \cdot (1.1 + 5.75 \cdot kz^{0.7}) \right] \quad (3.4)$$

The calculated capacity ice pressures are:



- $P_{web} = 1.67MPa$
- $P_{3h} = 1.69MPa$
- $P_{asym} = 1.99MPa$

The load height is found from calculation of the bow ice load characteristics: total impact force, line load, and pressure according to equation... The load height  $b$  is found to be  $2390mm$  and the load width  $w = 3104mm$ .

Figure 3.15 shows the load plotted as a function of load height.

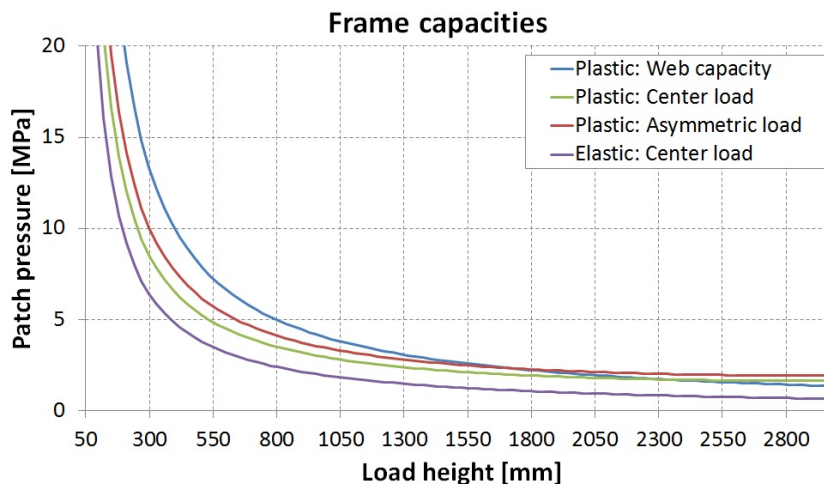


Figure 3.15: Frame capacities as a function of load height

### 3.9.3 Capacity Calculated from Simplified Theory

In the following simplified beam theory have been used to calculate the capacity of frame #232  $\frac{1}{2}$ . The theoretic beam is clamped at both ends and undergoes a uniform pressure over the whole span. Note that the loads calculated above have been applied to only a part of the frame span. The equation is basically the same as equation (3.1), but with  $l^2$  instead of  $l \cdot h$  since the whole beam is loaded, and with  $m_t = 12$  for the elastic case and  $m_t = 16$  for the plastic case. The following pressures are obtained:

- $p_{el} = 0.97MPa$
- $p_{pl} = 2.30MPa$

The subscript “el” refers to elastic theory which the FSICR are based on, and “pl” refers to plastic theory which the Polar Class is based on.



## Chapter 4

# Damage Reproduction with Finite Element Analyses

Two cases are investigated using finite element analysis (FEA). The first case is two of the frames which appeared to have undergone the largest deformations. The goal is to recreate the severe deformations and use the results as a guide line of how to continue with the main model. The main model, the second case, is the bow port side where the main part of the damage was seen.

MSC Patran 2012.1 is used for making the models in this thesis. Due to complications which arose when importing the models to Abaqus some of the modelling was more convenient to do in Abaqus. ABACUS/CAE 6.13-1 and -2 was used for parts of the modelling and running the analyses.

Because Patran is able to create surfaces with double curvature the programme is well suited for the modelling of the port side of the fore peak tank. The procedure was to create nodes and curves from coordinates given from the design drawings, see Appendix A. Surfaces were extruded between the curves, and shell thickness and material assigned to the surfaces. At the end the geometry was meshed, and 2D beam elements created for the smaller flanges and stiffeners in the model. The geometry, mesh, materials and properties was written to a .inp-file which is compatible with Abaqus. In Abaqus plastic properties were added to the material and boundary conditions created. A test load was applied to a test patch, and analysis steps created. Numerous test analyses had to be run in order to verify the model and detect errors.

In the following the details of the analysis setup is explained for the simplified frame analyses and the main model. This includes boundary conditions, loads, element meshing and analysis types. All of the models have the same material

properties and use the same analysis procedures. Therefore, the materials and analysis procedures are presented before going into more specific analysis details. Contact between elements and initial imperfections are not included in any of the models.

## 4.1 Material Properties

In design analyses the rule requirements define minimum yield required of a certain material for certain applications. In this case the design values are not of interest. To reproduce the damage as close to the real deformation as possible, the true stress-strain curve is central. The given design yield stress a plate is certified for is the minimum required value. The steel mill want to be sure the plate is strong enough and aims for a yield stress above the required value. If a significant number of plates of a certain steel grade are tested, the result will be normally distributed about a yield stress 10% above the required stress, see figure 4.1. For the lower steel grades the deviation is high, while for the higher steel grades the deviation is lower, giving a slimmer curve. In other words, a steel member will have more capacity than what the design proposes, and for increasing steel grade will the extra capacity decrease. In this case the extra yield stress capacity has been used when the ship side deformed, thus it's desirable to have the exact capacity for the materials.

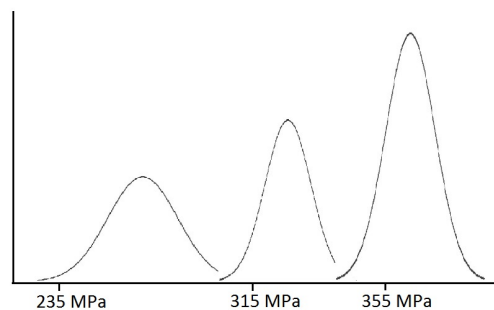


**Figure 4.1:** Example of distribution of steel quality, strictly illustrative

The yard that built the ship was able to present the material certificate for most of the members in the damaged area. A material certificate is a document which gives the chemical composition, strength, and capacity of a material. In other word the real qualities of the steel. Due to the large deformations seen in the photos it is important to have correct nonlinear properties of the materials in that area. Steel of three different qualities is present in the damage area of the ship:

- Mild Steel: NV A,  $\sigma_y = 235MPa$
- Higher Tensile Steel: NV A32,  $\sigma_y = 315MPa$
- Higher Tensile Steel: NV A36,  $\sigma_y = 355MPa$

Standard steel material data used, is as follows:

- Young's modulus:  $E = 210000MPa$
- Density:  $\rho = 7.85 \cdot 10^{-9}ton/mm^2$
- Poisson's ratio:  $\nu = 0.3$

### 4.1.1 Plate Materials

For the plastic part Abaqus allows you to specify the desired material curve. The curve is specified by entering coordinates for points along the curve as a value of stress and the respective strain. In this case the data from the material certificates is used. Unfortunately only the stresses are given, not strains. For the first point it does not matter because Abaqus defines the plastic part of the material curve as an individual curve with the first point being the yield stress at zero plastic strain. It is also common to assume the strain at upper yield to be equal to zero, since it is in the range of 0.002 due to the steep slope of the curve in the elastic area, the Young's modulus. The second point used in this case is at ultimate stress. In the certificate no strain information is given for this point. In order to find a good estimate, results from material tests done in the laboratory by DNV-GL are used as guidance, see figure 4.2.

The figure shows four curves. The curved curve with the lower stresses consists of two curves. In the first blue part, which makes up the elastic region and the plateau in the start of the plastic region, the elongation of the test specimen is measured with an extensometer. Unfortunately, this device isn't able to do good measurements in the plastic region, so in the connected green curve the elongation is taken from the displacement of the test rig itself. The output is a load-displacement curve which is converted to a stress-strain curve by dividing the force by the cross section area of the specimen, and dividing the difference in elongation with the original specimen length. Since these calculations assume the cross section of the specimen to be constant throughout the test the blue-green curve is the engineering stress strain curve. In reality the cross section of the specimen will become smaller as the elongation increases. By taking this into account the true stress-strain curve is gained. Since the engineering curve already is at hand the true

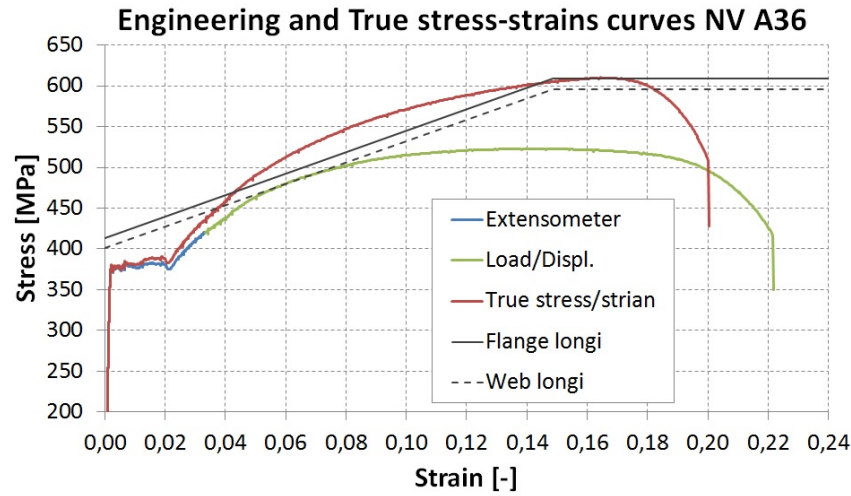


**Figure 4.2:** Stress-strain curves from test data, DNV-GL

curve can be found from a few simple formulas found e.g. in DNV-GL's Recommended Practice DNV-RP-C208 [16]:

$$\sigma_{true} = \sigma_{eng}(1 + \varepsilon_{eng}) \quad (4.1)$$

$$\varepsilon_{true} = \ln(1 + \varepsilon_{eng}) \quad (4.2)$$

By this the red curved curve with the higher stresses in figure 4.2 is found.

For NV A36 three different curves from tests DNV-GL has performed are available. Two test curves are available for NV A32. The values for ultimate stress and strain are as shown in table 4.1.

**Table 4.1:** Stress-strain values from DNV-GL test curves

Grade	$\sigma_{ult}$	$\varepsilon_{ult}$
NV A36	440	0.15
NV A36	523	0.16
NV A36	552	0.16
NV A32	467	0.13
NV A32	634	0.21

By assuming the same curve shape, yield at zero strain, and the ultimate stress occurring at same strain, an approximation of the ultimate strain can be found. For NV A36 the strain is taken to be 0.16 at ultimate stress. This value coincides with the proposed material curves found in DNV-RP-C208, [16]. By comparing

the mean values of NV A32 stress and strain from the DNV-GL curves with the mean ultimate stress from the yard's material certificate, the corresponding strain becomes 0.158. Due to the proximity to NV A36's estimated ultimate strain NV A32's strain is also taken to be 0.16.

**Table 4.2:** Material details for plating used in model, true stress and strain

<b>Grade</b>	<b>t</b>	<b>Y.P.</b>	$\varepsilon_{Y.P.}$	<b>T.S.</b>	$\varepsilon_{T.S.}$	<b>Where to be used</b>
NVA32	17,5	422	0	618	0.148	At the specific plate
NVA32	17,5	408	0	599	0.148	At the specific plate
NVA32	15,5	348	0	568	0.148	At the specific plate
NVA36	31,5	403	0	603	0.148	At the specific plate
NVA36	26,5	412	0	604	0.148	At the specific plate
NVA36	31,5	394	0	602	0.148	At the specific plate
NVA36	26,5	423	0	607	0.148	At the specific plate
Mean NVA32	-	393	0	595	0.148	For all other NVA32 plates
Mean NVA36	-	408	0	536	0.148	For all other NVA36 plates

Table 4.2 gives the input for the true plastic stress-strain curves for the exterior plating. The certificate provides information about the upper yield point and ultimate stress for all shell plates in the bow region, except for two plates. **Grade** refers to the steel grade of the specific plate, **t** is the plate thickness, **Y.P.** is the upper yield point,  $\varepsilon_{Y.P.}$  is the yield point strain, **T.S.** is the tensile strength also known as ultimate stress,  $\varepsilon_{T.S.}$  is the tensile strength strain. The stresses and strains given in the table are the ones inserted into the analyses in Abaqus.

Information about the quality of the internal plating is lacking. The plates are coming from the same mill, and by assuming the quality to be about the same within each steel grade, approximations of the quality of the internal plates can be done. Here, the mean value of each steel grade is utilized. These are the two bottom materials in table 4.2. Note the difference from true yield point to the design yield point for each material. The yield point for NV A32 used here is 25% higher than the minimum required value, while the yield point for NV A36 is about 15% higher. These numbers coincides well with the curves shown in figure 4.1, where the standard deviation of the yield strength of a steel grade decreases with increasing steel quality. Unfortunately, no information is given about plates of grade NV A. This will be discussed in the following section.

### 4.1.2 Frame Materials

For the stiffeners data for the actual material used in the ship was not available. Instead was data for some profiles of the same dimensions from the same mill available. Assurance was given that there should be negligible difference between profiles coming from the same mill, [17].

No tensile test curves for NV A steel was available from DNV-GL. The strain value for ultimate stress taken from DNV-RP-208 is therefore used, [16]. In RP-208 the upper yield and ultimate stress are lower than the values in the material certificate. Generally, the strain decreases for increasing ultimate stress, therefore should the strain used here be lower than the strain of 0.18 from RP-208. Without having any way of presuming a likely value, 0.18 is used here. This assumption is not expected to have a considerable effect on the analysis since the members in the damage area are of the other more well derived steel grades, A32 and A36, while NV A is only used for members outside the damage area and for smaller stiffeners.

**Table 4.3:** Material data for frames and stiffeners used in model, true stress and strain

Section	Grade	Dim.	Y.P.	$\varepsilon_{Y.P.}$	T.S.	$\varepsilon_{T.S.}$	Used for
Flat bar	NVA	12x150	334	0	551	0.166	
Flat bar	NVA	12x150	327	0	540	0.166	
Flat bar	NVA	12x150	316	0	516	0.166	
Mean	NVA		326	0	536	0.166	NVA stiff.
Web longi	NVA36	13,5	401	0	596	0.148	NVA36 web
Flange longi	NVA36	19x125	413	0	609	0.148	
Flange longi	NVA36	25x125	390	0	597	0.148	
Mean flange	NVA36		402	0	603	0.148	NVA36 flange
Mean	NVA36		401	0	600	0.148	NVA36 stiff.

Table 4.3 gives the certificate data for frames and stiffeners provided by the yard, and calculated true stresses and strains. In the column furthest to the right a short comment is given to where the material should be applied. The fourth row, “Mean NVA”, is the mean value of the three rows above. “Mean flange” is the mean of the two rows above, and “Mean NVA36” is the mean of “Web longi” and “Mean flange”.

In table 4.2 the information of a NV A plate is absent. By comparing the mean values of a NV A36 plate with the mean values of a NV A36 stiffener it is noticed that the numbers differs with no more than 1-2%. From one can draw the conclusion the material in the plates and in the frames in general is similar. Thus



is the plate NV A assumed to be the same as the mean frame NV A. The same procedure is done to find a value for the absent frame NV A32: it is put equal to the plate NV A32, as shown in table 4.4.

**Table 4.4:** Material data calculated from mean values

<b>Grade</b>	<b>Y.P.</b>	$\varepsilon_{Y.P.}$	<b>T.S.</b>	$\varepsilon_{T.S.}$	<b>Where to be used</b>
NV A	326	0	364	0,18	For all other NV plates
NVA32	393	0	513	0,16	For any NVA32 stiffener

In figure 4.2 the curve labeled “Flange longi”, meaning “flange of longitudinal”, is the material test of NV A36 from the certificate with the highest tensile strength, likewise is “Web longi”, meaning “web of longitudinal” the material test of NV A36 with the lowest tensile strength. Both can be found in table 4.3. By comparing these curves with the red “True stress/strain curve” it’s noted that the upper yield is about  $23 - 30\text{MPa}$  higher for the longitudinals than for the red curve. Following, the red curve has a curvature describing the strain hardening of the steel as the stress increases. Due to the lack of reference points the black curves are linear from the upper yield point to the ultimate tensile strength. At the point of the ultimate tensile strength the “Flange longi” coincides well with the red curve. The “Web longi” lies about  $15\text{MPa}$  below, indicating all of the NV A3 steels used in the analyses to be located within a range of  $15\text{MPa}$  of the red curve. Considering the sparse information given in the material certificates the estimated curves appears to be reasonable. After the last plastic curve point specified Abaqus assumes the curve to continue infinitely with zero slope. This is illustrated by the black curves. The red and green curves illustrate the real situation: loss of capacity and eventually fracture. In the analysis fracture is not included as a phenomenon, this will be discussed in section 4.5.

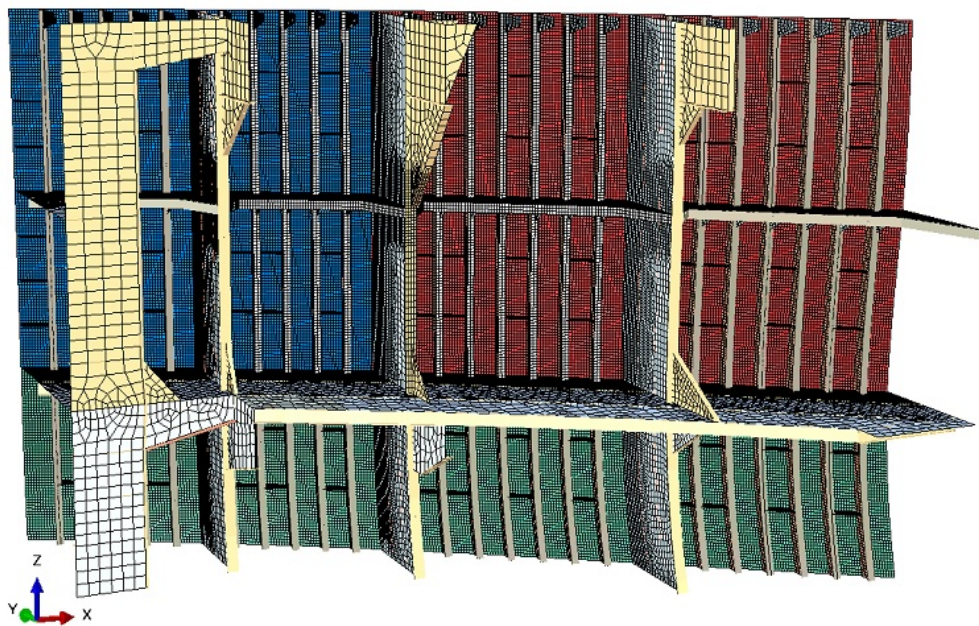
### 4.1.3 Material Summary

The total mean values for the three steel types are calculated from all the above numbers. Table 4.5 gives the result. These values are not used in the model but are purely for comparison with the minimum required design values. For NV A36, NV A32, and NVA the strength is respectively 14%, 25% and 39% above the minimum required value. The increase in difference with decreasing steel quality coincides well with the curves of normal distribution of the actual steel quality and the increasing standard deviation with decreasing steel quality.

**Table 4.5:** Summary of material data

Steel grade	$\sigma_y$	Frac.	Y.P.	$\varepsilon_{Y.P.}$	T.S.	$\varepsilon_{T.S.}$
NVA36	355	1,140	405	0	519	0,16
NVA32	315	1,248	393	0	515	0,16
NVA	235	1,386	326	0	454	0,18

Figure 4.3 gives a colour plot over the variety of materials used in the main model.

**Figure 4.3:** Different materials used in different parts of the model

## 4.2 Analysis Procedures

Abaqus provides a variety of analysis types depending on the problem at hand. For the case studied in this thesis the load is assumed to be static and it's the nonlinear deformations which are of interest. Among the various analysis types offered in Abaqus "Static, General" and "Static, Riks" are the best suited for this kind of problem, [18].

Steps are the sequences in which one defines the desired analysis procedures. The “initial step” is a default step Abaqus creates in the start of a model’s step sequence. After the initial step comes the user defined analysis steps. For the analyses performed here only one analysis step is used.

In a general analysis step any nonlinearity present in the model can be included, [18]. There are three types: material nonlinearity, geometric nonlinearity, and boundary nonlinearity. In the analyses run in relation with this thesis material nonlinearity is included as the plastic part of the material curves, as discussed previously. The geometric nonlinearity, or “large displacement formulation” is selected when creating the analysis, and is accounted for when Abaqus updates the nodal positions of the elements as the structure deforms, allowing the elements to distort from their original shapes. Boundary nonlinearities are e.g. contact problems, and are not relevant for this thesis’ analyses. In the static stress procedure inertia effects are neglected, nonlinearity can be included or excluded, and time depended material effects, e.g. creep, are ignored.

During the “Static, General” analysis step a time period is assigned to the analysis. Since the applied pressure from the load cases is time independent Abaqus/Standard uses the default time, which goes from 0.0 to 1.0 over the step. The analysis is then divided into time increments, or fractions of the time period. When running the analysis the pressure load in each time increment is applied as a fraction of the specified load value. At time = 1.0 the accumulated load is equal to the specified load. Newton’s method is used to solve the nonlinear equilibrium equations for each increment. Iterations are done within each increment to obtain equilibrium. Sometimes the increments must be kept small to endure correct modeling of history-dependent effects. Note that Newton’s method only works for analyses where the load-displacement curve of the model has a positive slope.

An alternative to “Static, General” is the “Static, Riks” procedure, intended for geometrically static problems that involve buckling or collapse behaviour. During some of the test runs of the ship side analysis collapse of one of the web frames was observed, see figure 4.6 at  $y = 40mm$ . At this point the response shows a negative stiffness and the structure must release strain energy to remain in equilibrium. The Riks method solves simultaneously for loads and displacement, requiring another quantity to measure the progress of the solution. In order to obtain solutions regardless of whether the response is unstable or stable Abaqus/Standard uses the arc length along the static equilibrium path. During a Riks step the load is ramped from an initial value, which is a fraction of the reference load. For each increment a another fraction of the reference load is either added or subtracted. From this the accumulated applied load within each increment can be calculated.

Static, General and Static, Riks are implicit analysis procedures available in Abaqus/Standard.

An alternative to the implicit method is the explicit procedures available in Abaqus/Explicit. In the latter analyses the dynamic response problems are solved using an explicit direct-integration procedure. The explicit dynamic analysis is computationally efficient for the analysis of large models with relatively short dynamic response times. At one point in the test analyses the model was not running with neither Static, General or Static, Riks. It was decided to try running the model as a quasi-static analysis using Abaqus/WxPLICIT. Some problems were experienced with this analysis procedure as well, and the focus was returned to searching for errors in the model.

### 4.3 Simplified Frame Analysis

As an introduction to the model of the whole damage area, a simple model of one frame, frame #232½, is analysed. The goal is to investigate the possibility of reproduction of the plastic deformations seen for the real frame, showed in figure 3.7. This type of displacement of a frame is known as tripping.

The frame model length is equal to the distance between the 2<sup>nd</sup> side stringer and the fore peak tank top. The shell is modeled as the plate flanges of an I-beam, and the width is equal to the frame spacing. The curvature of the skin, both in z- and x-direction, is assumed to be negligible due to the small area of the shell included in the simplified model. The frame web is transverse to the ship length while the shell has an water line angle of 38°, as illustrated in figure 3.10.

Table 4.6 and 4.7 gives the scantlings of frame #232 1/2.

**Table 4.6:** Scantlings of frame #232 1/2

Part	Symbol	[mm]
Frame span	L	2990
Frame spacing	s	470
Plate thickness	tp	26,5
Web height	hw	300
Web thickness	tw	13,5
Flange width	wf	125
Flange thickness	tf	19

**Table 4.7:** Materials of frame #232 1/2

Part	Material	$\sigma_y$ [MPa]
Plate flange	NV A36	412
Web	NV A36	401
Flange	NV A36	401

### 4.3.1 Element Meshing

In the element mesh Abaqus' S4R-element is used. This is a 4-node, quadrilateral, stress/displacement shell element with reduced integration and a large-strain formulation, [18]. Because the structural members are assumed to be thin walled, i.e. the stresses varying in two dimensions while constant in the third, this element is well suited for the purpose of the analyses. The solution will be sufficiently accurate for design verification using significantly fewer resources compared to using solid representation.

The element meshing is crucial for the results of a finite element analysis (FEA). Type of elements, element size, and method used for meshing needs attention. In Patran, Quad4 elements are used, and these elements are equal to the Abaqus S4R elements. The element size of the frame was chosen to  $50mm$ , following recommendations from experienced modellers at Høvik. There are six elements over the frame web height, ensuring deformations and stress variations being calculated with a sufficient accuracy for the comparison with the real deformations seen in the photos. In general a more accurate result can be obtained by refining the mesh, but at one point the increase in accuracy gained by using smaller elements is offset by the (quickly) growing computational cost of increasing the number of elements. A comparison of results from the frame analysis with various element sizes could have been performed, but because of limited time and since this isn't the main focus this paper, the advice from experienced modellers is followed.

### 4.3.2 Boundary Conditions

It is of high importance to choose the correct boundary conditions in order to obtain results which coincides with the purpose of the analysis. For the frame assessed here, which is a part of a plate field, it is important that the interaction with the plates on each side of the frame are accounted for in the boundary conditions.

When a plate field, clamped along all edges, is exposed to lateral loading some

of the loading will be taken by membrane capacity. Membrane effects are not accounted for in the IACS rules and are considered to be reserve capacity of a structure, [10]. By excluding the membrane effect in design calculations the design results are thought to be conservative. In the present case of the frame membrane effect is excluded by allowing the long edges to translate in  $x$ -direction. The bottom edge is also free to translate in  $z$ -direction. The top edges of the plate flange, web and top flange are fixed against any translations and rotations, illustrating the connection to the tank top. The long edges and bottom end are also fixed against rotations.

When a plate is deformed laterally the edges will displace inwards, towards the largest deformation observed at the middle of the plate for evenly distributed loading. Since the plate flange of the frame is part of a plate field it is restricted against such inwards deformation by the neighbouring plates. One way to express this through the boundary conditions is to limit the  $x$ -translation to a synchronized displacement of the long edge. In Abaqus this is done by the \*EQUATION function: one node is chosen as “master” while the rest of the edge are “slaves” and will have the same displacement as the master node in the specified degree of freedom (DOF). One of the long edge’s master node is restrained against  $x$ -translation, preventing rigid body displacement.

### 4.3.3 Loading

The load is the main focus of this thesis; to estimate the magnitude of the ice pressure which resulted in the severe damage. The initial loads used in the analyses are simply the design ice loads from the FSICR and IACS rules, for bow area of the ship in question, see section 3.9. Within the initial load analyses two cases are run:

- Load patch size from the FSICR, located at the centre of the frame span,  
 $w = s = 470mm, h = 300mm$
- Load patch size from the IACS rules, located at the centre of the frame span,  
 $w = s = 470mm, h = 2390mm$

In the rules the load is located at the centre of the frame span because this is the most critical location for the frame in bending failure. With a load located closer to one of the ends of the frame, the frame will have more bending capacity, but at the same time lose shear capacity, as discussed in section 2.2.3. In the case of the damaged cargo ship, the shipowner reported the draught at the time of the incident was about  $13m$ . When applying the load in the analyses this should be taken into account. By assuming the density of ice to be  $920kg/m^3$  and the density of sea

water  $1025\text{kg}/\text{m}^3$  the result will be 10% of the ice above water and 90% of the ice submerged in water. The frame analysed starts at  $10.29\text{m}$  above base line and ends at  $13.28\text{m}$ . With a water line at  $13\text{m}$ , the load patch starts at  $2440\text{mm}$  from the bottom of the modelled frame and ends at  $2740\text{mm}$  for the FSICR patch. The IACS PC patch starts at  $559\text{mm}$  from the frame bottom, and ends at  $2949\text{mm}$ . The two new load cases (LC), with the ice load patches located 10% above and 90% below the water line, are as following:

- Load patch size from the FSICR, located at the water line,  
 $w = s = 470\text{mm}, h = 300\text{mm}$
- Load patch size from the IACS rules, located at the water line,  
 $w = s = 470\text{mm}, h = 2390\text{mm}$

Figure 4.4 shows a single frame, with mesh, boundary conditions, and a span centred load patch, ready for analysis.

#### 4.3.4 Double Frame

In addition to the single frame is a double frame also analysed. It consists of the neighbouring frames #232 and #232 1/2, including two tripping brackets connecting the webs. The materials are the same as for the single frame, only including the tripping brackets consisting of NV A steel with thickness  $16\text{mm}$  and yield stress  $326\text{MPa}$ . The scantlings, mesh, boundary conditions, and loads are the same as for the single frame. This model is mainly included to account for the effect of the tripping brackets.

Centred load cases for the double frame:

- Load patch size from the FSICR, located at the centre of the frame span,  
 $w = s = 940\text{mm}, h = 300\text{mm}$
- Load patch size from the IACS rules, located at the centre of the frame span,  
 $w = s = 940\text{mm}, h = 2390\text{mm}$

Water line cases for the double frame:

- Load patch size from the FSICR, located at the water line,  
 $w = s = 940\text{mm}, h = 300\text{mm}$
- Load patch size from the IACS rules, located at the water line,  
 $w = s = 940\text{mm}, h = 2390\text{mm}$

Figure 4.4 shows the double frame with mesh, boundary conditions, and load.

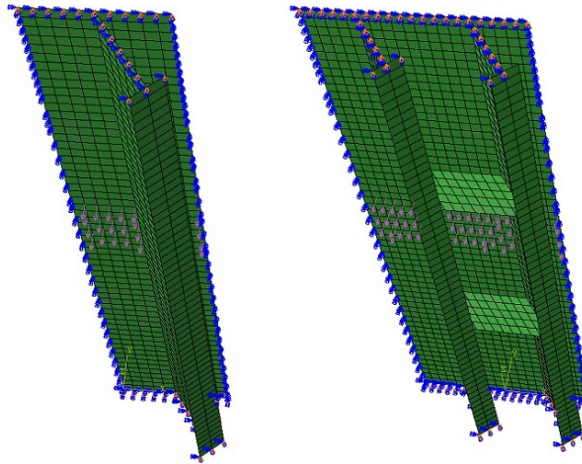


**Figure 4.4:** Single and double frame with mesh, boundary conditions, and load

## 4.4 Analysis of Ice Damaged Hull Structure

For the main analysis a model presenting the whole area of the severe damages is used. The initial model was from the bulk head at frame #227 to the bulk head at frame #241, from center line including everything port to the center line, and from the base line and to the fore peak tank top. Positive x-axis is defined in the forward longitudinal direction, positive y-axis to port side, and the positive z-axis from the base line and up. Due to several problems with the model it was reduced in size, as will be discussed in Chapter 4.5. The model used for the analyses goes from bulk head at frame #227, to the fore bulk head of the fore peak tank: frame #241. In vertical direction the model goes from the 4<sup>th</sup> side stringer, to the fore peak tank top. In transverse direction the model starts at the shell and ends at the edge of the 3<sup>rd</sup> side stringer. The reasons for the choice of this geometry is discussed in section 4.5. Figure 4.5 shows the model used in the main analysis.

This model was created from scratch for use in the work with this thesis. The geometry, mesh, and materials and properties are modeled in Patran while boundary conditions, loads, and analysis steps are added in Abaqus. Some remodeling was also done in Abaqus.



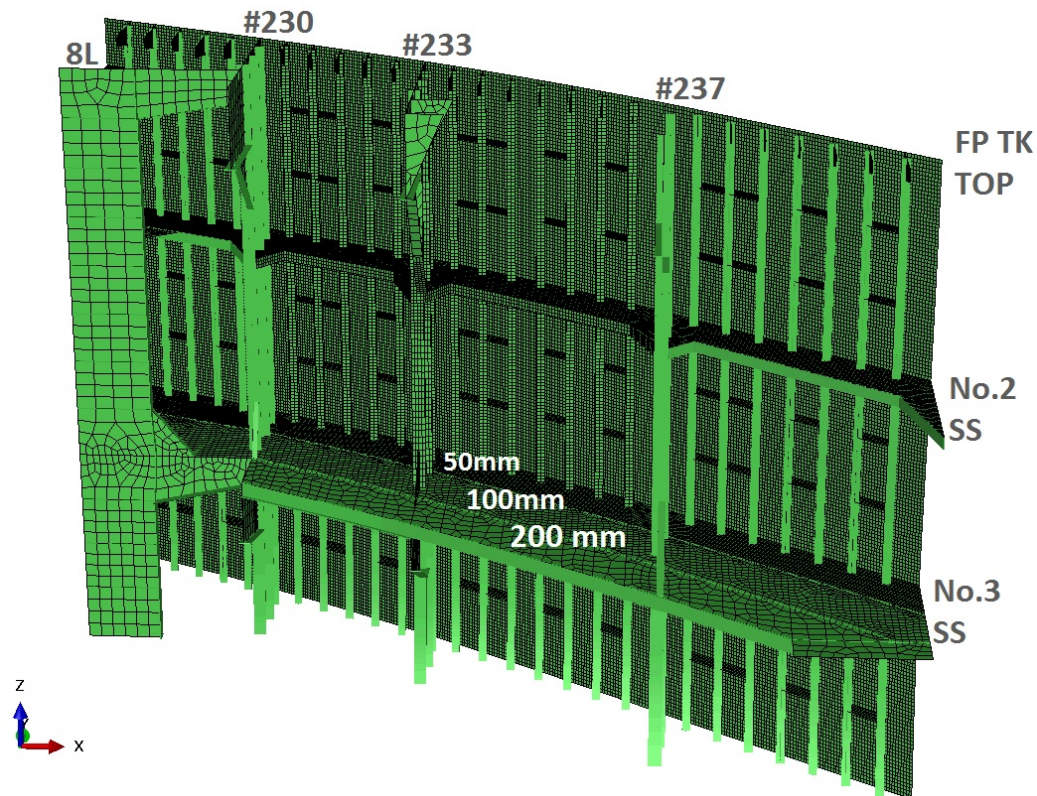


Figure 4.5: Main analysis model with mesh

#### 4.4.1 Element Meshing

As in the simplified analyses, the deformation of the frame webs are of interest. Thus is the element size of  $50\text{mm}$  kept in this area. However, the model is fairly big some changes are done to reduce the element number and run time. The element size is kept  $50\text{mm}$  over most of the ice strengthened area, from the tank top and down to  $4.29\text{m}$  above base line, and  $1.8\text{m}$  towards the center line. Beyond this the mesh is increased first to  $100\text{mm}$ , and next to  $200\text{mm}$  furthest away from the damage area, see figure 4.5. The model consists of about 131 000 elements.

The major part of the model consists of shell S4R elements, the same as in the frame analysis. In addition, 1D beam elements, or B31; 2-node linear beams, are used for smaller stiffeners and flanges. B31 is a “Timoshenko beam”, which allows transverse shear deformation. They can be used for thick as well as slender beams, [18]. In the area of the largest deformations the beam elements was replaced with shell elements (S4R) after the preliminary analyses showed that the beam elements did not cope with the large strains associated with the deforma-

tions. This will be further discussed in Chapter 4.5.

#### 4.4.2 Boundary Conditions

The boundary conditions used in the main model are constraints assigned to x-, y-, and z-translations and rotations. The model given in figure 4.5 is constrained along the five planes the model borders to, excluding the sixth plane parallel to the ship side.

At the top the shell plate, frames, frame brackets, and web frames are fixed in all six degrees of freedom (DOF) to illustrate the connection to the fore peak tank top. This is done under the assumption that the tank top has a stiffness much larger than the structures connected to it, hence being rigid. The same assumption is used for the boundary conditions for the structures ending in the bulk heads fore and aft of the tank. Towards the center line and down towards the 4<sup>th</sup> side stringer all six DOF are fixed, but here the assumption is that these boundaries are far enough from the load and deformed area as not to interfere with the solution. If the fixation is done close to the deformation area it can influence the structure to deform differently. The girders under the tank top at frame #230, #233, and #237 are considered to be close enough to the deformation area to have an effect on the structure. Therefore symmetry about the z-axis is assumed, which means that translation is fixed in y-direction because of the direction of the load and in z-direction because of symmetry, and rotations are fixed about x because of symmetry.

#### 4.4.3 Loading

An investigation is done to whether hydrostatic pressure should be included in the load cases. Two analyses was run on one of the test models. The first model was loaded with an ice patch load of width 3090mm and height 2380mm. In the second case the same patch used together with hydrostatic pressure. Figure 4.6 gives the result for the two analyses as load-displacement curves, the lower red line indicating the analysis that includes hydrostatic pressure.

As expected, the curve for the analysis including hydrostatic pressure is shifted a bit towards higher deformations for an arbitrary load. This shift is simply the result of the force added by the sea pressure. The shift is relatively small since the total force from the hydrostatic pressure is about half of the total ice patch force, and distributed over an area about 23 times the size of the patch. At patch pressure = 2,5MPa the difference in displacement is about 4mm. When considering the

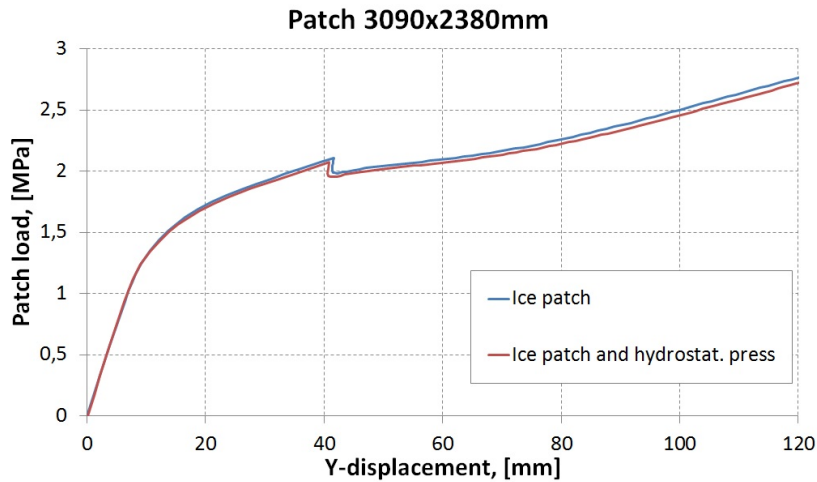


**Figure 4.6:** Comparison plots of model with and without hydrostatic pressure

sources of errors discussed in section 3.8 and including errors and assumptions from the modeling and analysis, the  $4mm$  representing the hydrostatic pressure becomes negligible. Therefore, the hydrostatic pressure is excluded in the following load cases and analyses.

#### 4.4.4 FSICR and IACS Ice Patch

The first two load cases are the FSICR ice patch and the IACS PC ice patch, as described in the following. The patches are centered at web frame #233 since this is where the largest deformations are seen, see figure 3.3.

- **LC FSICR:** The design load patch from the FSICR has a height of  $300mm$  and width equal the spacing of the structure in question. Large deformation of the web frames is seen in the photos, e.g. figure 3.5 and 3.7, therefore is the web spacing chosen as patch width,  $3290mm$ , see table 3.10.
- **LC IACS:** The design patch from IACS PC is calculated in Chapter 3.9 giving a patch height of  $2390mm$  and width  $3104mm$ .

#### 4.4.5 Proposed Ice Patches

Several load cases was initially planned for the main model. The first three was based on the deformations seen in figure 3.2. Because Riks is the procedure used in the analyses, the load magnitude doesn't have to be considered, only the area

of application. More information about procedures are given in Chapter 4.2. Following are the three load cases listed:

- – Long patch:  $w = \text{model length}$ ,  $h = 1000\text{mm}$
- Rectangle:  $w = \#229\text{-}\#235 = 5640\text{mm}$ ,  $h = 1000\text{mm}$ , located below the long patch
- – Long patch:  $w = \#229\text{-}\#238 = 8460\text{mm}$ ,  $h = 3500\text{mm}$
- – Long patch:  $w = \text{model length}$ ,  $h = 1500\text{mm}$
- Rectangle:  $w = \#228\text{-}\#238 = 9400\text{mm}$ ,  $h = 2500\text{mm}$ , located below the long patch

None of the above analyses were completed successfully. The first thought was that the large areas of the patches led the analysis to crash, and the patches were reduced. The photos of the damage are the main source of inspiration for the creation of load cases. The load distribution which proved to be successful, is made from a visual estimate based on the deformation seen in photo 3.3. This load is also used as the first load case in the full analysis, and can be seen in figure 4.7.

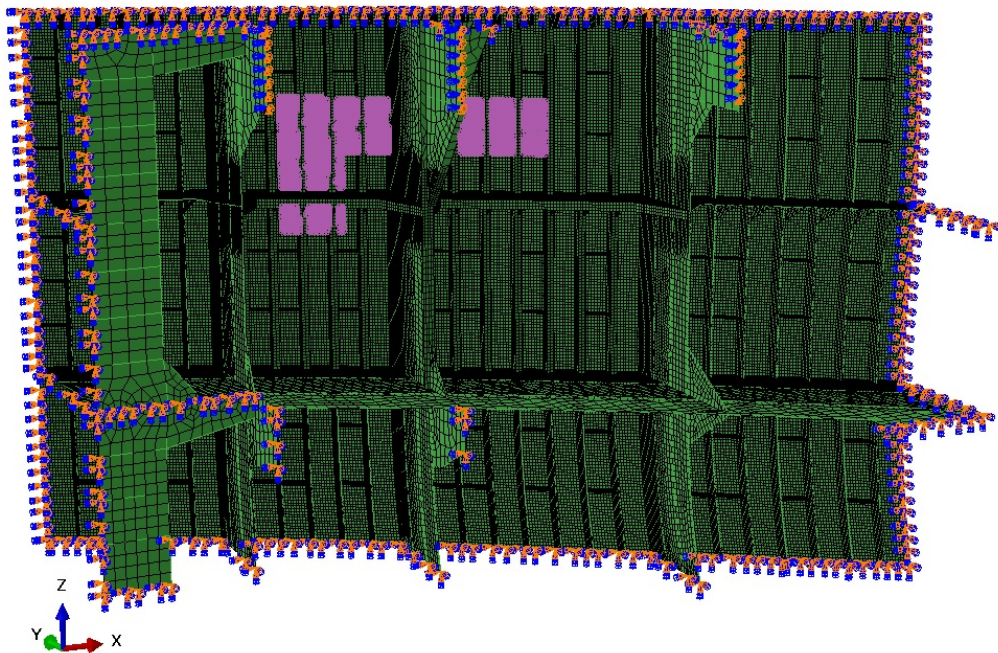


**Figure 4.7:** Load and boundary conditions applied in LC1, from Abaqus

- **LC1:**
  - Uniform pressure

- Reference load =  $5\text{MPa}$
- L-shaped area about  $5.78\text{m}^2$
- **LC2:** Same as LC1, with horizontal patch part extended to web frame #237, adding  $1.40\text{m}^2$  to the area of LC1
- **LC3:** Same as LC1, including patch extending to web frame #230, adding  $1.96\text{m}^2$  to the area of LC1

LC3 aborted early in the analysis, and thoughts were given to whether the patch was too big again, but after running two additional analyses with load centred about #230, as listed below, it became clear that the area was not the problem. For more details, see Chapter 4.5.

- **LC4:** Patch at #230 with an area of  $2.73\text{m}^2$
- **LC5:** Same as LC4, including a patch below the original patch, adding  $1.37\text{m}^2$  to the area of LC4

In the load cases the reported water line is ignored as the patch location is purely based on the deformations in photographs. Figure 4.8 shows LC2 and how the patch from LC1 is extended. Figure 4.9 shows the load patch for LC3.

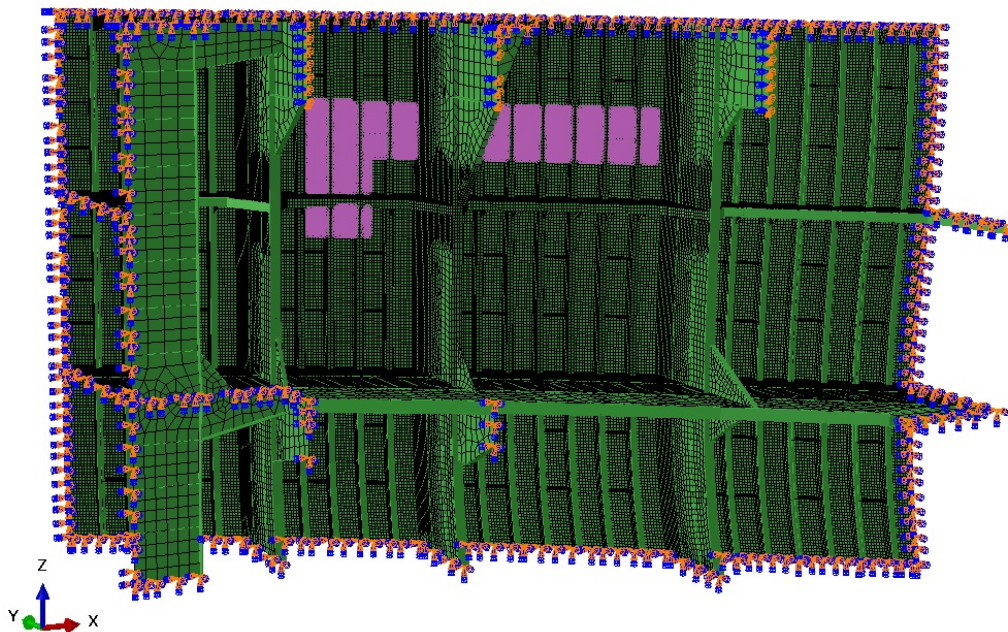


**Figure 4.8:** Load distribution of load case 2

Figure 4.10 shows how the patches in LC4 and LC5 are applied. The upper horizontal rectangle belongs to LC4, while the lower vertical rectangle is added in LC5.

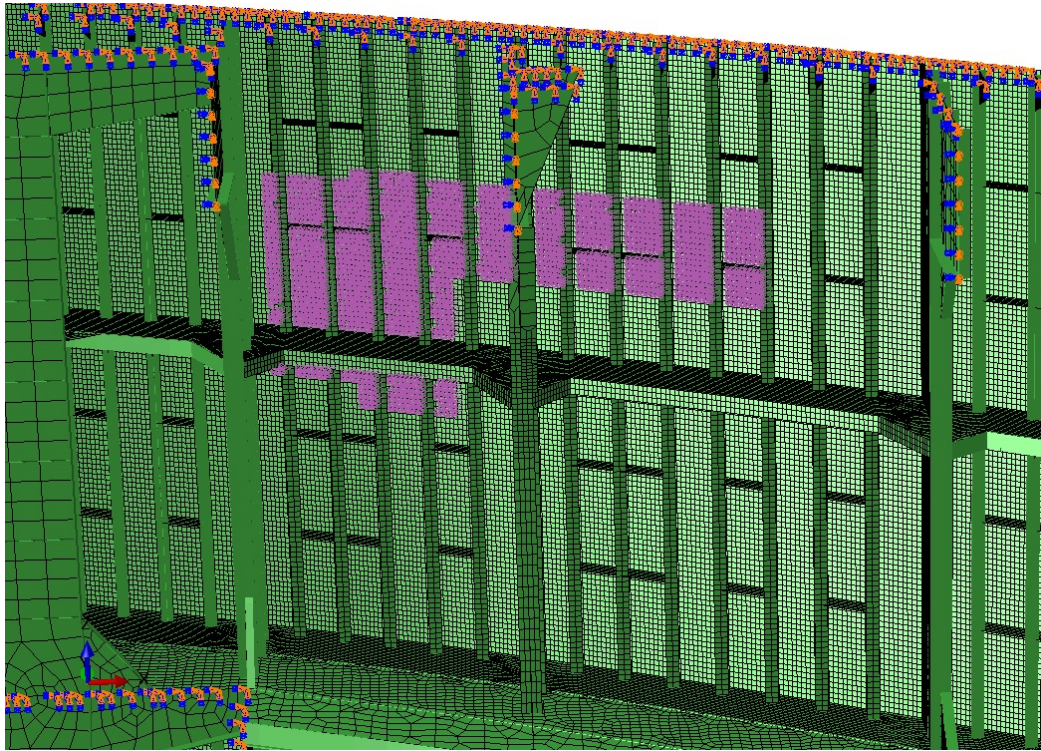


**Figure 4.9:** Load distribution of load case 3

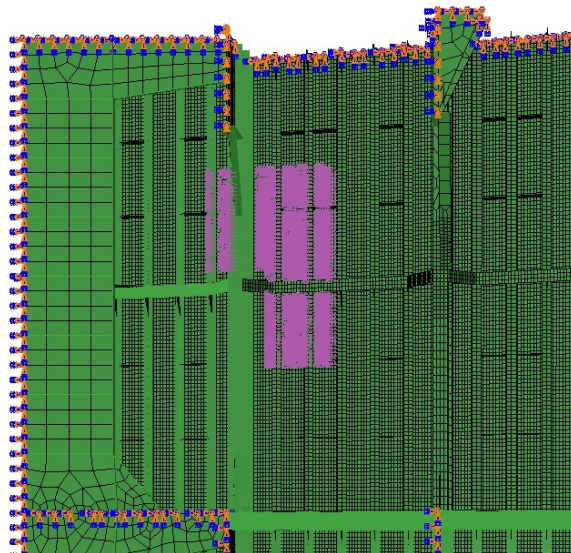


**Figure 4.10:** Load distribution of load case 4 and 5

## 4.5 Analysis Challenges

For the main analysis of this thesis a lot of time and effort was put down to make a complete model of the damaged area. The initial idea was to end the model at larger structural parts, to make the choice of boundary conditions easier. This will be discussed in the following sections. Figure 4.11 shows the first version of the main analysis model. The geometry is modeled in Patran.

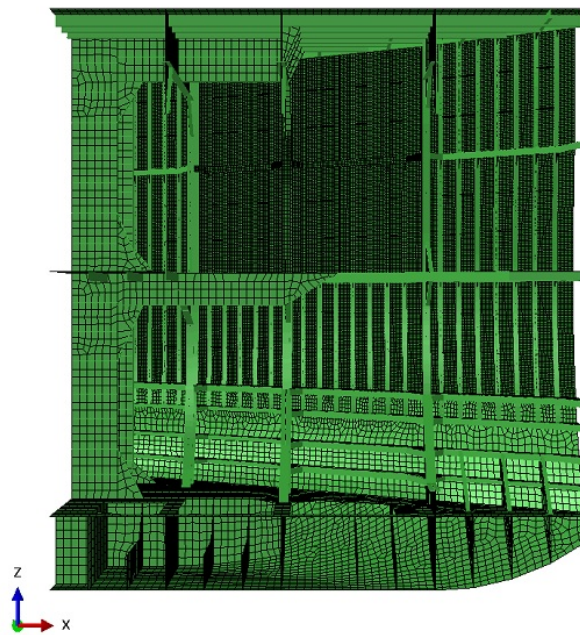


**Figure 4.11:** The full model as it initially was intended to be, seen from center line

Several test runs were performed for the first version of the model without any success. The analyses aborted and reported error messages long before the desired deformation of the ship side was reached, and one point the analyses didn't start at all. Some of the errors was related to mistakes done while creating the mesh, and will be discussed in the next section. But even after correcting the element errors Abaqus still was not able to complete a desired analysis. After having changed the mesh, the elements, loads, boundary conditions, and materials without any luck the problem appeared to be the size of the model. Large plastic deformations are observed in the damage area, and even though the damage area in total covers most of the ship side of the model, severe deformation of individual frames or web frames are small compared to the whole model. Every member of the model can be considered as a spring when the material is in the elastic region. The

model is loaded at the port side with high pressure patches, and fixed against displacement and rotation at the center line. (The model is fixed other places as well and this will be discussed in the following section, but is left out here to simplify the explanation of the model problems.) The deformed area stretches about 2m from the shell and towards the center line. This means that about 7/9 of the members between the center line and the shell acts as springs compressed between the load and the translation and rotation constraints. These springs make it very hard for Abaqus to mathematically control the deformations happening at a distance in the model. When running the analysis with Riks Abaqus will try to unload the structure when a load carrying member is about to collapse. This unloading procedure becomes difficult when there are a lot of springs in between interacting with the response from the collapsing member. One solution to this problem is to remove some of the springs, hence reduce the model in y-direction, removing members that didn't have considerable deformations. In z-direction the double bottom and some of the lower side shell with frames was removed to cut back run time and file sizes. This was done under the assumption that the members in question is located at a distance from the damage area great enough to not have any influence. Figure 4.7 shows the reduced model used in the analyses.

The preliminary model was limited in positive z-direction because the fore peak tank top seems to be little deformed and a good place to apply boundary conditions. However, in a report of the improvement of the damage area, provided by ship owner, the ice damage is sketched to go over a metre above the fore peak tank top, see figure 3.1. Since the draught of the vessel was assumed to be about 13m when the damage occurred, thick ice could have inflicted deformations above the fore peak tank top. On the other hand, the report on the damage improvement shows that the shell plating and frames was replaced only from the tank top and below. This should be proof that no great deformations was seen above the tank top. In addition, the area above the tank top wasn't mentioned in the surveyor report. A model including structure above the fore peak tank top could have been created, and analyses run to compare with results from the models stopping at the tank top. Due to the limit in time, such a model was not created.

The material curves proved to be challenging to estimate due to the sparse information available in the material certificates. Thoughts were given to estimating curves with a curvature illustrating the strain hardening, e.g. using the method of the "Power law" or "Ramberg-Osgood", but this was not done as the material is only a small part of the whole thesis and the time limited. Another material feature considered is the fracture criterion. In the material certificates the strain percentage at fracture is given. By using the element length as basis one can calculate the elongation of the element to fracture in mm, and specify this in a fracture feature in Abaqus. The only fractures seen in the photographs are at minor details



as brackets, therefore this property is excluded from the analyses.

The B31 beam elements appeared to be a problem in areas of large deformations; the elements are not made for extreme distortion and displayed the response of the structure poorly. The challenges with the beam elements were simply solved by deleting all beam elements in the area under the highest load and replacing them with shell elements. This is seen as the darker area in the middle of the model in figure 4.11. Figure 4.12 shows to the left the junction of the 2<sup>nd</sup> side stringer and bracket by web frame #233. To the right is the same junction at web frame #237. First of all, the geometry is erroneously modelled since the end flange of the stringer is supposed to end at the web frame, not at the bracket. In addition, the flanges should have been sniped and not connected. When looking

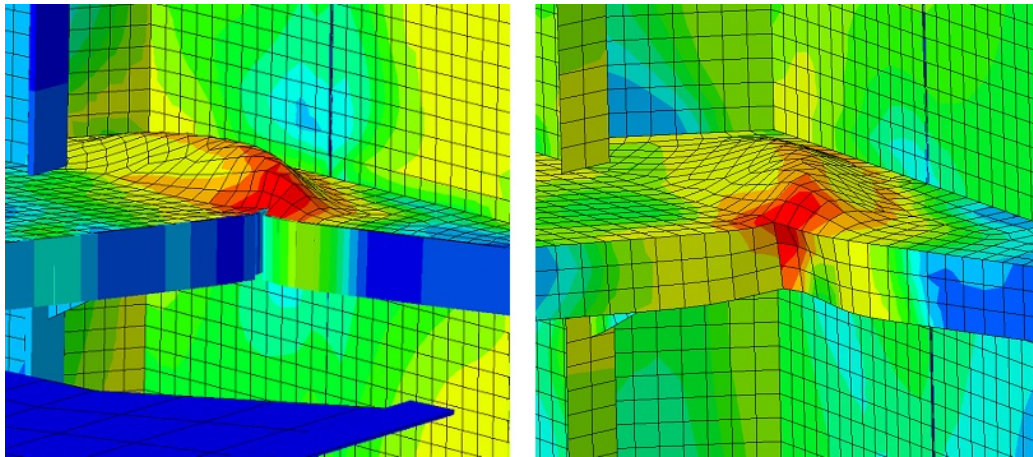


**Figure 4.12:** Deformed stringer junction with beam and shell elements, respectively - von Mises stress distribution

at the stress distribution it is clear that the shell elements gives the most precise stresses. Also, since the beam elements have a height to width ratio of 6:1, the deformations are very poorly expressed with the beam elements to the left. The online Abaqus Manual states: “Abaqus assumes that the transverse shear behavior of Timoshenko beams is linear elastic with a fixed modulus and, thus, independent of the response of the beam section to axial stretch and bending.” In other words, the B31 beam elements are not designed for nonlinear analyses and should not have been included in the model in the first place.

It’s conservative to assume the tank top to be completely rigid, especially when the load is applied very close to the boundary, and even to elements which which together makes the boundary. By fixing all DOF at a boundary, the structure will quite stiff in this area. This means that the fixation at the tank top can prevent the

model to deform to a degree similar to the real ship. Which in the next step can lead to over-prediction of the force needed to deform the ship side.

The uncertainty connected to the geometry modeling, materials, elements, and boundary conditions discussed above, make these factors contributing to potential modelling errors.

### 4.5.1 Verification of the Model

The results gained from the initial test analyses appeared to be quite large, in the range of  $7\text{MPa}$ . Even though the nominal pressure used for calculation of the design ice pressure in the FSICR is  $5.6\text{MPa}$ , see equation (2.1), some checks of the model were done to see if the forces and energy are in equilibrium. The first check is the control of the reaction forces: the reaction force shall be equal to the applied force. Figure 4.13 shows the comparison plots of the applied force (ice

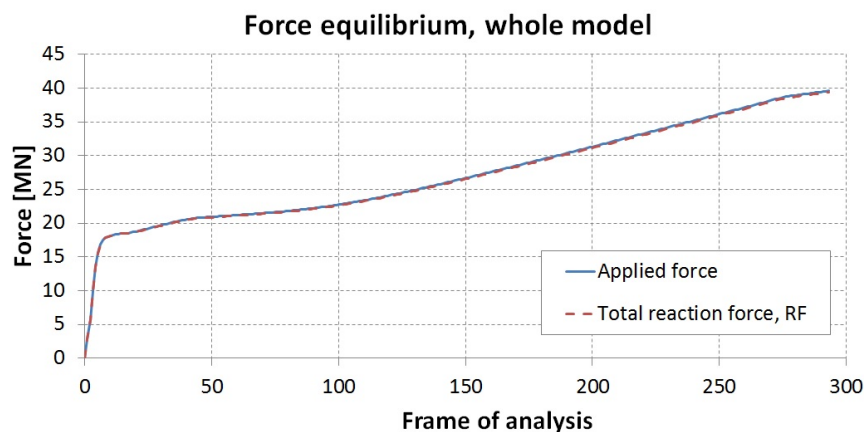


**Figure 4.13:** Curve of the applied force and the reaction force

pressure over a patch) and the total reaction force. The two curves are basically on top of each other, which means that all of the force applied is correctly absorbed as reaction force. The largest difference between the curves is 0.6%, in other words negligible.

The next control done is the energy equilibrium. Figure 4.14 shows the curve for the external energy applied to the model, and the energy absorbed by the model; internal energy. The curves are coinciding, which means that all the external work is correctly absorbed as deformations and strain.

The two curves above verify that the analyses are in equilibrium, and that no numerical errors arise.

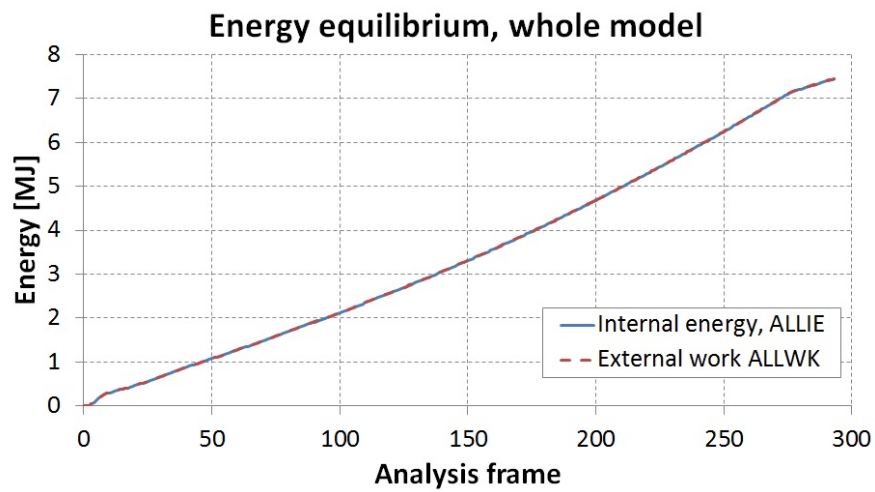


**Figure 4.14:** Curve of the internal energy and the external work



# Chapter 5

## Results from Finite Element Analyses

Three different models are used for analysing the ice loading and deformation response. The simplest model is a single frame, the second is two neighbouring frames with tripping brackets in between, and the third is the main model which is the whole length of the fore peak tank.

All the following results have been found using the “General, Riks” procedure in Abaqus, hence the magnitude of the applied load does not matter since it is only used as a reference throughout the analysis.

### 5.1 Simplified Frame Analyses

The two frame models, the single and the double, are analysed first with the load located at the centre of the frame span. Next the same analyses are done with the load located at the water line.

#### 5.1.1 Initial Loads, Centred

Figure 5.1 shows the load-displacement curves for the single and double frame with the span centred loading calculated from the FSICR in chapter 3.9. The load deformation is plotted for the node at the center of the plate flange; at the largest deformation of the frame. Both of the curves have a steady slope at lower loads since the material here is in the elastic range. As the load increases the slope

decreases as the material yields and reaches the plastic region. In the plastic region the slope is positive but small compared to the slope in the elastic region, until it reaches the ultimate strength of the material. Here the curve is flat. After this point the frame doesn't have any more capacity and the slope of the curve is negative. The frame will continue to deform but not as much load as before is required to do so. Note that the double frame deforms at a lower load level than the single frame. This is because the load is given as a pressure, and for the double frame the area to which the pressure is applied is the double of the single frame area. The dark dot on the single frame curve indicates the frame capacity calculated in Chapter 3.9. Since the rule formulas don't have displacement as a variable the value is inserted where the curve from the analysis is equal to the capacity load. The corresponding displacement indicates at which analysis displacement the rule capacity is expected to be reached. The formula for the capacity is derived for a single frame, therefore the curve for the double frame doesn't have a similar dot.

**Table 5.1:** Initial load analysis for center loading, FSICR rules

Frame	$h$ [mm]	$w$ [mm]	$P_{max}$ [MPa]	U2 at $P_{max}$ [mm]	$P$ at U2 = 168mm[MPa]	$F_{max}$ [MN]
Single	300	470	14.46	123	1.93	2.04
Double	300	940	8.96	68	7.8	2.53

Table 5.1 gives some key values from the plot in figure 5.1.  $h$  is the load height, and  $w$  the load width.  $P_{max}$  is the capacity of the frame for the given loading, and in the following column the displacement at the capacity is given. The desired deformation is 168mm as measured for frame #232 1/2 in table 3.1. The force  $F_{max}$  is simply found by multiplying the capacity load pressure by the patch area.

**Table 5.2:** Initial load analysis for center loading, IACS PC rules

Frame	$h$ [mm]	$w$ [mm]	$P_{max}$ [MPa]	U2 at $P_{max}$ [mm]	$P$ at U2 = 168mm[MPa]	$F_{max}$ [MN]
Single	300	470	2.94	147	2.9	3.31
Double	300	940	1.65	98	1.53	3.70

Figure 5.2 shows the load-displacement curves for a single and a double frame loaded at a span-centred patch calculated according to the IACS PC rules for frame capacity. The double frame deforms at a lower load level than the single frame since the single frame has only half the area of the double frame. Table 5.2 shows the key values from figure 5.2. Figure 5.4 and 5.5 are taken from the visualization in Abaqus' output database for the analyses with centred loading. The frames loaded with the FSICR load patch have sharp bend in the location of the applied

load. The IACS PC loading gives a more smooth curvature of the frames. The deformation is scaled 1:1.

To make it easier to compare the frame analyses with centred loading, the force is plotted as a function of displacement in figure 5.3. The frames under IACS PC loading are able to withstand higher loads than the frames under FSICR loading because the load in the latter case is applied to a very narrow area, almost acting as a point load on the frame.

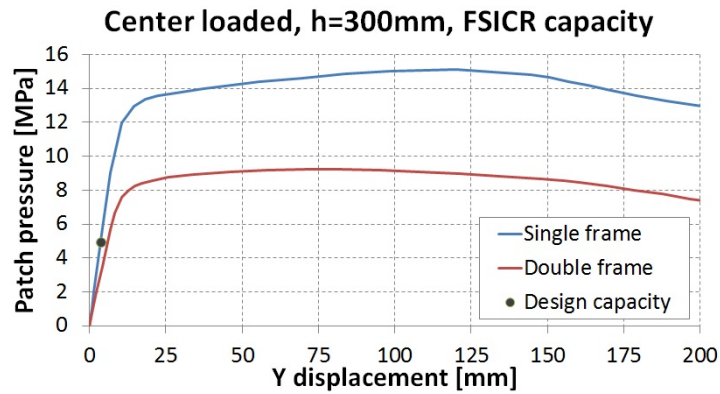


**Figure 5.1:** Load-displacement curves for frames under FSICR capacity loading

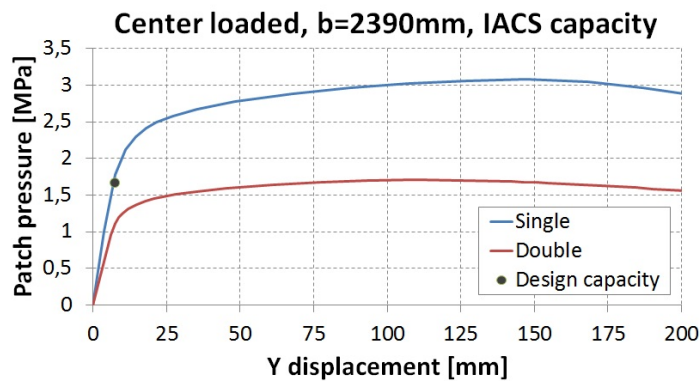


**Figure 5.2:** Load-displacement curves for frames under IACS PC capacity loading

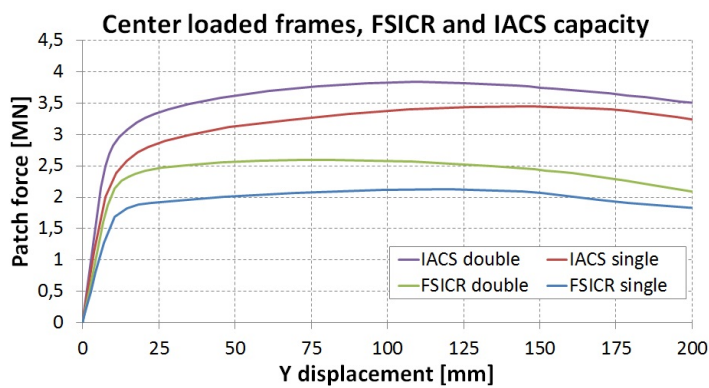


**Figure 5.3:** Force-displacement curves for centred loaded frames, FSICR and IACS



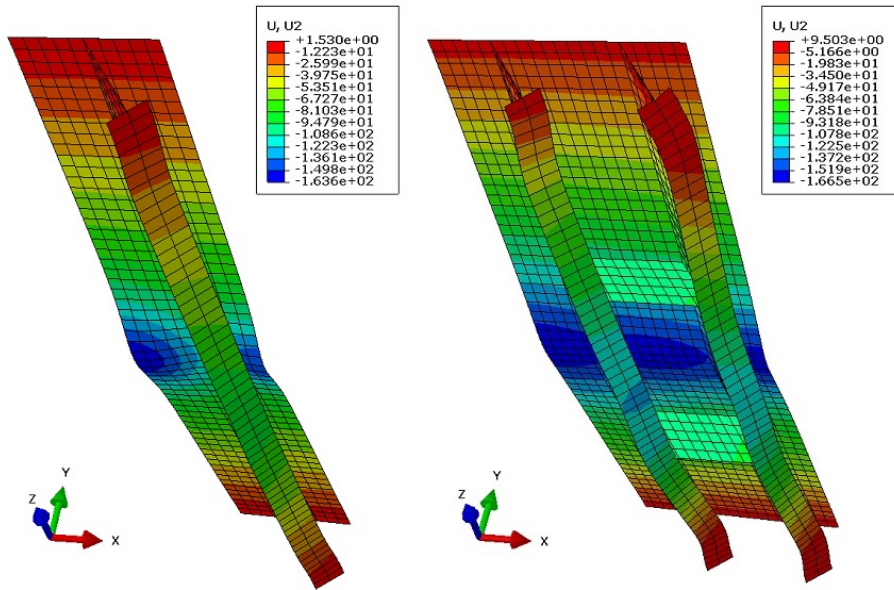


**Figure 5.4:** Distribution of U2 displacement at  $U2_{max} = 168mm$ , for single and double frame with centred FSICR patch

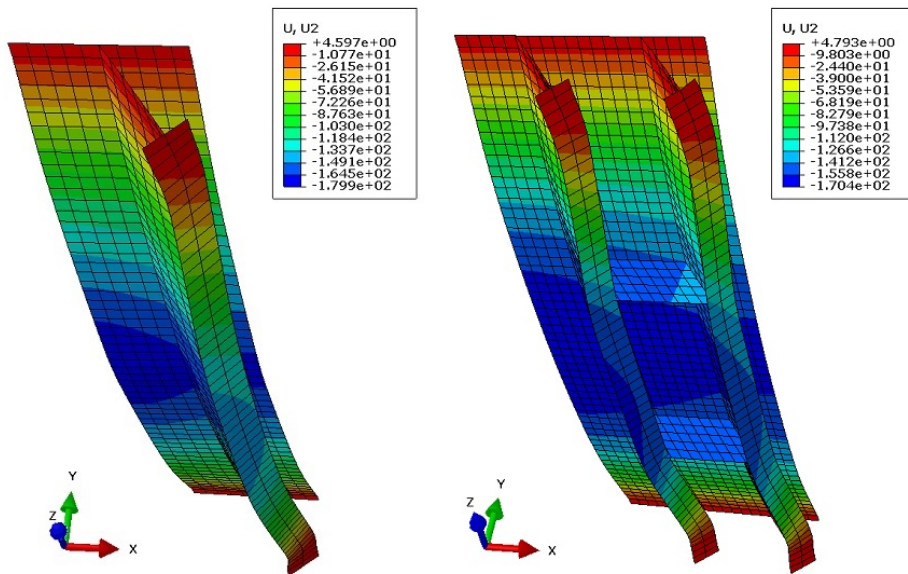


**Figure 5.5:** Distribution of U2 displacement at  $U2_{max} = 168mm$ , for single and double frame with centred IACS PC patch

### 5.1.2 FSICR and IACS Ice Patch Analysis of Single and Double Frame

In the following two analyses the load patches are located at the water line. Figure 5.6 shows the load displacement curves for the single and double frame under FSICR loading. Note that the capacity of the frames are higher when the load is located towards one of the ends of the frame. The difference in  $P_{max}$  is only 6% for the double frame, while it's 32% for the single frame. This is because the loading acts more as a shear loading as it is located further away from the centre of the frame. The combination of shear and moment capacity will make it possible for the frame to withstand a higher loading. Table 5.3 shows the input and result for the frame analysis in figure 5.6.

**Table 5.3:** Results from nonlinear FEA of single and double frame with FSICR patch at water line

Frame	$h$ [mm]	$w$ [mm]	$P_{max}$ [MPa]	U2 at $P_{max}$ [mm]	$P$ at U2 = 168mm[MPa]	$F_{max}$ [MN]
Single	300	470	19.08	120	18.5	2.69
Double	300	940	9.56	42	8	2.70

Figure 5.7 presents the load-displacement curves for the single and double frame analysis with IACS patch centered at the water line.

The results from the frame analyses are shown in table 5.4. As for the water line patch from the FSICR the capacity for the water line IACS PC patch is somewhat higher than for the centered patch. The difference is less for the latter since the patch height is close to the frame span.

**Table 5.4:** Results from nonlinear FEA of single and double frame with IACS patch at water line

Frame	$h$ [mm]	$w$ [mm]	$P_{max}$ [MPa]	U2 at $P_{max}$ [mm]	$P$ at U2 = 168mm[MPa]	$F_{max}$ [MN]
Single	2390	470	3.03	139	3.00	3.40
Double	2390	940	1.69	89	1.50	3.80

Figure 5.8 gives the force-displacement curve for the four analyses with ice load patches at the water line. Figure 5.9 and 5.10 shows the displacement distribution and deformation of the frames under loading at the water line. The FSICR patch

**Table 5.5:** Results from nonlinear FEA of single and double frame with patch at water line

<b>Frame</b>	<b>Rule</b>	<b>Load height</b> [mm]	<b>Load Width</b> [mm]	<b><math>F</math> at U2 =</b> 168mm[MN]
Single	FSICR	300	470	2.69
Double	FSICR	300	940	2.70
Single	IACS	2390	470	3.40
Double	IACS	2390	940	3.80

results in a sharper bend in the frames than for the frames with IACS PC patch. The deformations are also more distributed for the latter.

Table 5.5 gives an overview of some of the key numbers of the above analyses. The last column gives the force needed to reach the desired deformation of 168mm for each of the four cases.

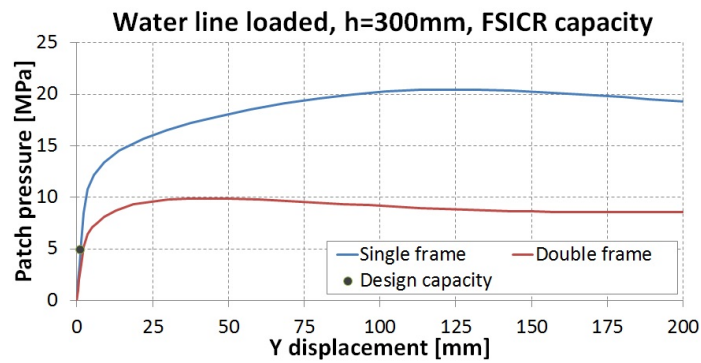


Figure 5.6: Load-displacement curves for frames under FSICR capacity loading

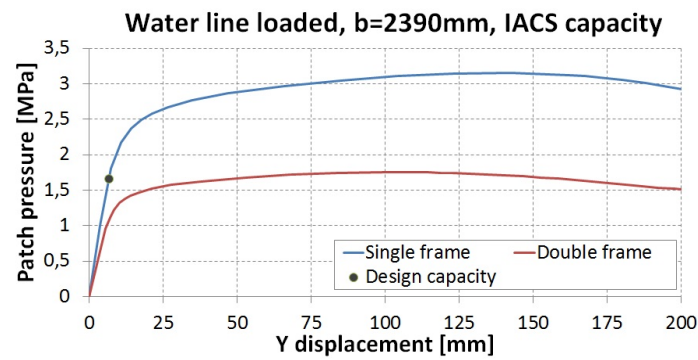


Figure 5.7: Load-displacement curves for frames under IACS capacity loading

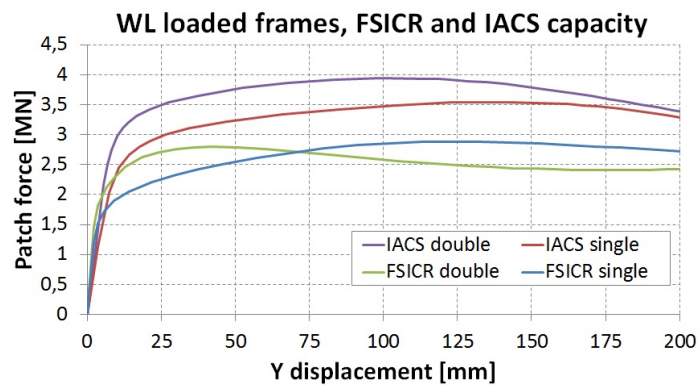
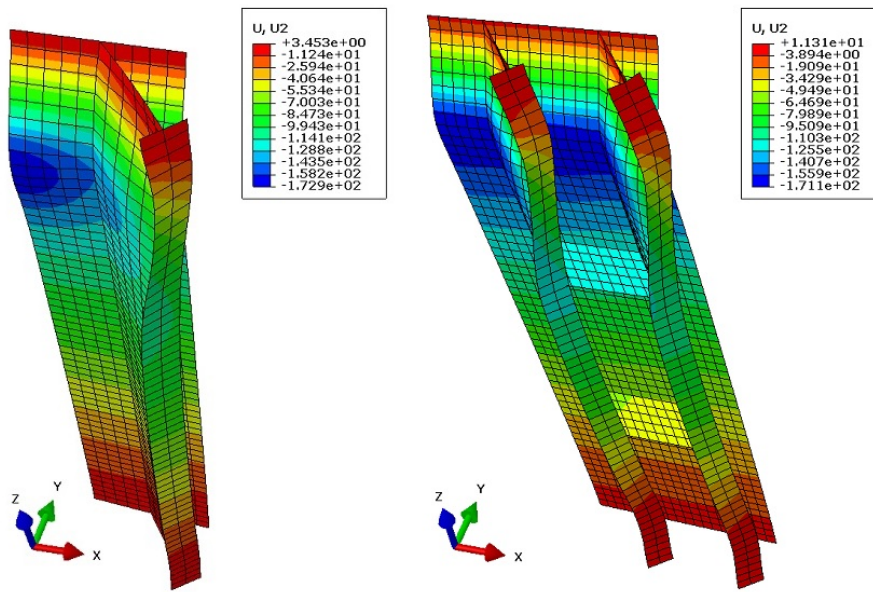
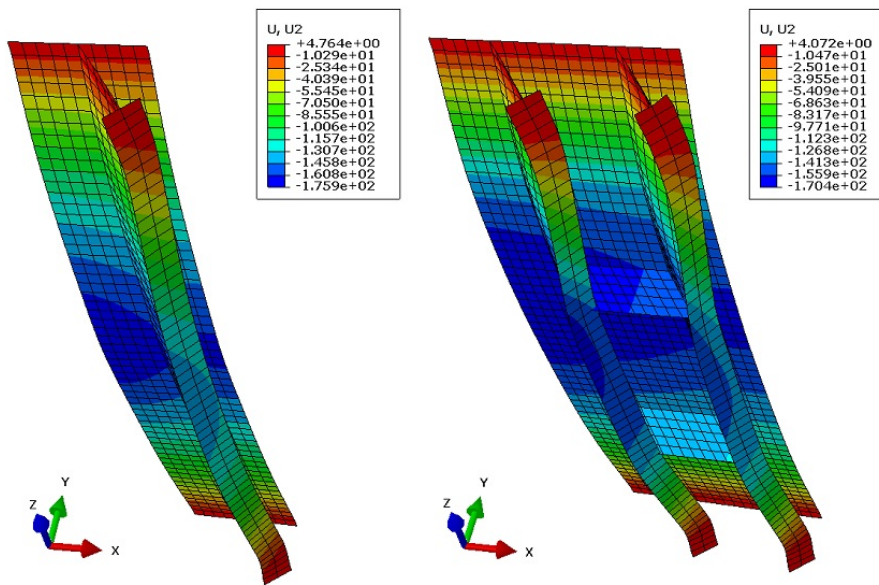


Figure 5.8: Force-displacement curves for frames under loading at the center line



**Figure 5.9:** Distribution of U2 displacement at  $U2_{max} = 168mm$ , for single and double frame with FSICR patch at the water line



**Figure 5.10:** Distribution of U2 displacement at  $U2_{max} = 168mm$ , for single and double frame with IACS patch at the water line

## 5.2 Main Model Analysis

The main model has been analysed in Abaqus using “General, Riks” with nonlinear geometry. The first load cases analysed are the rule calculated frame capacity loads. Following are different load cases suggested to mimic the real deformations.

### 5.2.1 Analysis with FSICR and IACS Ice Patch

The first analyses performed with the main model were the “LC FSICR” and “LC IACS” from chapter 4.4.3. Figure 5.11 shows the load-displacement curve from the analysis with FSICR ice patch. The pressure is applied over a relatively small area compared with the area from IACS PC, and a very high loading is obtained. The deformation is linear in the start and the structure absorbs the loading without deforming much. At about  $13MPa$  however, web frame #233 starts to collapse and a sharp bend is seen in the curve. After this point the curve is relatively flat while the web frame deforms. The neighbouring frames starts resisting the load as the slope of the curve increases again. In the visualization of the output database from the analysis it was discovered that the frames actually deform through the shell plating from patch pressure equal  $31MPa$ . This is possible because the load is narrow giving large deformations in a limited area, and because contact between elements wasn't defined in the element model. In the figure the curve is stippled after this point of contact, and here the curve is not realistic. Figure 5.14 shows the deformed ship side with frames deformed through the shell.

Figure 5.12 shows the load-displacement curve from the analysis with the IACS ice patch. Here, as well, the curve is steep and approximately linear in the start where mainly the shell and frames aft of web frame #233 deforms. At  $2.2MPa$  the web frame collapses rapidly and deforms under the loading with little increase in resistance. In the following the resistance increases as the neighbouring frames absorb more of the loading. At  $35.6MPa$  another collapse occurs. This time it is the bottom part of the flange of web frame #233, as seen in figure 3.12. Note that the curve stops at a deformation equal  $200mm$ . This is because Abaqus has had problems finding equilibrium in the calculations and hence been tanking very small increments. Due to lack of time no new analyses were run trying to obtain the desired deformation of  $285mm$ .

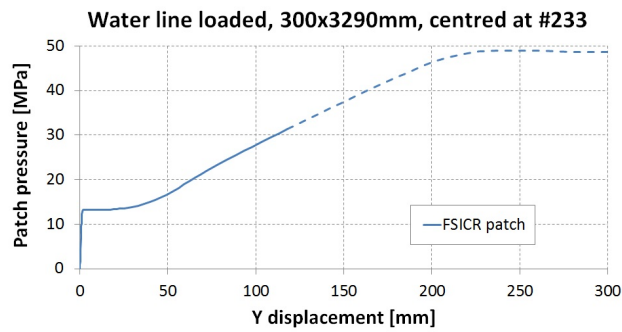


**Figure 5.11:** Load-displacement curve of main model loaded with FSICR patch at water line and web frame #233

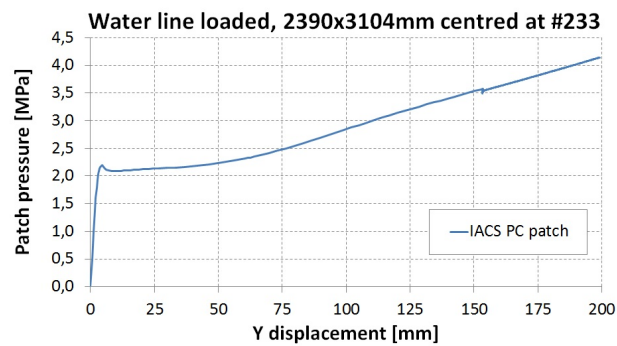


**Figure 5.12:** Load-displacement curve of main model loaded with IACS patch at water line and web frame #233

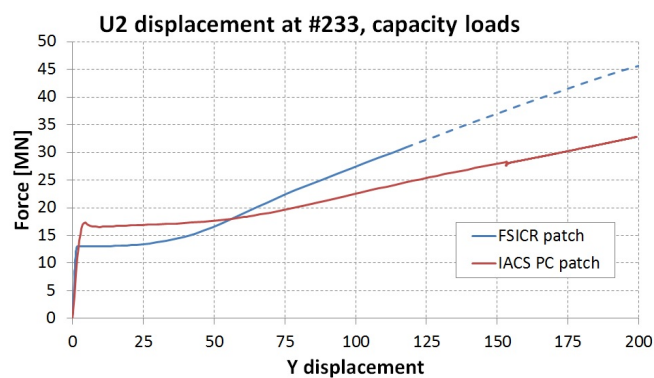


**Figure 5.13:** Load-displacement curve of main model loaded with IACS patch at water line and at frame #232<sup>1/2</sup>

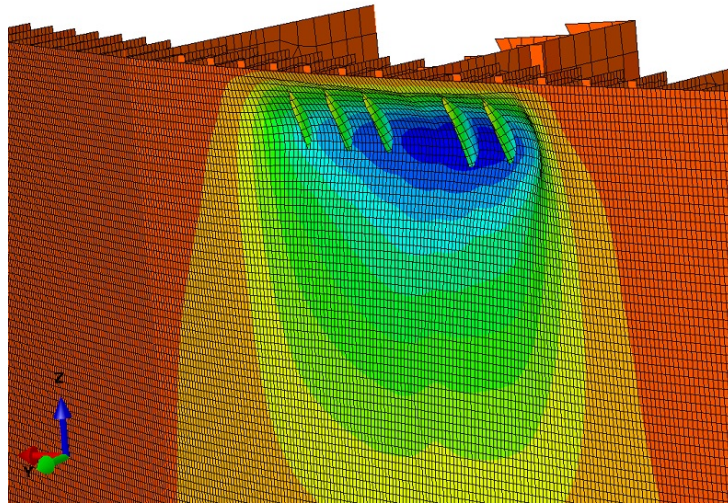


**Figure 5.14:** Distribution of U2 displacement at  $U2_{mac} = 285mm$ , FSICR patch

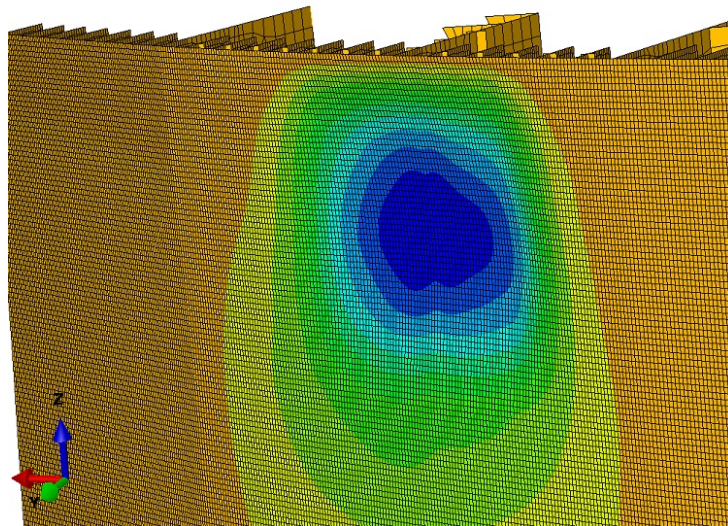


**Figure 5.15:** Distribution of U2 displacement at  $U2 = 200mm$ , IACS PC patch



For comparison are the force-displacement curves for the two analyses up to  $U2 = 200mm$  plotted in figure 5.13. With the larger patch area for load application the model with the IACS patch is able to absorb more loading in the elastic region than the model with the FSICR patch. At  $18MN$  the two models absorb the same amount for loading for the same displacement of web frame #233. After this point the FSICR patch model is actually able to absorb more loading than the IACS PC patch model. This is because the patch is narrow and only a part of the frames have large deformations, while a sufficient part of the frames are deformed under the larger IACS PC patch. But again, from  $32MN$  and out the FSICR patch curve is invalid due to the lack of physical interaction of the elements in the model. Here the curve is stippled.

Some key numbers from the plots are given in table 5.6. Due to the analysis problems no values are available for the desired web frame displacement of  $285mm$ .

**Table 5.6:** Results from nonlinear FEA of main model with FSICR and IACS PC ice patch at water line

<b>Patch</b>	$h$ [mm]	$w$ [mm]	$P_{max}$ [MPa]	<b>U2 at <math>P_{max}</math></b> [mm]	<b><math>P</math> at <math>U2 = 285mm</math></b> [MPa]	$F_{max}$ [MN]
FSICR	300	3290	31.34	118	-	30.93
IACS	2390	3104	4.14	199	-	32.79

## 5.2.2 Analyses with Proposed Load Cases

In the following the results from the proposed load cases, LC1-LC5, are presented.

### Results from LC1 Analysis

The first load case run purely with the intent of reproducing the ice damage, is load case 1 (LC1) from Chapter 4.4.5. Figure 5.16 shows the distribution of displacement in U2 for the whole model. The loading results in a deformation of the model which at first glance looks like the desired deformation. Note the resemblance to the shaded area in figure 3.1. One of the nodes in the darkest blue area is selected for the plotting of the load displacement curve in figure 5.17. The first part of the curve is linear, where the material is in the elastic range, up to about  $2.3MPa$  patch pressure. After this point the plastic range is entered and the displacement increases quicker than the load is increased, thus giving a curve with

a less steep slope. At about  $3.6\text{MPa}$  and  $77\text{mm}$  a small vertex is present. By investigating in the analysis results it is observed that the reason for its existence is the collapse of web frame plating #233. It's reasonable to expect this collapse since the load is located about the web frame. After the vertex the slope is a bit less steep again before increasing into a fairly constant slope. Figure 5.18 gives the distribution of von Mises stress for the whole model in LC1.

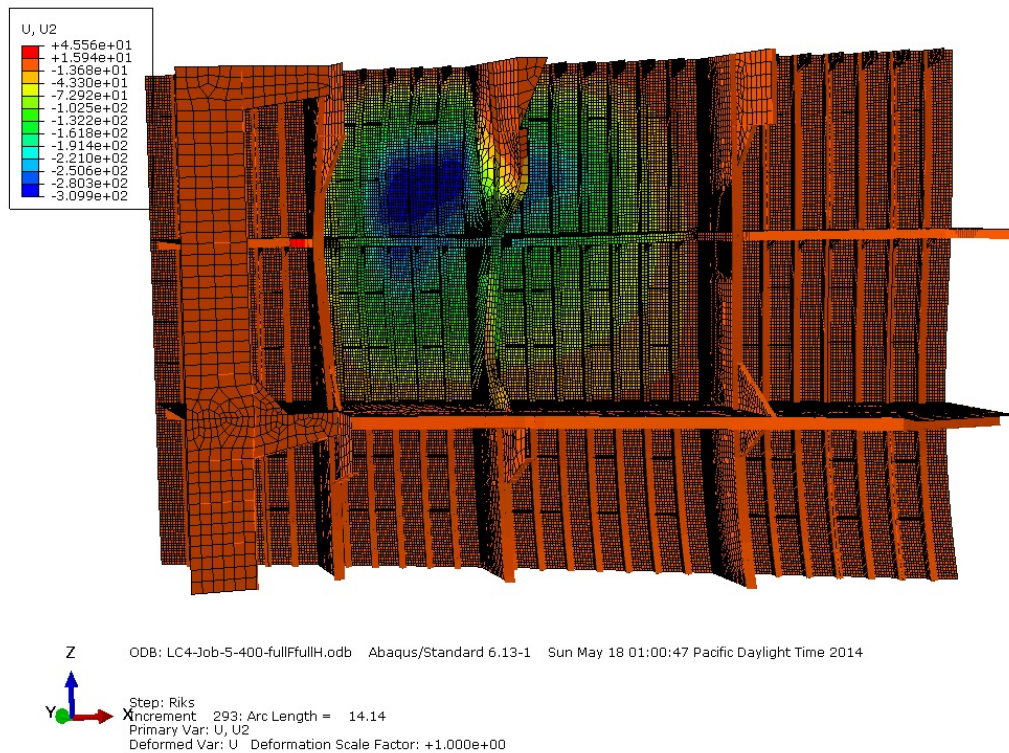


**Figure 5.16:** Distribution of U2 displacement for LC1

Table 5.7 and 5.8 gives a comparison of the displacement values measured from the photos and on the deformed model after analysis. In general, the measurements from the photos seem underestimated compared to the analysis measurements. The deformation in U2 direction (which equals negative y-direction) of web frame #233 has been used as a reference when running test analyses of the model. Note therefore that the two numbers are almost the same. For web frame #230 on the other hand, the deformation in U2 is too low in the model compared to the photo measurement. Regarding the U1 displacement of web frame #233, attention should be paid to figure 6.5 where the upper bracket and bracket flange of web frame #233 appear to have a larger deformation than seen in the photos.

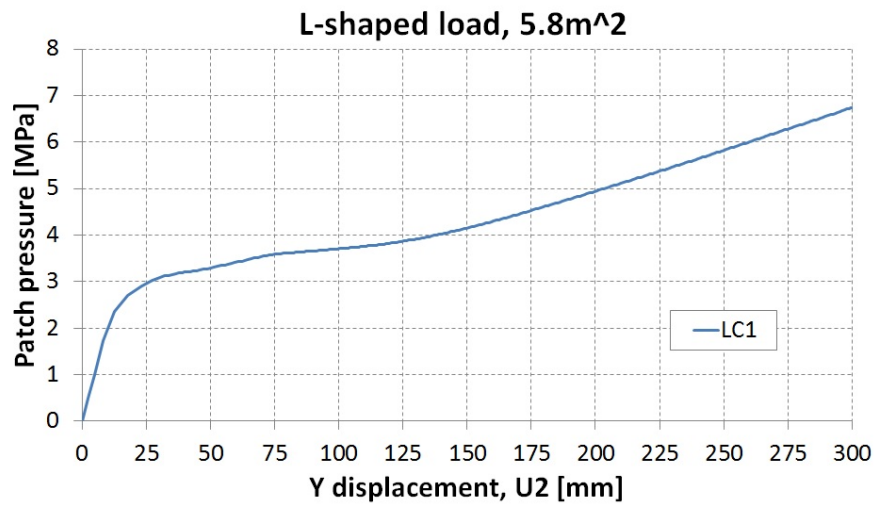


Figure 5.17: Load-displacement curve for LC1

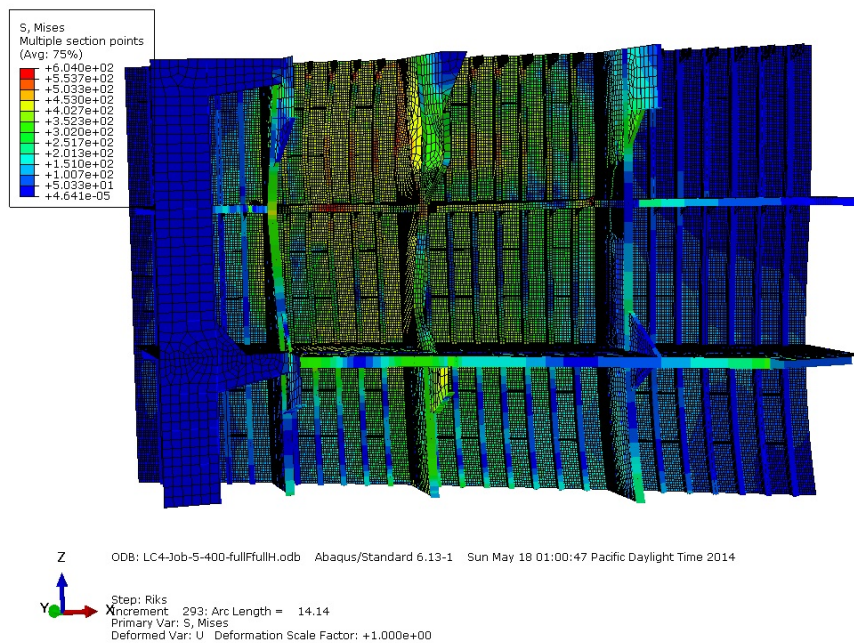


Figure 5.18: Distribution of von Mises stress for LC1

Following are the measurements for the frames between bulk head #227 and web frame #230. Here the numbers measured from the model are basically zero. Next are the displacements of the frames from web frame #230 to #233. The numbers from the model is considered to be the most reliable since these coincide with

**Table 5.7:** Comparison of measurements from photos and from analysis

Frame	Structure	Direction	Photo	Photo [mm]	LC1 [mm]
230	Web frame	U2	3.3	199	14
233	Web frame	U2	3.3	285	288
230	Web frame	U1	3.5	-212	-202
233	Web frame	U1	3.5	-50	-73
228½	Frame flange	U1	3.6	-17	0.2
229	Frame flange	U1	3.6	-27	0.6
229½	Frame flange	U1	3.6	-53	0.5
232	Frame web	U2	3.7	62	288
232½	Frame web	U2	3.7	162	287
233	Frame web	U2	3.7	85	288
231½	Frame flange	U1	3.7	50	128
232	Frame flange	U1	3.7	91	137
232,5	Frame flange	U1	3.7	80	140
232	Frame web	U2	3.8	100	270
232½	Frame web	U2	3.8	86	262
233	Frame web	U2	3.8	133	288

**Table 5.8:** Comparison of measurements from photos and from analysis

Frame	Structure	Direction	Photo	Photo [mm]	LC1 [mm]
233½ top	Frame flange	U1	3.9	42	23
233½ mid	Frame flange	U1	3.9	-66	-119
234 top	Frame flange	U1	3.9	-84	24
234 mid	Frame flange	U1	3.9	-17	-115
234½	Frame flange	U1	3.9	-94	-62
235	Frame flange	U1	3.9	-56	-80
235½	Frame flange	U1	3.11	-56	-25
236	Frame flange	U1	3.11	-56	-11
236½	Frame flange	U1	3.11	-27	7
232½	Frame flange	U1	3.12	-23	-13
234	Frame flange	U1	3.12	38	-14
234½	Frame flange	U1	3.12	31	-13

the measures from the photo of the exterior hull, and because the model has been tested and calibrated to give correct results in this area. The next three lines are measured in the same area but from a photo with a different view of the structure. The latter is assumed to give more correct numbers since the deformations are measured over a larger span, showing more of the global deformation. Even

though, the measurements are lower than numbers taken from the model. Next are the frames from web frame #233 to #237. Here as well differences are seen in the numbers.

### Results from LC2 Analysis

In figure 5.19 the load displacement curve from LC1 and LC2 are plotted together. The analysis of LC2 stopped before reaching a maximum displacement  $U_2$  of  $200\text{mm}$ . Therefore is no further comparison with the measurements from the photos done. It is observed that the curve for LC2 has a larger displacement than the curve of LC1, for a given load.

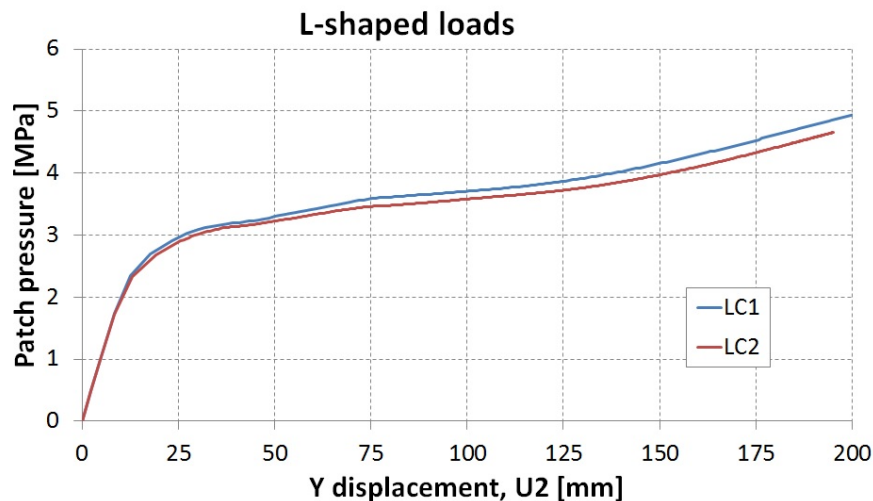


**Figure 5.19:** Comparison of load-displacement curve from LC1 and LC2

### Results from LC3 Analysis

The load-displacement curve of LC3 is given in figure 5.20. This analysis aborted even earlier than LC2, even though the load application area is smaller. It's also noted that the model under the LC3 loading enters the plastic region for a lower pressure than LC1 and LC2.

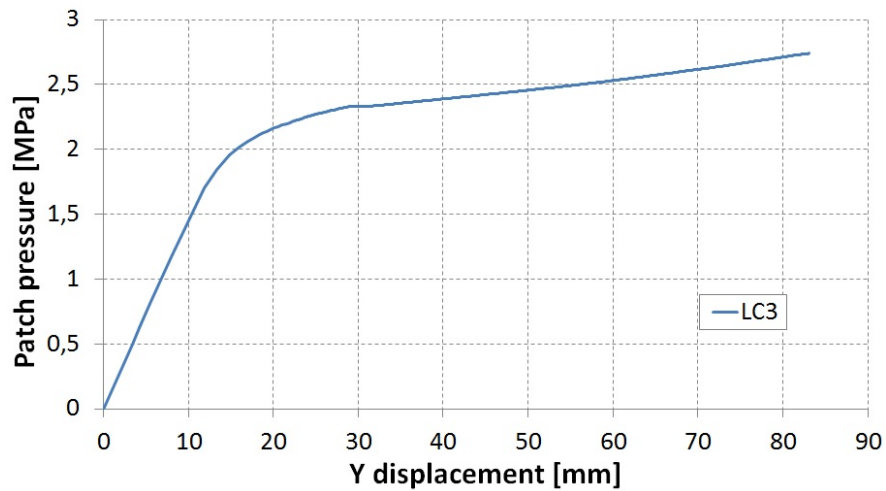


**Figure 5.20:** Load-displacement curve from LC3 analysis

### Results from LC4 Analysis

Figure 5.21 shows the load displacement curve of LC4. The vertex of the curve at  $U_2 = 27\text{mm}$  is the collapse of frame #230 $\frac{1}{2}$ . Unfortunately the analysis aborted at  $U_2 = 115\text{mm}$ . The analysis of LC5 gave a maximum  $U_2$  displacement of only  $29\text{mm}$  before aborting. Due to this and LC5's resemblance to LC4 the load-displacement curve of LC5 is excluded from the thesis.

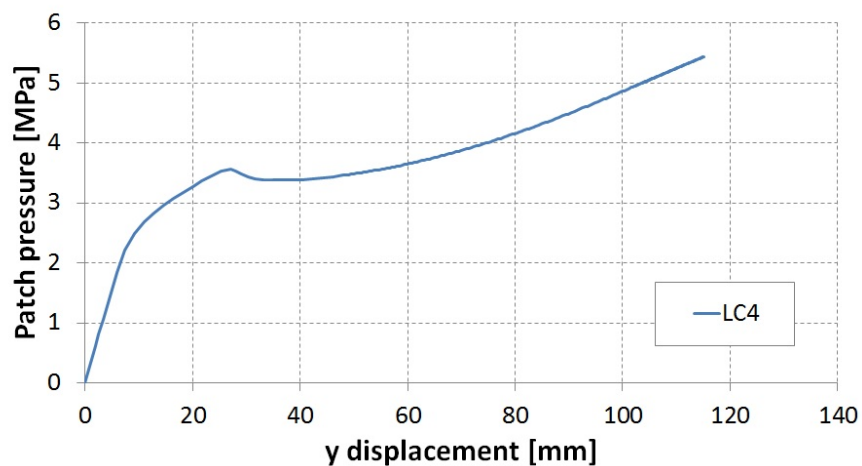


**Figure 5.21:** Load-displacement curve from LC4

# Chapter 6

## Discussion of Results

In Chapter 5 the results from the nonlinear finite element analyses were presented. In the following these results will be discussed.

### 6.1 Comparison of Analysis Results and Real Damage

The scope of the thesis is to find the load case that inflicts deformations which resembles the damage seen in the photographs. Hence, the focus of the Discussion is to compare the analysis results with the real damage.

#### 6.1.1 Single and Double Frame

For the frame analyses in Chapter 5.1 the desired deformation of  $168mm$  is obtained after the capacity of the frame is reached. Therefore, the loading at  $U2 = 168mm$  is lower than the maximum pressure the frames have resisted. Table 6.1 gives a summary of the capacities calculated in Chapter 3.9. The top line refers to from which theory the capacity is calculated and the two latter columns are respectively “elastic theory” and “plastic theory”. All of the numbers are given in  $MPa$ . Note that the capacities calculated from the FSICR and IACS PC are for a specific ice load height while the elastic and plastic theories assumes loading over the whole span of the frame.

Table 6.2 gives the capacities obtained in the nonlinear finite element analyses for span-centred and water line (WL) centred loadings. Note that the narrow FSICR

**Table 6.1:** Calculated capacities for a single frame, [ $MPa$ ]

<b>FSICR</b>	<b>IACS PC</b>	<b>El. theo.</b>	<b>Pl. theo.</b>
4.94	1.67	0.97	2.30

loading results in a high pressure, basically having the same effect as a point load. A point load will generally induce membrane and bending resistance while a more distributed load will induce bending and shear resistance. Membrane capacity is not included in neither the rules nor theories considered here and is a factor which increases the conservatism in design calculations. Thus, the FEA shows that the frames have a considerable amount of capacity beyond the level the rules and theory predict. For example does the single frame with water line centred FSICR patch loading resist a loading of  $19MPa$  while the predicted value is not more than  $5MPa$ . For the IACS PC patches however, the calculated capacities are much closer to the FEA results. For the frame with the centred IACS PC patch the resistance was about  $2.9MPa$  while the predicted capacity was  $1.7MPa$ . This is because little membrane resistance is active under the wide loading, and because the IACS PC rules accounts for shear capacity as well as bending capacity. Still, the FEA shows that the frames have more capacity than the rules predict.

**Table 6.2:** Capacities for a single frame from FEA, [ $MPa$ ]

<b>Centred FSICR</b>	<b>Centred IACS PC</b>	<b>WL FSICR</b>	<b>WL IACS PC</b>
14.46	2.94	19.08	3.03

In their IACS UR PC rule derivation Daley et al. state: “The design limit states used in the UR proposals are idealized plastic collapse onset mechanisms. The simplified mechanisms include conservative assumptions - for example, they ignore the beneficial effects from membrane stresses and strain hardening. Consequently, the real structure can be expected to have a substantial reserve capacity beyond the design condition. The design limit states thus represent a condition of substantial plastic stress, prior to the development of large plastic strain and deformations.” [13]. In other words, capacity calculations done following Daley’s formulations will give an underestimate of the structure capacity. This is easily seen from figure 5.2 where the “design capacity dot” is located at a pressure about half of the capacity of the (single) frame. Also, it should be noted that the scale of the x-axis makes it look like the “dot” is located in the elastic region of the curve. By changing the scale the “dot” appears to be located more correctly; in the start of the plastic region. See figure 6.1. A similar scaling would show a similar results for curves in figure 5.1, 5.6, and 5.7 as well.



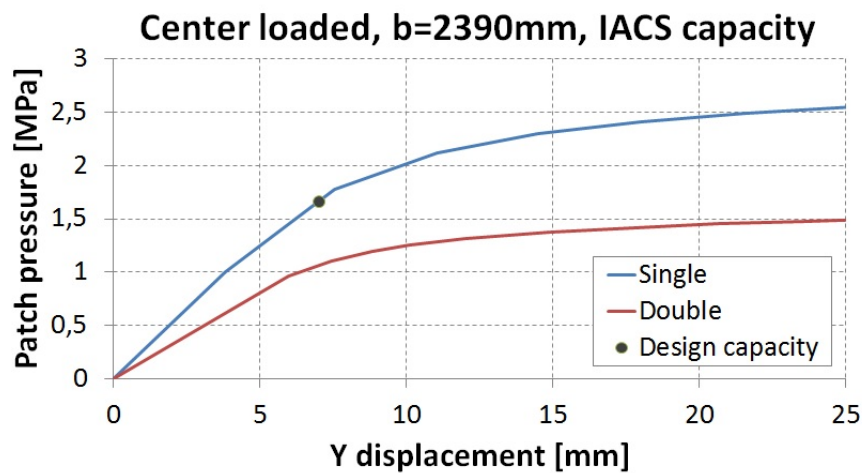


**Figure 6.1:** Transition from elastic to plastic region, from figure 5.2

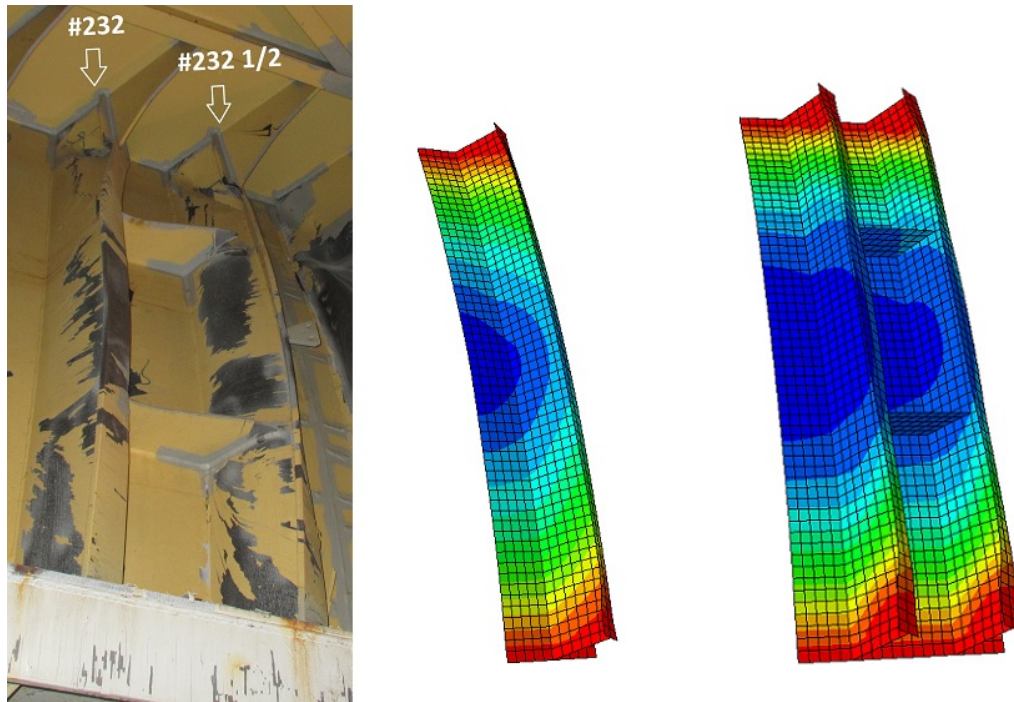
The FSICR gives an underestimate of the capacities, as well. However, where the conservatism comes from is more unclear in these rules. Several scaling factors are applied when calculating the design ice pressure, plate requirements, and frame scantlings, see Chapter 2.1, and the physics behind gets lost on the way.

Figure 6.2 shows a comparison of the frames in the ship with the largest deformations and the single and double frame from the FEA. The single frame is intended to be frame #232  $\frac{1}{2}$ , and the double frame to be frame #232 and #232  $\frac{1}{2}$  with tripping brackets in between. Generally the deformations seem to be similar. The lack of top brackets in the element models results in a more continuous deformation there than can be seen for the real frames in the photograph. In the photograph frame #232  $\frac{1}{2}$  seems to have more curvature to its web than obtained with the models. The models' webs resembles more the web of frame #232.

## 6.1.2 Main Model

### FSICR and IACS Ice Patch

The two first load cases for the main model were the patches calculated from the FSICR and IACS PC. By looking at the displacement distribution in figure 5.14 and 5.15 one can assume that neither was the loading which inflicted the deformation to the ship side. On the other hand, both analyses failed to reach the desired displacement of 285mm, and one cannot know if a displacement similar to the one seen in figure 3.3 could have been obtained later on if corrections were done



**Figure 6.2:** Comparison of real damage and single and double frame from analysis

to the model.

### Load Case 1

The next load case, LC1, has an L-shape which resembles the overall shape of the displacement seen in the photos. This analysis proved to be the most successful one, both by reaching the desired deformation of  $285\text{mm}$ , and through general resemblance to the deformations seen in the photos, see Chapter 6.2.

The load-deformation curve for one of the shell nodes with the largest U2 deformation gave a load of  $6.9\text{MPa}$  at the desired deformation of  $285\text{mm}$ . In table 6.3 this result is compared with the design loadings from other IACS Polar Classes. The case study ship has notation PC-7 and is referred to as “LC1 (PC-7)”. The numbers following are, however, taken from the FEA. Above are the design loading for PC-7 and for notations with design magnitudes on the same level as the FEA results. First of all, the design force for PC-7 is  $19\text{MN}$ , half of the actual loading needed in the analysis to create the desired deformations. Dimensioning following the rules of PC-2 would be necessary to obtain a design pressure higher ( $9.2\text{MPa}$ ) than the pressure from the FEA ( $6.9\text{MPa}$ ). If the area is taken

into account and the total applied force considered PC-4 would be sufficient with  $47MN$ .

**Table 6.3:** Comparison of design loads from IACS PC and FEA results

<b>Class</b>	$P_{av}$ [MPa]	$A$ [m <sup>2</sup> ]	$F$ [MN]	<b>Numbers from</b>
PC-2	9.2	11.0	102	Rule design
PC-3	6.3	9.7	63	Rule design
PC-4	5.1	9.2	47	Rule design
PC-5	4.0	8.0	32	Rule design
PC-7	2.5	7.4	19	Rule design
LC1 (PC-7)	6.9	5.8	40	FEA

By assuming the pressure and not the force to be the dimensioning quantity the case study ship would have needed a notation five notations above the one it is classified for to avoid the severe damages. The deformations would have been smaller for a notation lower than PC-2 as well, but to figure out which notation would be the one to prefer would be a discussion regarding levels of allowable damages. Such a discussion is not included in this thesis.

A short discussion should be done regarding the total kinetic energy. From figure 4.14 the kinetic energy absorbed from external loading is found to be  $6.52MJ$  at analysis frame 258 (which is the frame in which  $U2 = 285mm$  is obtained). Since the ship displacement is known the velocity of the ship at impact can be calculated from the equation of kinematic energy, equation (6.1). The velocity is found to be  $0.4m/s$ . For comparison, NORSOK N-004, [19], uses  $11MJ$  for bow collision of a  $5000t$  ship at  $2m/s$ . If the case study ship had a velocity of  $2m/s$  the kinetic energy from the impact would be  $173MJ$ .

$$E_k = \frac{1}{2}m \cdot v^2 \quad (6.1)$$

Figure 6.3 shows the ship kinetic energy as a function of velocity. Due to the mass of the ship the kinetic energy is high, even for low velocities.

Several times it has been stated that the LC1 analysis gives a good reproduction of the damage. However, when looking at the numbers compared in table 5.8 and 5.7 the accuracy of the reproduction can be discussed. For, instance is the  $U2$  displacement of the shell at web frame #230 only  $14mm$  in the analysis and  $199mm$  in the photo. This indicates that more load should be applied around web frame #230. However, when considering the displacement in  $U1$  direction (x-direction) it is clear that the model coincides well with photo measures. An

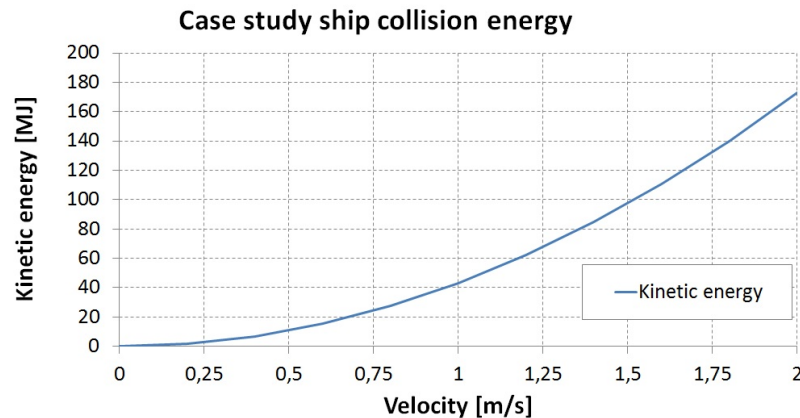


**Figure 6.3:** Ship kinetic energy as function of velocity

increase in load about web frame #230 could lead to an increase in U1 deformation of the frame, which wouldn't be desirable. For the frames between bulk head #227 and web frame #230 the numbers measured from the model are basically zero. This is likely a result of the lack of load applied to this area.

### Load Case 2-5

For load case 2 (LC2) the load-displacement curve shows that the application of more load on the fore side of web frame #233 leads to an increase of displacement aft of web frame #233. This indicates that the desired deformation of 285mm could be obtained for a lower patch pressure by increasing the patch size. However, when increasing the patch towards web frame #230, as in LC3, the analysis aborted before any results of interest was produced. LC4 was created to test whether the patch size was the reason for the analysis abortion. The analysis with LC4 obtained a larger displacement than LC3, but smaller than LC2 even though the load application area for LC4 is less than for LC2. The patch in LC4 is located on top of web frame #230. Aft of this web frame the frames have beam elements as flanges. As discussed in Chapter 4.5, the beam elements used are not intended for nonlinear analysis. Beam elements are also used fore of web frame #237, and are the reason for the abortion of the analyses when the load patch get close to these web frames.

LC1 is the only analysis where an U2 over 300mm is achieved, and where the highest load resistance is gained. The discussion of the beam elements in the previous paragraph imply that LC1 is successful because the load patch is centred about web frame #233, and is not close to web frame #230 or #237.

Table 6.4 gives a summary of the load cases. Note that the patch pressures are taken at different displacements for each load case. The displacement is the maximum U2 displacement within each load case, and are not measured at the same location in the model.

**Table 6.4:** Summary results from load case 1-4

<b>Class</b>	$P$ [MPa]	<b>At U2=</b> [mm]	$A$ [m <sup>2</sup> ]	$F$ [MN]
LC1	6.9	288	5.8	40
LC2	4.7	195	7.2	34
LC3	2.7	83	7.8	21
LC4	5.4	115	2.7	15

### 6.1.3 Discussion of Validity of Comparisons

Due to the sources of error discussed in Chapter 3.8 there are most likely differences in the location of the measurements in the photos and from the element model. The above discussion is valid under the assumption that the measurements are done in the same locations.

The specifications of the actual load which interacted with the ship is the main scope of this thesis and also the part with most uncertainties related to it. The load is assumed to be a uniformly distributed pressure to make the calculations and following assumptions easier. In other words, the mechanical properties of the ice itself are ignored. Examples of how ice mechanics can influence the load are:

- the ice consisting of softer ice with pockets of harder ice, inflicting a varied pressure over the contact area
- the ice breaking several times giving several different shapes of the load application area
- ice rubble accumulating by the ship side creating a large contact area and influencing the capacity of the ship side
- rolling loading, meaning the ice slides along the ship side

A uniformly distributed pressure can be close to the true ice load, but it can also be a very poor simplification.

## 6.2 Comparison of Photos and Analysis Model

In the following figures from Abaqus analysis of LC1, at basically the same location as the photos, are given. Unfortunately, Abaqus' Viewport doesn't have the same (extreme) visualization of depth as seen in some of the photos.

Figure 6.4 shows the exterior damage to the ship side. The analysis displacement distribution seems to be shorter in the longitudinal direction than the actual deformation.

Figure 6.5 shows an overview of the internal damages. When taking the cracked and missing coating into consideration, the maximum deformation appears to be closer to the FP TK TOP in the photo than in the model.

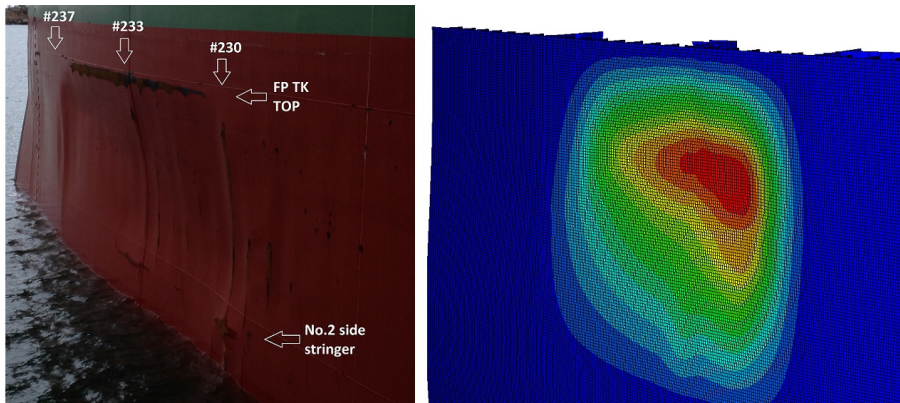
Figure 6.6 shows a close up of the damage area with the largest U2 deformations. Generally the deformations appear to be similar. Note the resemblance in buckling of web frame #233 and the top of the frames.

Figure 6.7 shows the same area as figure 6.6, but from a greater distance and a different angle. Here as well, the frame tops and web frame #233 should be noted for the resemblance in deformation.

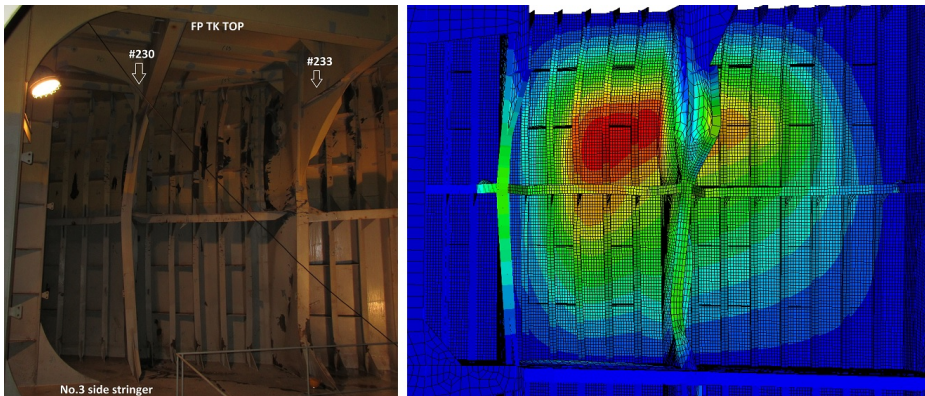
Figure 6.8 shows the fore side web frame #233. Here the deformations of the model are less than seen in the photo.

Figure 6.9 shows the buckling of the lower part of web frame #233. The deformation of the flange in the model is close to the deformation seen in the photo.

Figure 6.10 shows the deformation of a stringer corner. Large deformations are seen both in the photo and for the model, but the resemblance is limited. Note that the model is incorrectly modeled.



**Figure 6.4:** Comparison of figure 3.3 and analysis model



**Figure 6.5:** Comparison of figure 3.5 and analysis model

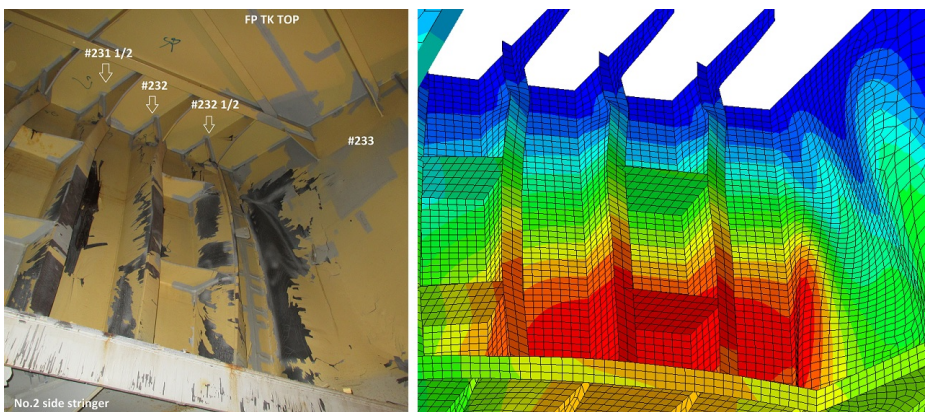


**Figure 6.6:** Comparison of figure 3.7 and analysis model

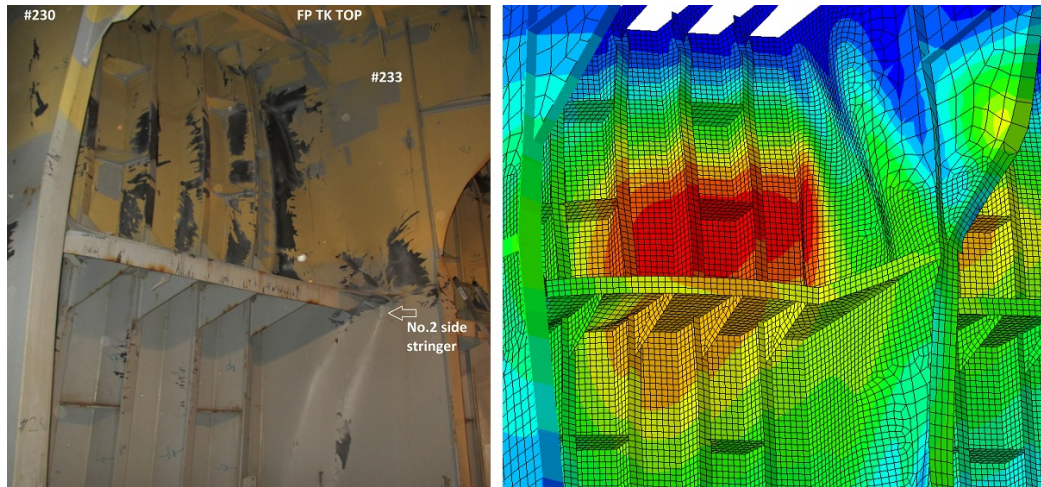


**Figure 6.7:** Comparison of figure 3.8 and analysis model

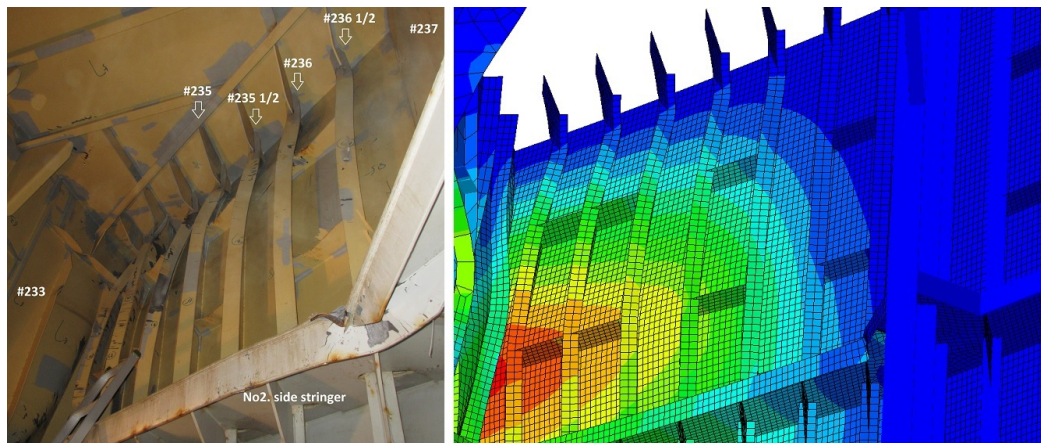


**Figure 6.8:** Comparison of figure 3.11 and analysis model



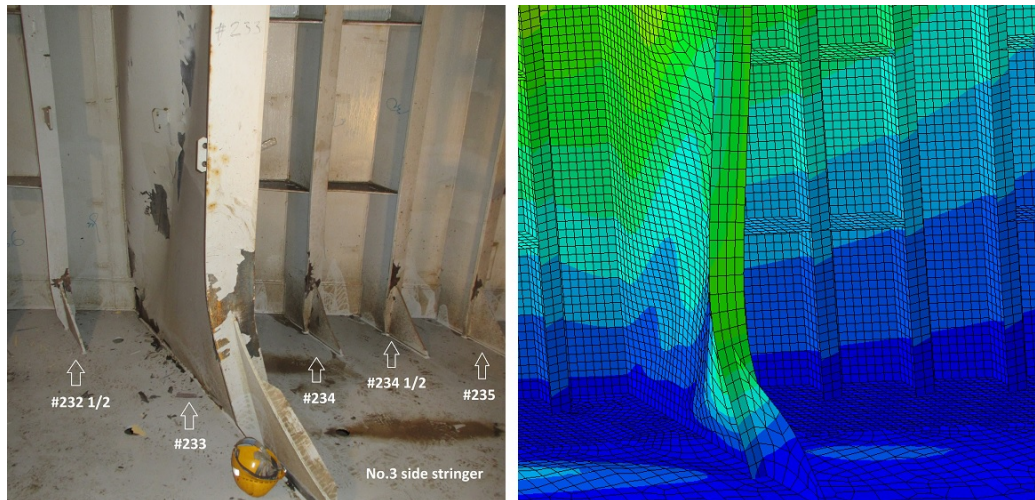


**Figure 6.9:** Comparison of figure 3.12 and analysis model

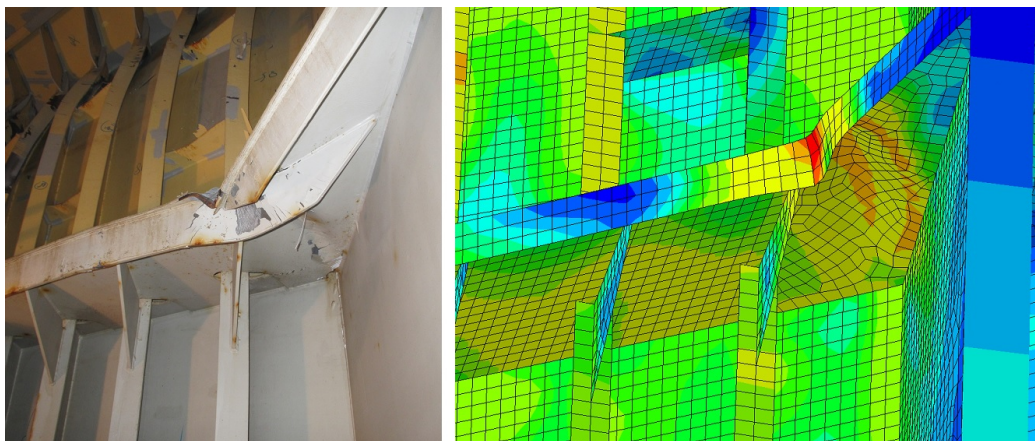


**Figure 6.10:** Comparison of photo and analysis model



# Chapter 7

## Conclusion

The aim of this thesis is to reproduce the hull side deformations of a case study ship in order to estimate the loading which inflicted the damage. The thesis intend to find the loading case with the closest resemblance to the original load, and compare this loading case's characteristics with the design ice load characteristics from the Finnish-Swedish Ice Class Rules (FSICR), which are adopted by DNV-GL, and the International Association of Classification Societies' Unified Requirements for Polar Class (IACS UR PC). The load is assessed as a uniformly distributed pressure over an application area.

The FSICR and the IACS PC are reviewed with focus on the derivation of plating and framing requirements, and the design loads are calculated for the ice class notation of the case study ship. A considerable difference is seen in in the designs load characteristics. The load height of the FSICR is small compared with the span of the structure it is applied to, and is acting more as a line load than as a uniform distributed pressure. The IACS PC ice load on the other hand, has a load height almost equal to the frame span. This load is thus close to acting as a uniform distributed pressure over the whole span. The difference in application area imply a difference in the total applied force, even though the design pressures are of the same order of magnitude. The loads are applied to three finite element models in order to reproduce the deformation of the hull structure: a single frame with plate flange, two neighbouring frames with tripping brackets in between, and a ship side model including the whole damage area. Nonlinear analyses are run and the deformations recorded. Through measurements of photographs from the damage survey, the actual deformation of the side hull of the case study ship is estimated. The photos are of poor quality, and a lot of uncertainty is related to the measurements. The original deformations are compared with the deformations from the finite element analysis in order to verify the applied load cases.

Only one of the proposed load cases proved to reproduce the deformations sufficiently. The analysis shows that a force about ten times the FSICR design load, or twice the IACS PC load, is needed to produce the same deformations. The large difference in the ratio for the FSICR and the IACS PC force originates from the difference in the size of the load application area. These rules present conservative design loads, as the finite element analyses reveal a considerable amount of load carrying capacity beyond the design load level. Hence, these rules are not suited for calculation of the actual capacity of a structure. By looking on the results from a different angle, and assuming the rules' design loads to be sufficient for the conditions they're meant for, the case study ship would need an ice class 3-5 notations higher than the notation it is classified for, depending on how the numbers are evaluated. This implies that the ship in question has been sailing in waters with ice conditions it was not designed for.

The above conclusion is done assuming that the deformation measurements are correct, and that the finite element analyses are producing reliable data. A lot of uncertainty is related to the photo measurements, and many assumptions have been made for the analyses' input, hence there is an uncertainty related to the output of the analyses, and the conclusions based on these. After all, both are approximations to the real damage, and it is challenging to draw a conclusion based on the comparison of the two.

# Chapter 8

## Recommendations for Further Work

This thesis is meant as complete investigation of the ice load needed to inflict large deformations in a ship side. Due to time limitations the finite element model used for the ship side analyses was simplified and assumptions for made for the inputs. Further investigations can be done for the input, including verification studies of: the size of the model itself, the element mesh size and element types, and boundary conditions. In this thesis an extensive study of the material curves are performed, but more focus can be given to strain hardening effects, fracture, and initial imperfections. Due to the erroneously application of elastic beam elements in a nonlinear analysis model, a remodeling of all beam element to shell elements are strongly recommended.

As a continuation of the work in this thesis, an assessment of the necessary reinforcement of the ship side scantlings in order to with stand the ice loading, can be performed.



# Bibliography

- [1] Det Norske Veritas. *Ships for Navigation in Ice*. DNV-GL, 2012. Rules for Classification of Ships, Part 5, Chapter 1.
- [2] International Association of Classification Societies. *Requirements Concerning Polar Class*. IACS, 2011. IACS Req. 2006/Rev.02, 2010.
- [3] K. Riska. *Development of the Finnish-Swedish Ice Class Rules Using Recent Research Results*. Port and Ocean Engineering under Arctic Conditions (POAC), Espoo, Finland, 2013.
- [4] DNV-GL Internal e-mail correspondence.
- [5] DNV-GL Surveyor Report.
- [6] Det Norske Veritas. *Hull Structural Design, Ships with Length 100 metres and above*. DNV, January 2014. Rules for Classification of Ships, Part 3, Chapter 1.
- [7] Finnish Winter Navigation Research Board and Swedish Maritime Administration. *A Preliminary Risk Analysis of Winter Navigation in the Baltic Sea*. Etida Prima Oy, Helsinki, 2005.
- [8] Det Norske Veritas. *DNV Hull Structural Rules - Development, Background, Motives*. DNV, 2005. Part 5, Chapter 1, Ships for Navigation in Ice.
- [9] Det Norske Veritas. *Passenger and Dry Cargo Ships*. DNV-GL, 2014. Rules for Classification of Ships, Part 5, Chapter 2.
- [10] C. Daley A. Kendrick. *Derivatio and Use of Formulations for Framing Design in the Polar Class Unified Requirements*. 2000. IACS Ad-hoc Group on Polar Class Ships, Transport Canada.
- [11] International Maritime Organization. *Guidelines for Ships Operating in Polar Waters*. IMO, 2010.

- 
- [12] Claude Daley. *Background Notes to Design Ice Loads*. Memorial University, 2000. IACS Ad-hoc Group on Polar Class Ships, Transport Canada.
- [13] Appolonov Daley, Kendrick. *Plating and Framing Design in the Unified Requirements for Polar Class Ships*. POAC'01 VOL.2 p.779, Ottawa, August 2001.
- [14] A. Kendrick C. G. Daley. *Framing Design in the Unified Requirements for Polar Ships*.
- [15] Drawings from. DNV-GL Ship Database.
- [16] Det Norske Veritas. *DNV-RP-C208: Determination of Structural Capacity by Non-linear FE analysis Methods*. Det Norske Veritas, 2013.
- [17] E mail correspondence with on-site surveyor at yard.
- [18] *Abaqus Analysis User's Manual*. 3DS SIMULA, 2013.
- [19] Standards Norway. *NORSOK STANDARD N-004: Design of Steel Structures*. Standards Norway, 2004.



# **Appendix A**

## **Drawings**

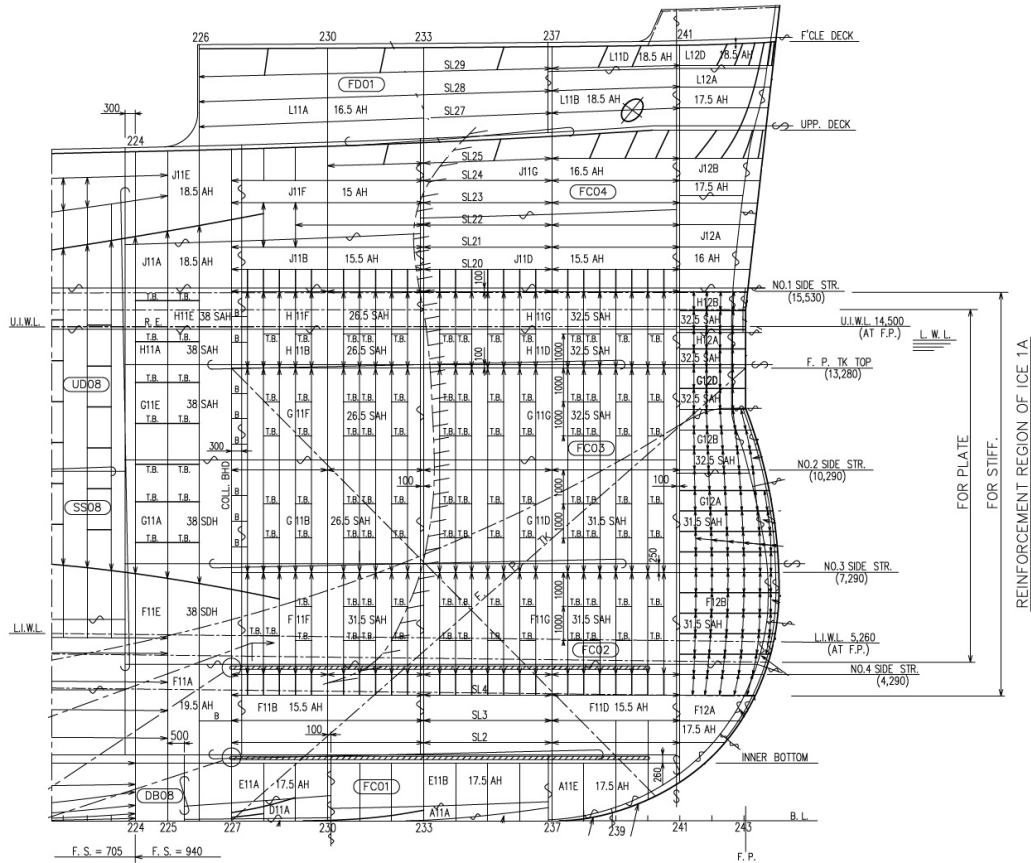


Figure A.1: Shell expansion, [15]

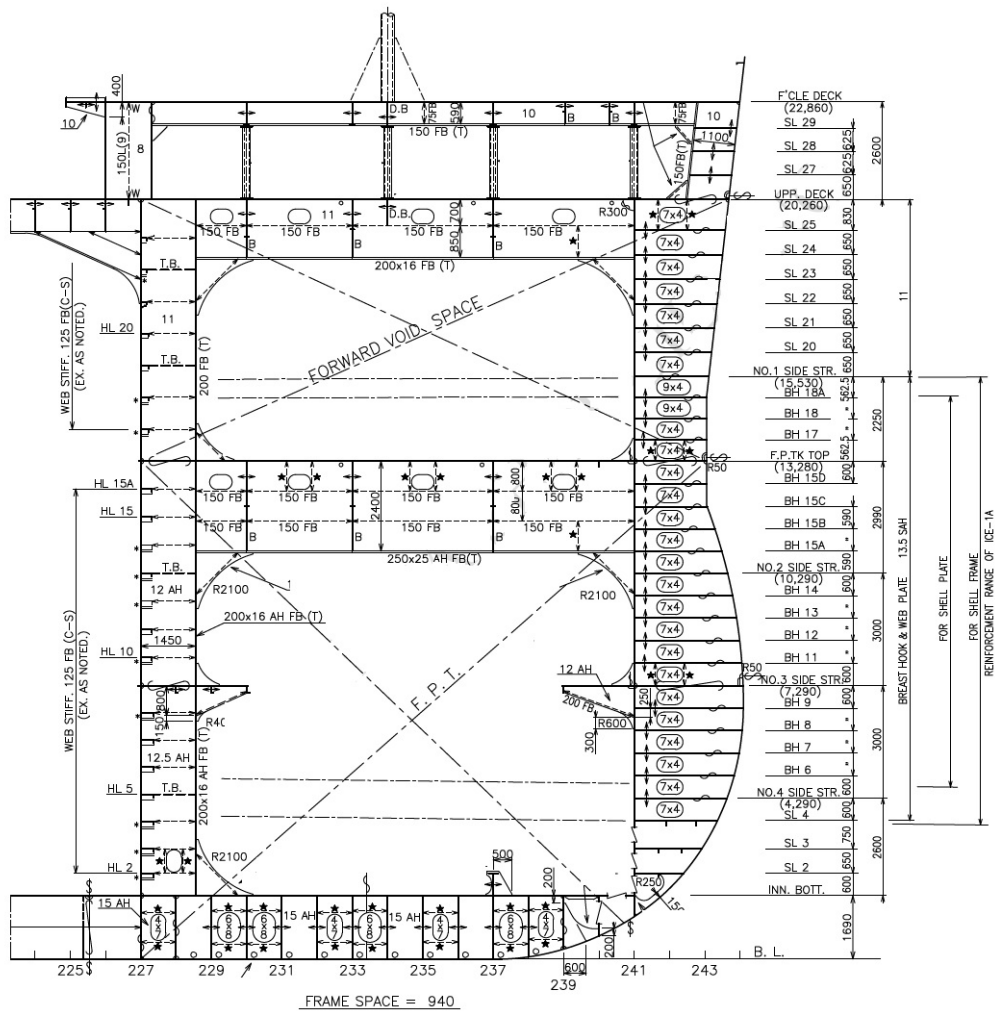


Figure A.2: Center line, [15]

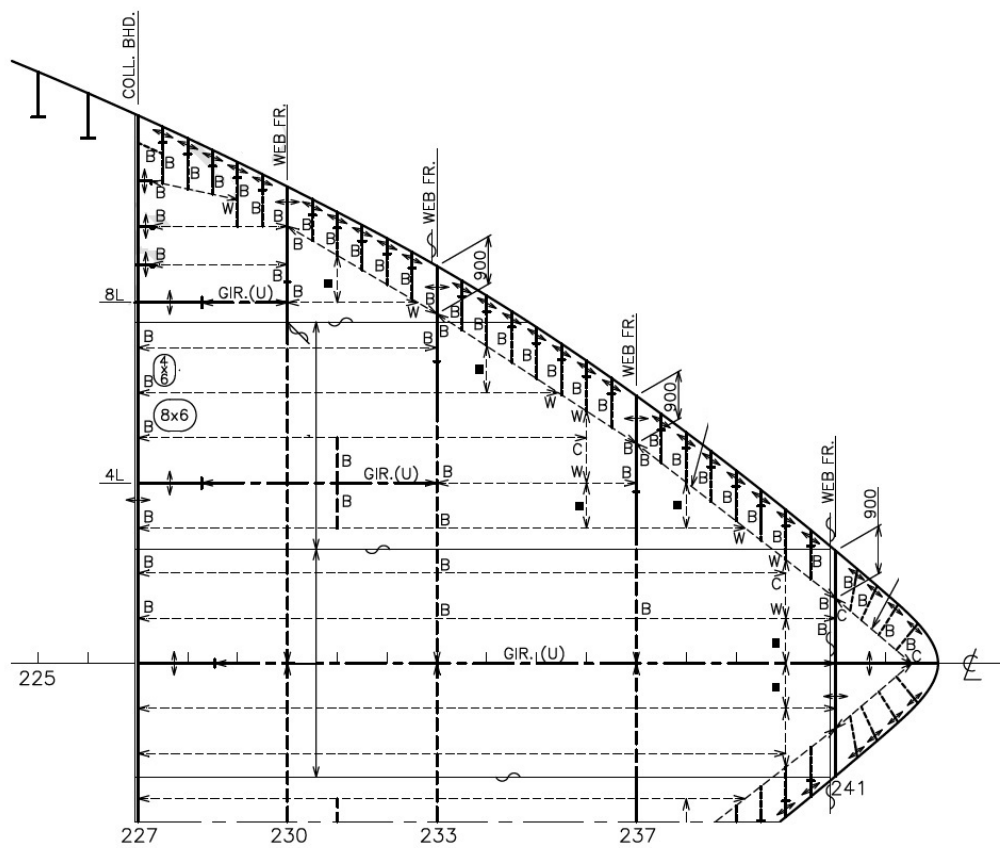


Figure A.3: Fore peak tank top, [15]

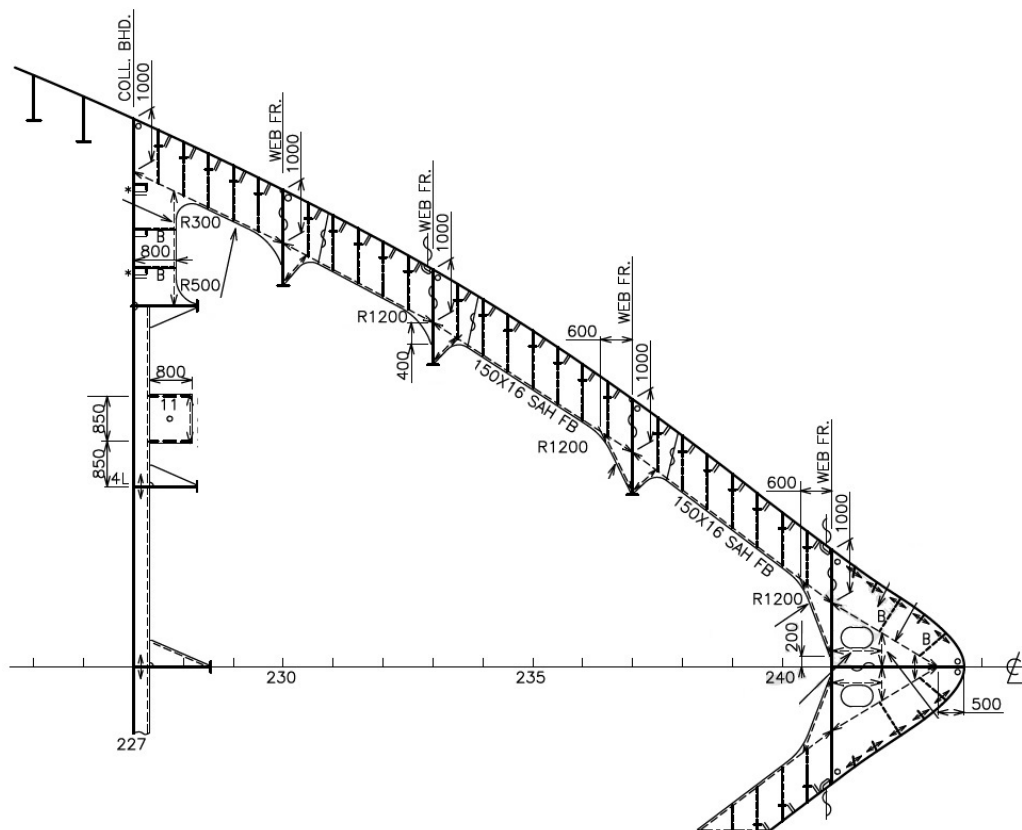


Figure A.4: No. 2 side stringer, [15]

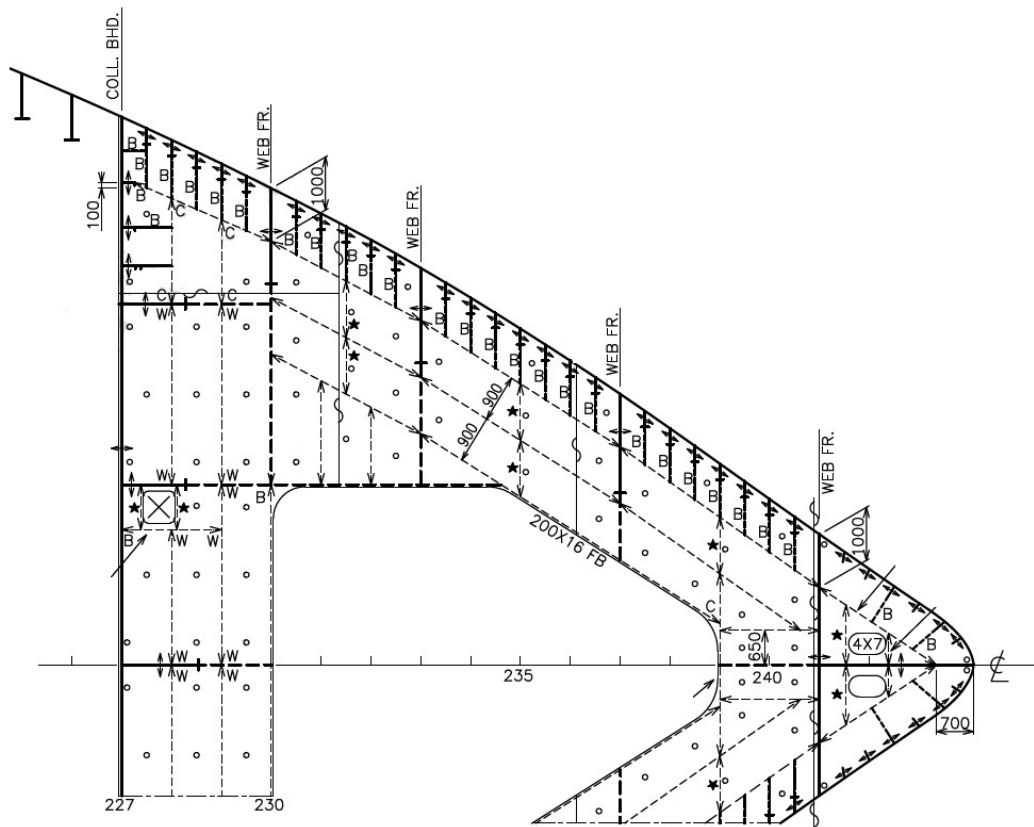


Figure A.5: No. 3 side stringer, [15]

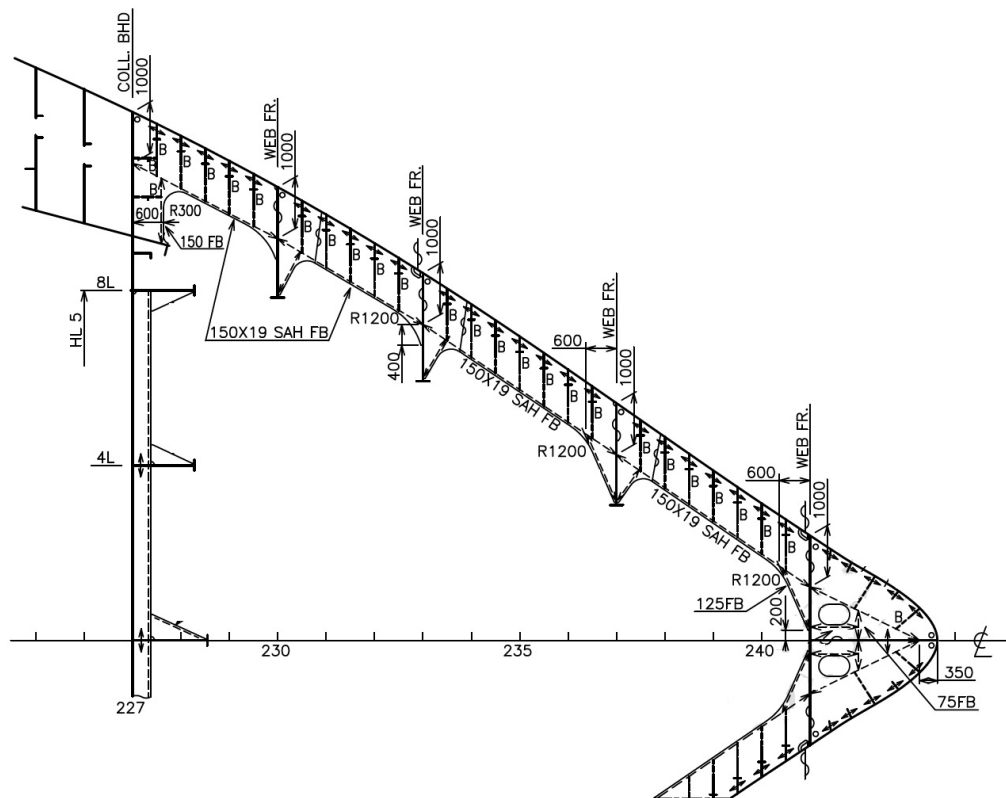


Figure A.6: No. 4 side stringer, [15]

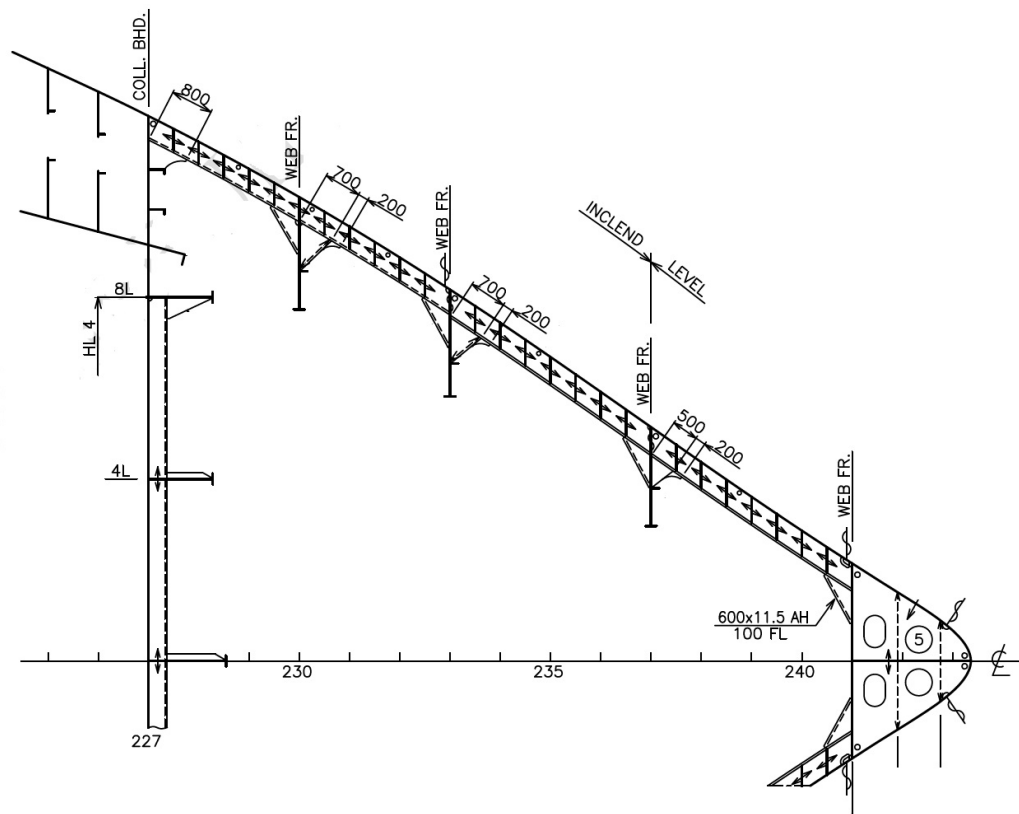
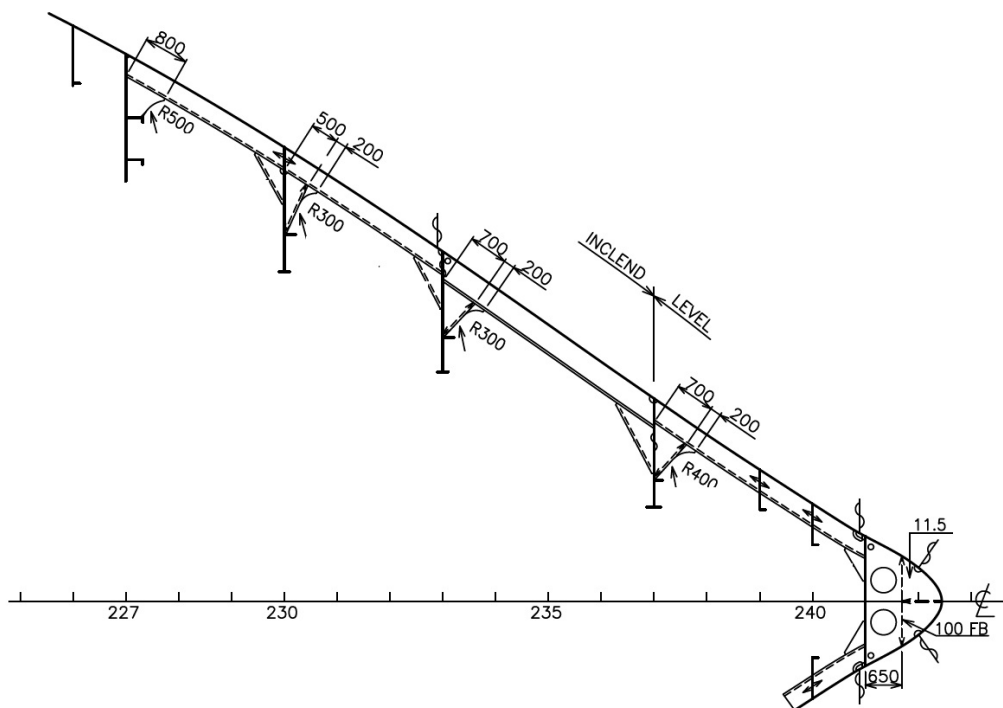


Figure A.7: Side longitudinal 4, [15]





**Figure A.8:** Side longitudinal 2 and 3, [15]

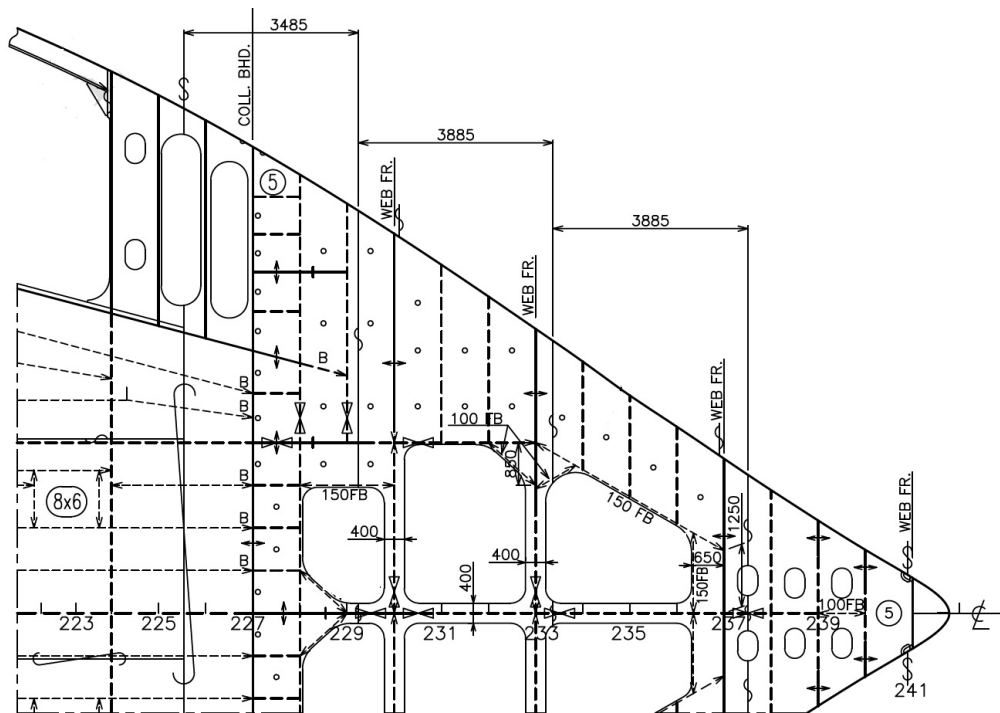


Figure A.9: Inner bottom, [15]

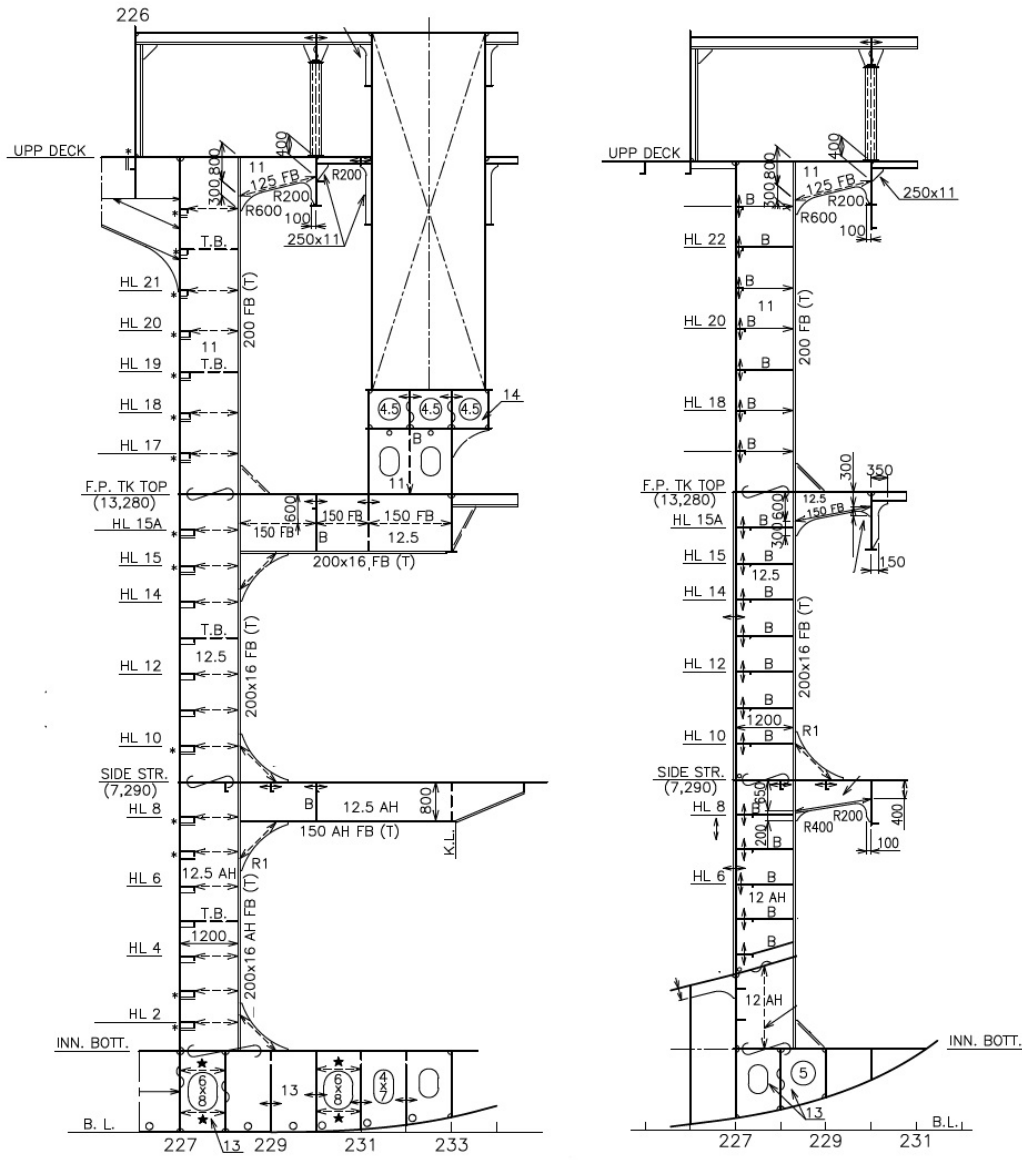


Figure A.10: Longitudinal 4 and 8, [15]

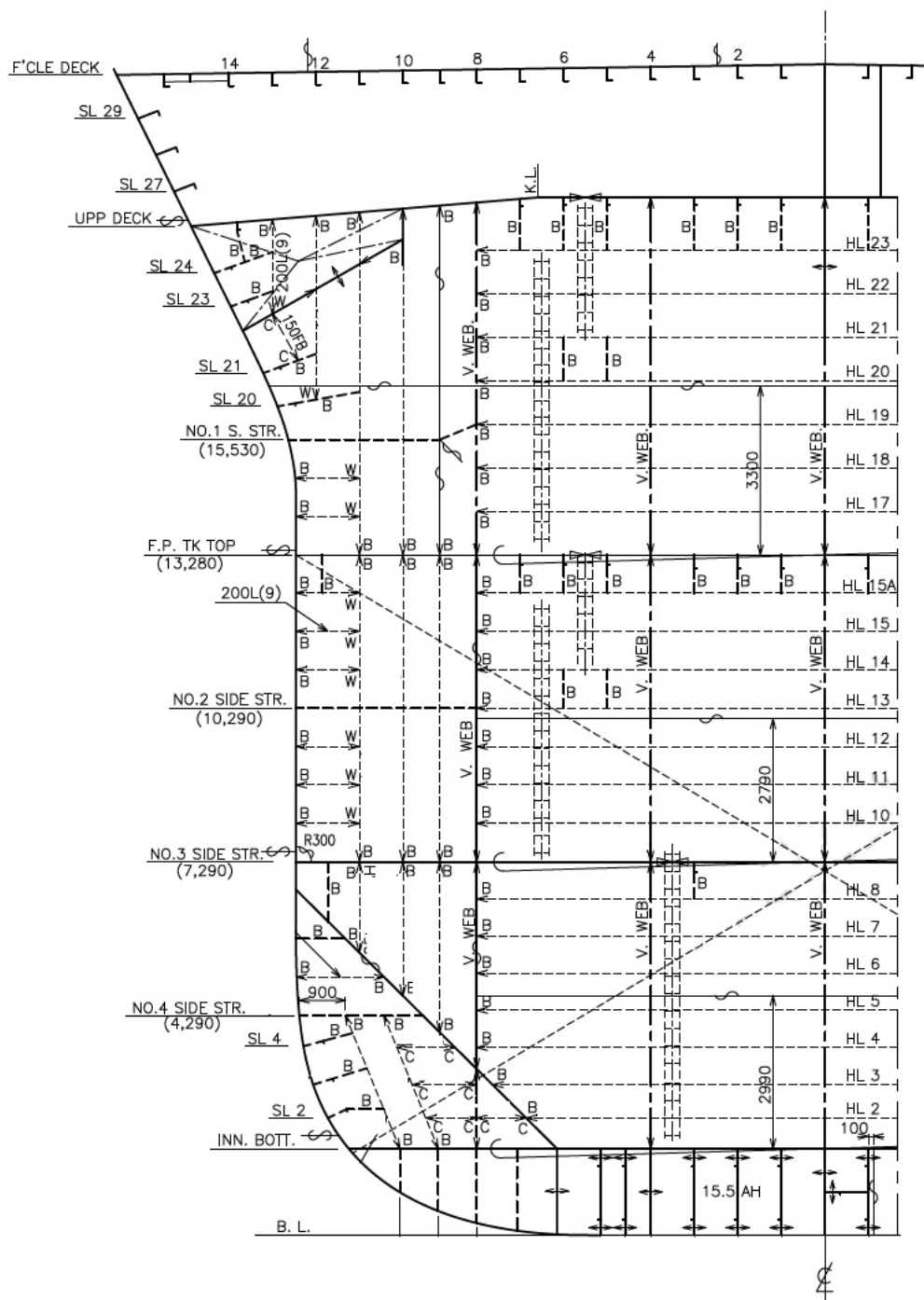


Figure A.11: Web frame #227, [15]

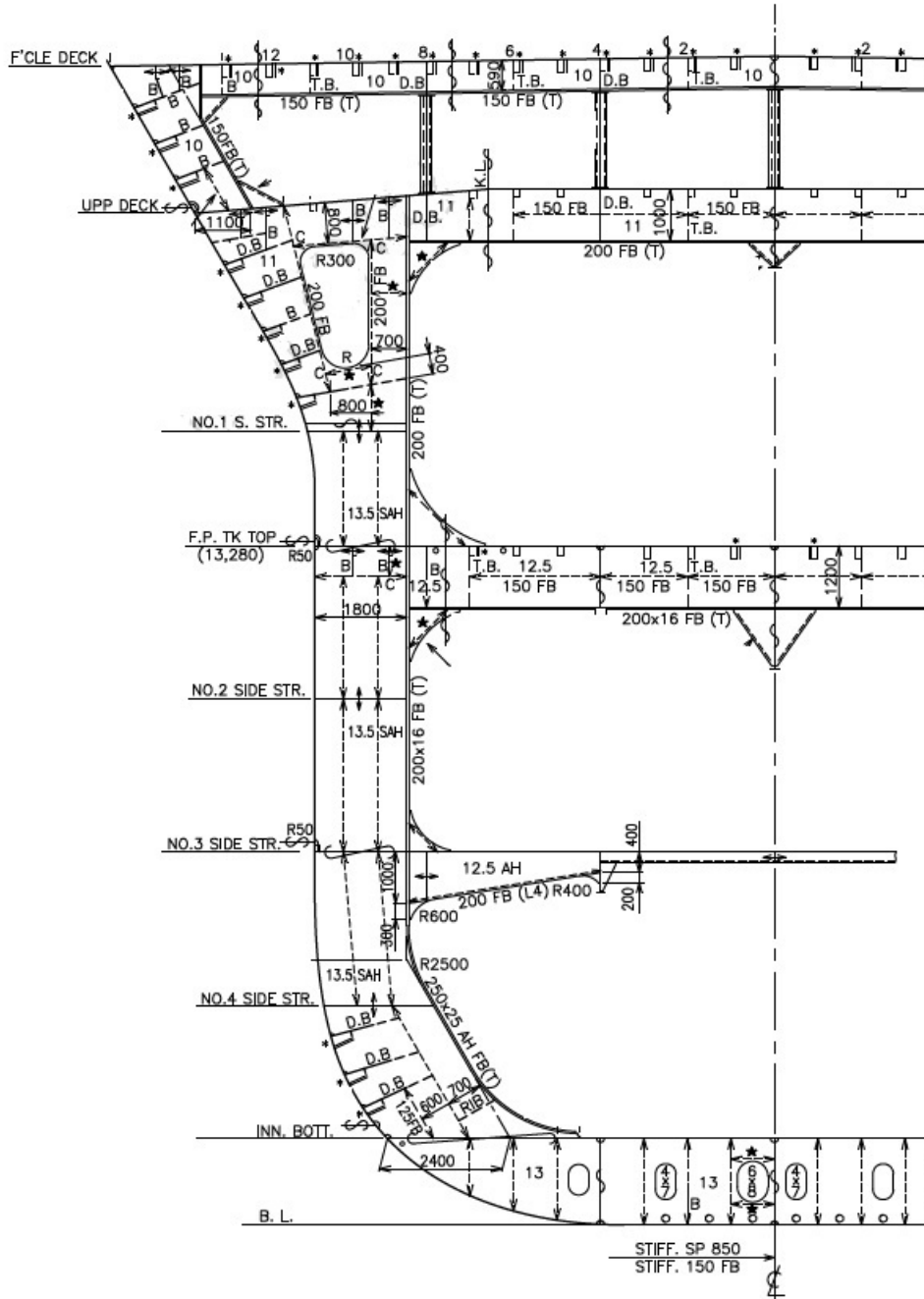


Figure A.12: Web frame #230, [15]

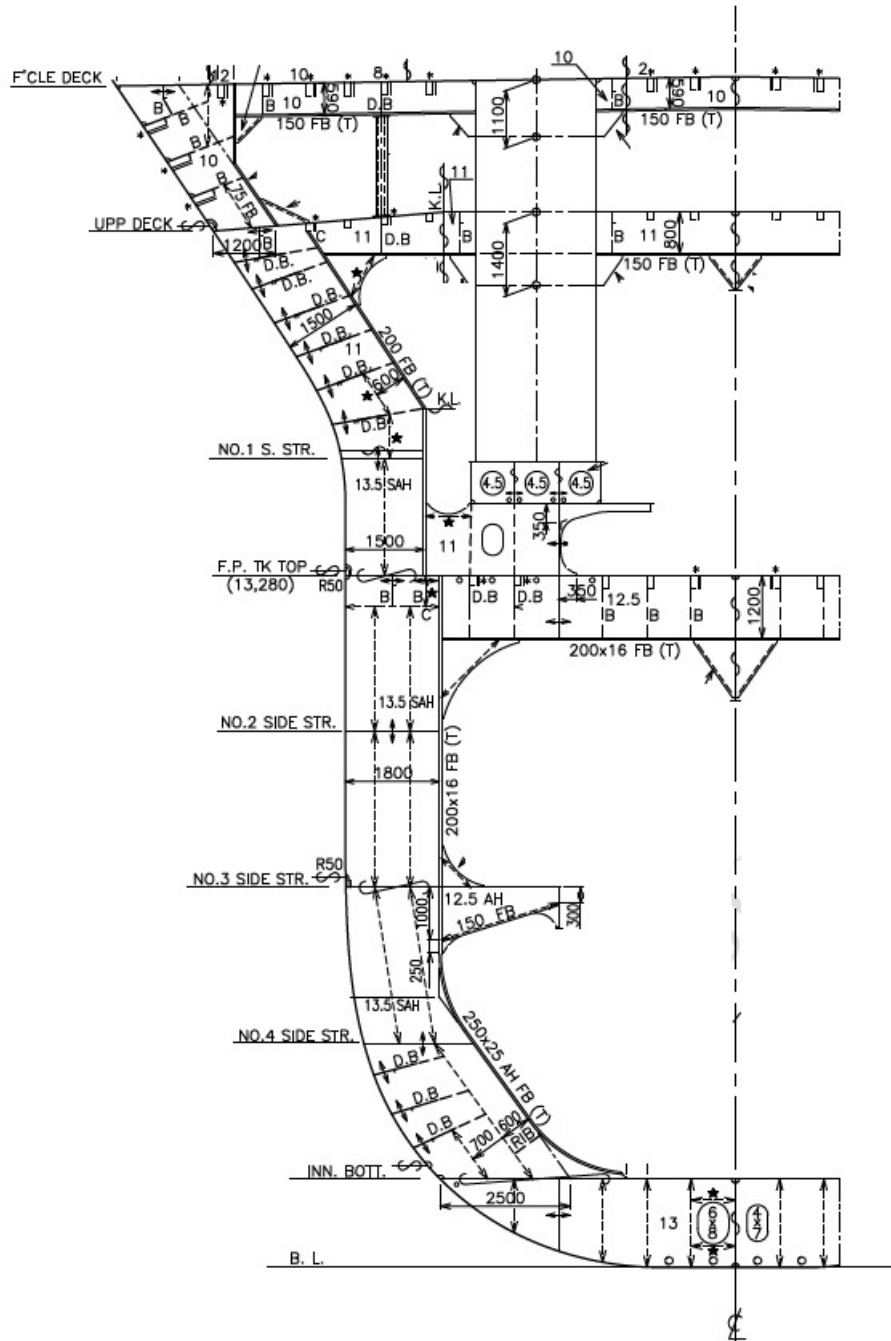


Figure A.13: Web frame #233, [15]

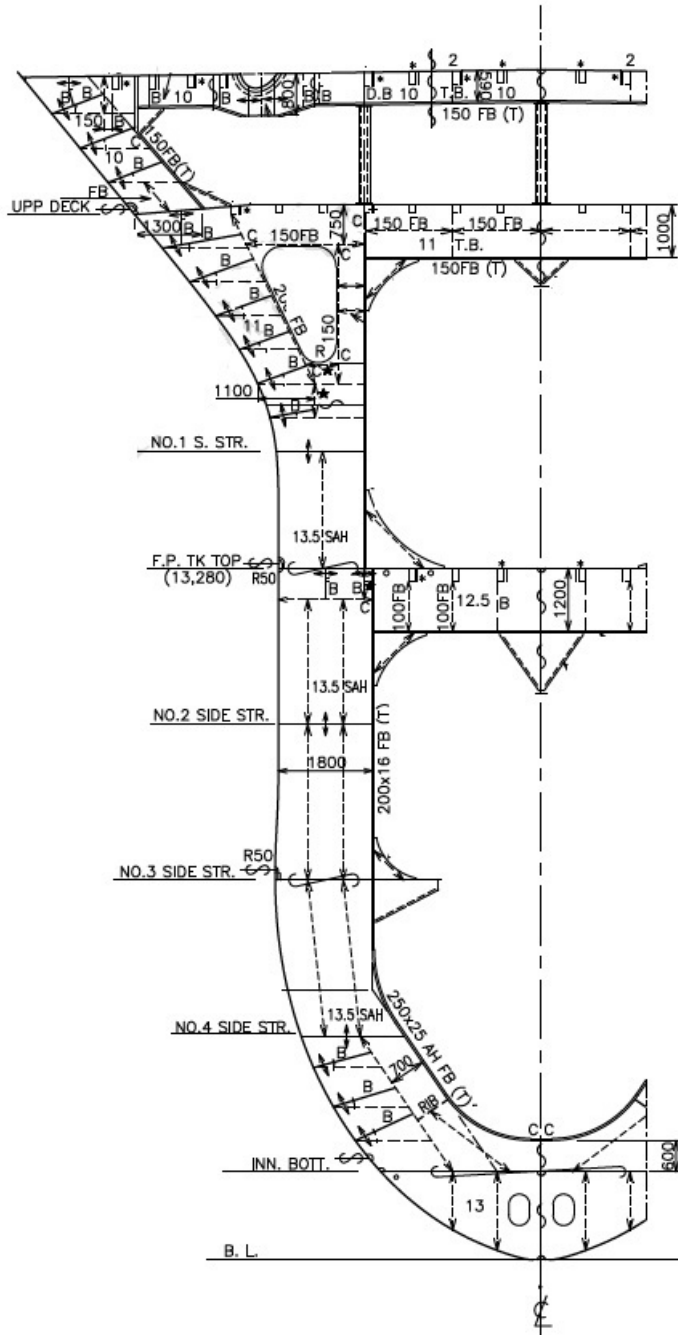


Figure A.14: Web frame #237, [15]

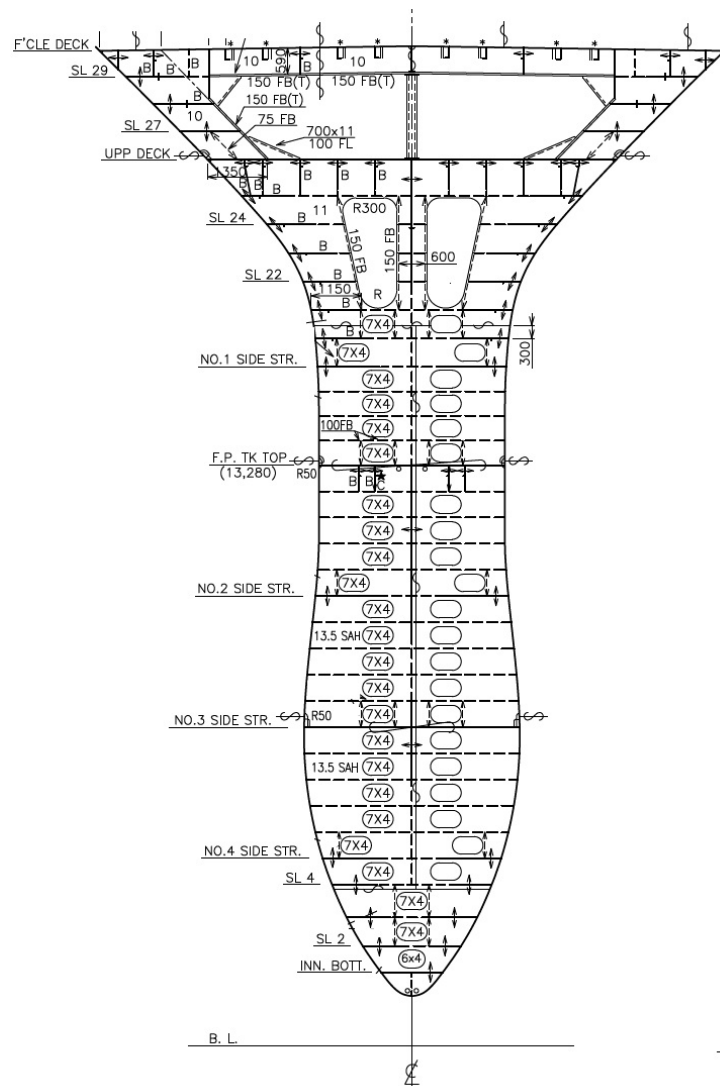


Figure A.15: Web frame #241, [15]